UNIVERSITY OF PARDUBICE

FACULTY OF CHEMICAL TECHNOLOGY

DOCTORAL THESIS

2018 Simon Cousy

University of Pardubice

Faculty of Chemical Technology

Preparation and study of simonkolleite and zinc oxide from aqueous precipitation of zinc chloride

Simon Cousy

Doctoral thesis

2018

I hereby declare:

This thesis was prepared separately. All the literary sources and the information I used in the thesis are listed in the bibliography. I got familiar with the fact that the rights and obligations arising from the Act No. 121/2000 Coll., Copyright Act, apply to my thesis, especially with the fact that the University of Pardubice has the right to enter into a license agreement for use of this thesis as a school work pursuant to § 60, Section 1 of the Copyright Act, and the fact that should this thesis be used by me or should a license be granted for the use to another entity, the University of Pardubice is authorized to claim a reasonable contribution from me to cover the costs incurred during making of the thesis, according to the circumstances up to the actual amount thereof. I am aware that my thesis will be accessible to the public in the University Library and via the Digital Library of the University of Pardubice in agreement with the article 47b of the Act No. 111/1998 Coll., on Higher Education Institutions, and on the Amendment and Supplement to some other Acts (the Higher Education Act), as subsequently amended, and with the University Pardubice's directive no. 9/2012.

In Pardubice on 5. 12. 2018

Simon Cousy

Acknowledgement

As the author, I would like to thank a few people without whom I would have not realized this work. First and mainly I would like to thank my supervisors Ladislav Svoboda and Jiri Zelenka for giving me the opportunity to realize this work, as well as their guidance and support all along my research. Additionally, I would like to send special thanks to Nataliia Gorodylova and all the people from the university of Pardubice as well as the company Toseda with whom I had the chance the cooperate. Additionally I would like to thank Jakub Houdek for his help, and the Center of materials and nanotechnologies through projects ED4.10011.0251 and LM2015082. Finally, I send all my gratitude to my parents, my friends and my supporting girlfriend who gave me the motivation and strength to go through difficult times, and to finish this work.

TITLE

Preparation and study of simonkolleite and zinc oxide from aqueous precipitation of zinc chloride.

ANNOTATION

This work deals with the preparation of simonkolleite and zinc oxide from zinc chloride. The main motivation for this work was the preparation of nanoparticles using no surfactant, inexpensive setup and chemicals. A wet precipitation method was chosen for the synthesis, using potassium hydroxide as a precipitation agent for the zinc chloride salt. The precipitation mechanism was studied, as well as the influence of the synthesis parameters on the morphology and nature of the product. Additionally, the addition of butanol to the aqueous suspension was studied, as a stabilizer for simonkolleite suspension. Simonkolleite was synthesized in the shape of nano-platelets, whereas zinc oxide exhibited aggregates of nano and microspheres. Both simonkolleite and zinc oxide had limited dispersion stability in water suspension and showed some sedimentation. Finally, three different potential applications were studied for the products: as an anti-corrosive agent, as a photocatalyst, and as a filler for polymer reinforcement.

KEYWORDS

Zinc oxide, simonkolleite, wet precipitation, composite, zinc chloride

ANOTACE

Tato práce se zabývá přípravou simonkolleitu a oxidu zinečnatého z chloridu zinečnatého. Hlavním cílem bylo připravit nanočástice bez použití surfaktantů s možností využití nenákladného uspořádání zařízení a dostupných chemikálií. Metoda mokrého srážení pomocí hydroxidu sodného jako srážecího činidla byla použita pro syntézu nanočástic z chloridu zinečnatého. Všechny experimenty byly prováděny tak, aby bylo možné studovat mechanismus srážení a vliv parametrů syntézy na morfologii produktů. Dále byl studován vliv přídavku butanolu do vodné suspense simonkolleitu za účelem její stabilizace. Simonkolleit byl syntetizován ve formě nano-destiček, zatímco připravený oxid zinečnatý vykazoval agregáty. Nicméně obě látky, jak simonkolleit, tak oxid zinečnatý, jsou ve vodné suspenzi omezeně stabilní a částečně sedimentují. Na závěr práce byly pro studované produkty zkoumány tři potenciální aplikace jako antikorozní činidlo, fotokatalyzátor a plnivo do polymerů.

KLÍČOVÁ SLOVA

Oxid zinečnatý, simonkolleit, mokré srážení, kompozit, chlorid zinečnatý

Contents

List of figures and tables

Figures

Tables

List of abbreviations and acronyms

AAS	atomic absorption spectrometry
AFM	atomic force microscopy
CVD	chemical vapor deposition
DEL	double electrostatic layer
DLVO	Derjaguin Landau Verwey Overbeek
DMA	dynamic mechanic analysis
DSC	differential scanning calorimetry
IR	infra-red
LDH	layered double hydroxides
LHS	layered hydroxide salts
LZH	layered zinc hydroxide
RIR	reference intensity ratio
SEM	scanning electron microscopy
TEM	transmission electron microscopy
Tg	glass transition temperature
USA	United States of America
UV	ultra-violet
VdW	Van der Walls
VLS	vapor-liquid-solid
WAXS	wide angle X-ray scattering
XRD	X-ray diffraction

Introduction

The motivation behind the presented lied in studying easy and cost-efficient ways how to valorise recycled $ZnCl_2$. Many publications describe the use of other zinc salts, namely zinc acetate for the preparation of zinc oxide. Another motivation to this work was to avoid the use of surfactants, that might plasticize polymeric systems. Finally the synthesis methods should be performed in mild synthesis conditions, while avoiding the use of expensive or sophisticated equipment.

A promising lead was to synthesize ZnO that found numerous applications due to its interesting properties, namely its piezoelectric constant, photoluminescent properties, photocatalytic activity in the UV range, and low toxicity. There are many known ways how to synthesize ZnO, which can be sorted in a few categories: processes where the reactives are in vapor phase, usually requiring high temperatures; processes where the reaction takes place in a solid form, namely mechanochemical process; electrodeposition processes; and other wet precipitations excluding any oxydo-reduction reaction.

Alternatively, it is possible to synthesize simonkolleite, a layered hydroxide salt of zinc, under similar synthesis conditions to ZnO. Simonkolleite has a layered structure and is a potential source for nano sheets, and showed few promising properties as well. Layered hydroxide salts have the general formula $M^{2+}(OH)_{2-x}\ A^{m-}_{x/m}\ .nH_2O$, and show good anionic exchange capacity, exfoliation and intercalation of different molecules. Among layered hydroxide salts, simonkolleite and other layered zinc hydroxide salts have been studied because of their interesting catalyst support, drug carrier, UV and visible light absorption, and corrosion inhibition properties.

The main goals of this thesis are to first test two possible synthesis methods for the synthesis of ZnO and/or simonkolleite, both based on a precipitation of salts in aqueous media. The most promising method will be studied more closely to understand the precipitation mechanism, and the influence of different synthesis parameters on the product. Further the effect of n-butanol on simonkolleite and ZnO stabilization in aqueous suspension will be studied, both after and during the synthesis process. Finally, three potential applications will be explored for the synthesized products: ZnO as a photocatalyst, simonkolleite as an anticorrosive agent, and simonkolleite as filler for a polymeric matrix.

1. Theoretical and literature part

1.1 Nano-effect phenomena

Obviously, the mass or volume fraction of the filler has an influence on the composite material, but the size of the filler has also its importance. Nano-effect is often linked to surface effects, since when decreasing the size of particles, the specific surface is increasing. The specific surface is the ratio between the surface and the weight of an object or groups of objects. This effect was demonstrated by Galileo (the square-cube law), and can be easily demonstrated for a cube or sphere. In the case of mechanical reinforcement, a higher aspect ratio will allow more efficient stress transfer between the matrix and the filler. A bigger surface will increase the stress transfer between the matrix and the filler. The filler will then take more of the load, and the composite deformation will be lower, as well as its resistance to break. Furthermore, it also can increase the resistance to fracture. Indeed, the decrease in size will increase the amount of particles at constant size. When a crack is initiated in the matrix, it has a higher chance to be stopped by a particle.

However, some other nano-effects are not linked to this increase of specific surface, but the size of the system studied. Laws of physics on a macro and meso-scale are different from those on a nanoscale. These effects are more complicated and will not be discussed in detail in this essay, but should be taken into consideration while studying nano-composites.

The first effect is the quantum effect and Heisenberg's uncertainty. This effect is non-deterministic, meaning that all properties of an elemental particle such as electron or photon cannot be known with precision simultaneously. As a result, when put in a confined space, the other properties of an electron will be less predictable. Another effect is the Brownian motion. This effect is the nanoscopic equivalent of temperature. Single molecules are moving according to a random path, having multiple collision with each other. The random motion of the molecules can be partially transmitted to small particles, which will start to move randomly as well. Laws of diffusion are for instance based on the Brownian motion. By the use of statistics and a large amount of molecules, the random factor will be attenuated, and general laws can be drawn. However, when confined in small space such as nanotubes, the travelling distance is too small to attenuate the random factor, and laws of diffusion do not apply anymore. Finally, each surface, or interface between the bulk particles and the external media, has an energy. This energy can explain surface tension, and why mosquito can walk on water, or why smaller bubbles of soap will be cannibalized by bigger

ones. For big particles, the surface energy can be ignored, but for nanoparticles it will have an important influence. This effect can be referred as border effect and will alter the properties of the particle such as the conductivity or energy levels for semi-conductors.

1.2 Colloid stability

Compared to a bulk material, small particles have a higher free energy arising from the atoms on its surface. Indeed, the content of atoms on or near its surface is increasing for smaller particles, and the total free energy of the particle is significantly increased. This energy is called surface energy, and can be measured easily for liquids, but is trickier to determine by a direct measurement for solids. This energy will give rise to an attractive force that will ultimately lead to the aggregation of the particles, in the view of reducing their total specific surface. This force has however a limited range, and will only be significant at low distances. This means that the aggregation rate will be driven mainly by diffusion laws.

In the case where additional forces are present, especially repulsive, this can lead to a potential barrier which can reduce the aggregation rate to several orders of magnitude. This is called the stabilization of colloids, and can arise mainly from two factors: steric hinderance, and double electrostatic layer.

Steric hinderance is caused by macromolecules or polymers, coated on the surface of the particles. The macromolecules have usually at least two different kinds of chemical building blocks. One will be poorly solvated and rather bind to the particle surface, while the other will be well soluble and be rather freely pending in the solvent, outward from the particle surface. When the particles get closer to each other, the macromolecules start to interpenetrate, and their movement freedom is reduced, leading to an increase in entropy. Moreover, the increased concentration of the polymer creates an osmotic pressure, where the solvent will try to get in the space between the two particles. The solvent is quite important as it should well solute the pending paret of the macromolecule, but not the one attached to the surface. When the solvent is soluting the whole macromolecule, it will deplete totally the surface of the particle, and the steric stabilisation effect will be lost. On the contrary, when the solvent does not solute any part of the macromolecule, it will form a densely packed shell on the surface of the particle, and again the steric stabilisation effect will be lost. In this case the polymer will merely reduce the surface energy of the particles. The steric effect is quite difficult to quantify with theories and schemes, as it depends from case to case, on the density of the polymer, on the surface, the fraction anchored to the surface and the fraction of units

pending perpendicularly to the surface. It also depends on the interaction coefficient between the polymer and the solvent (chi). This coefficient determines whether the polymer will decrease its free energy when being soluted by the solvent.

The second stabilisation effect is due from the electrostatic charge of the particle surface. In this case, a soluted electrolyte will concentrate near the surface via electrostatic attraction and the whole system will form a double electrostatic layer. This phenomenon is quite well quantified in the DLVO theory, which accronym refers to its major contributors: Derjaguin, Landau, Verwey, and Overbeek. In this theory, only two interparticles forces are taken into account: Van der Walls and the electrostatic interactions form the double electrostatic layer around the particles. The van der Walls (VdW) forces arise from the different dipole-dipole interactions between molecules. They are quite weak compare to other chemical interactions, but can have a significant contribution if they are a great number of them. They are generally attractive, but fades at distances greater than 0.6 nm. In the case of two infinite flat surfaces, the sum of VdW forces can be summarized as:

$$\Delta G_{VdW} = -\frac{A_H}{12\pi d^2} \tag{1}$$

Where d is the distance between the two surfaces, and A_H is the Hamaker constant, including the sum of the interactions of the induced and permanent dipoles present in the material. The calculation of the Hamaker constant can be quite complicated and tedious, but it can be approximated using the Ninham-Parsegian method. This method assumes that materials are made of a continuous media, and establish a relationship between the dielectric response and the frequency. This representation has no direct physical basis but is based on the value of static dielectric constant, index of refraction, and infrared, ultraviolet and microwave absorption spectra. The accuracy of the calculation depends greatly on the accuracy of the infra-red (IR) and UV spectra used to construct the Ninham-Parsegian function for the material. The method is well described in the literature [1–3], and will not be discussed in further details in this document.

The calculated Hamaker constant is valid for two particles in vacuum, however the presence of the fluid medium, the mutual attraction between the two surfaces will be reduced. It is therefore necessary to calculate the effective Hamaker constant, based on the constants of both the particle and the liquid in vacuum, according the following equation:

$$A_{Heff} = \left(\sqrt{A_{H1}} - \sqrt{A_{H2}}\right)^2 \quad (2)$$

In the case of the interaction between two spherical particles of diameters *r*, and in the case where $d << r$, the following developed function can be approximated, were the higher order terms $A_n \left(\frac{d}{r}\right)^n$ are neglected:

$$\Delta W_{VdW}(d) = -\frac{A_H}{12\pi d^2}\left[1 + \frac{3/4 d}{r} + \sum_{n=2}^{\infty} A_n \left(\frac{d}{r}\right)^n\right] \quad (3)$$

Schemes for different shapes can be further found in the literature, and schemes get more complicated as the size distribution is wider, but this will not be discussed here.

The second contributing forces are arising from the double electrostatic layer (DEL). This layer is formed in the case were the particles have a net charge on their surface. To keep the overall neutrality, a soluted countercharge will be present, and usually additionally extra electrolytes if the solution has not been deionized. The thickness of the layer depends on the competition between diffusion and electrostatic attraction. When the concentration of the electrolyte is smaller, the diffusion will be stronger and the counterions will have a tendency to go towards the rest of the solution, increasing the thickness of the DEL layer (Figure 1).

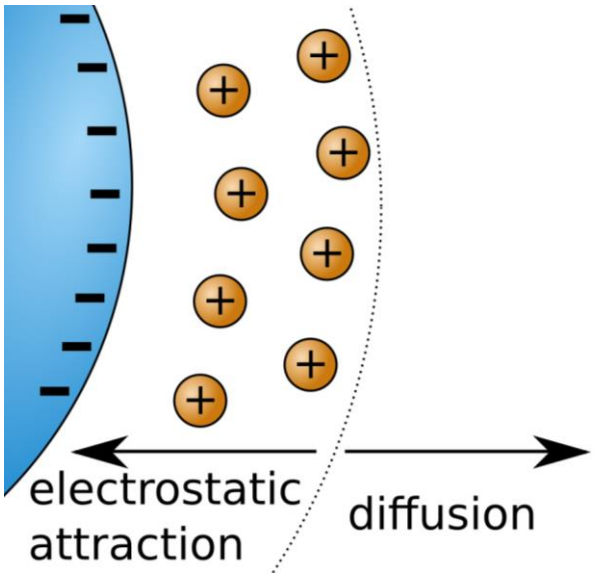

Figure 1: Illustration of the double electrostatic layer, with the layer thickness indicated by the dashed curve

The repulsive force of the electrostatic layer decreases with increasing concentration of electrolytes, according to the following equation:

$$W_{dl}(d) = \frac{2\sigma_+\sigma_-}{\varepsilon_0\varepsilon_r\kappa}\exp(-\kappa d) \quad (4)$$

Where σ_+ and σ_- are the charge surface density on both sides of the electrostatic layer, ε_0 and ε_r are respectively the absolute and relative permittivity, d the distance between two particles, and κ the inverse Debye length, calculated according to the following equation:

$$\kappa^{-1} = \left(\frac{k_B T\varepsilon_0\varepsilon_r}{2q^2 N_A I}\right)^{1/2} \quad (5)$$

Where k_B is the Boltzmann constant, T the absolute temperature, q the elementary charge, N_A the Avogadro number, and I the ionic strength of the solution.

The overall forces of the model system comprising two particles in a solution can be written under the following form (eq.6), and the total free energy can be plotted against the distance between the two particles. In the Figure 2, the free energy is plotted in function of the interparticular distance using the following parameters:

- $A_H = 5.10^{-21}$ J
- $\sigma^+ = \sigma^- = 5$ mC.m^{-2}

$$W_{dl}(d) + W_{WdV}(d) = \frac{2\sigma_+\sigma_-}{\varepsilon_0\varepsilon_r\kappa}\exp(-\kappa d) - \frac{A_H}{12\pi d^2} \quad (6)$$

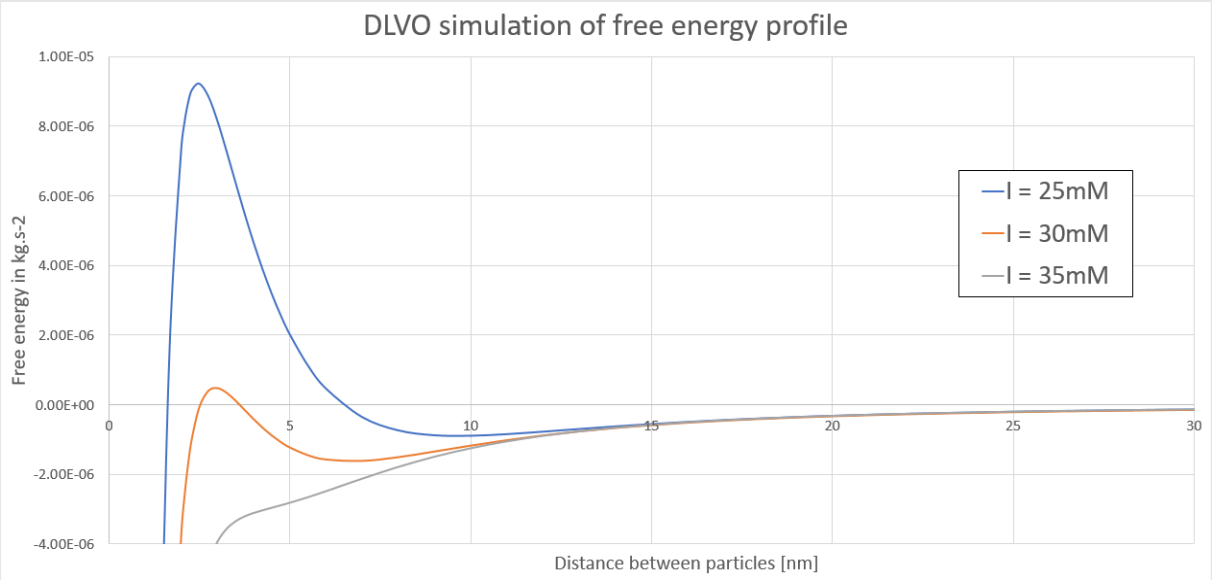

Figure 2: Energy profile simulation according to DLVO theory with a surface charge density of 5mC.m^{-2}

Contrary to the case where no stabilization was present, a barrier of potential free energy is present, which will slow down the aggregation of the particles, depending on its height. Its height increases with a decreasing ionic strength, therefore the addition of salts can be used to precipitate a colloid. It is interesting to note as well, that for an ionic strength of 30 mM in our example, a secondary smaller potential well appears, at a greater distance than the potential barrier. Since this well is not so deep, this is considered a metastable aggregation that can be easily reversed with relatively low input of dispersion energy. This can also produce some interesting structures with opalescent optical properties upon aggregation. Finally, for an ionic strength of 35 mM, no barrier is visible, meaning the effect of the double electrostatic layer is not strong enough to fight the attractive VdW forces.

1.3 Surfactants

By using molecules with a certain affinity to the material surface, it is possible to hinder the growth and aggregation of the particles. By reducing the growth rate, the nucleation and uniform growth are favored. It usually results in smaller particles and more homogeneous size distribution. Such molecules are designated as surfactant and can have different affinities with different crystal planes. This can result in anisotropic growth and the possibility to obtain different shapes. There are two ways how to see this effect: by hindering the growth of certain planes, or by reducing their surface energy and surface tension, allowing them to increase their surface more than the other planes. The result for both explanations is the same, the crystal will grow more slowly perpendicularly to this plane, and the particle will be more stable. Using those molecules can help reduce the size until a certain point. To be stable, a nuclei must have a minimum radius, or the surface tension will be too big and cause the nuclei to dissolve. Those molecules can reduce this radius to a certain point, but for too high concentration, the molecules might start to form a second phase and increase the particle size.

Several kinds of surfactants exist: anionic, cationic, non-ionic, and amphoteric. Surfactants are usually amphiphilic molecules with two sides. They are usually terminated on one side by alcohols, carboxylic acids, thiols, sulfates, sulfonates, phosphate groups. These groups can be adsorbed on the surface of nanoparticles, while the tail will point toward the solvent, or pack closely to form a shell around the particle. The tail is usually a chain of hydrocarbons, saturated or unsaturated. It can also be a polymeric chain, from polyethylene glycol for example.

The surfactants can be used during the synthesis to improve the quality of the particles, but also to improve their stability in a suspension, or their compatibility with the structure, they will be incorporated in. Once synthesized, there is a possibility for the particles to pack together and create either physical bonding, or even to merge via thermal sintering, dissolution/ precipitation, or atom mobility in the crystal. In the first case, the agglomeration of particle is not so critical, and the particle can be separated and dispersed in a new media by mixing, ultrasonic treatment, swelling… However, the redispersion procedure might damage the particles, especially the ones with a high aspect ratio. In the second case, aggregates need to be broken by the use of strong treatment which will for sure damage the primary particles. Moreover, this treatment might not be complete and results in big heterogeneities. It is therefore preferable in most cases to keep the particles in a suspension and prevent them from getting too close to each other.

Surfactant can help in this matter by inducing repulsive forces between particles. Those forces can be electrostatic or steric. For electrostatic repulsion, it is necessary to have ionic molecules, preferably with no tail or short, otherwise the charge would be hindered. Sometimes, electrostatic charges are already on the material surface, for example after oxidation of the surface. Metal oxides usually have OH groups on their surface, which can be dehydroxylated at higher potential hydrogen (pH). Electrostatic stabilization is quite efficient, and can be quantified as the zeta potential. However, such suspension can be easily disrupted in the presence of additional ions, which are present in the case of wet precipitation from salts.

Steric stabilization should not be affected by the presence of ions but requires the use of long chains, possibly of polymeric nature. At low concentration, and if the surfactant chain is well soluble in the solvent, there is a possibility for the chains to interpenetrate each other, and if the solvent is evaporated, it will lead to the creating of a polymeric composite. On the contrary, if the polymeric chains are not well soluble in the solvent, they will tend to pack closely around the particle, limiting the possibility to interpenetrate with chains from another particle.

In the case of nano-composites, the particles material might have a bad affinity with the matrix material, resulting in a bad synergy. A good surfactant can create an interface between the particle and the polymer, and improve their compatibility. Indeed, in case of a bad compatibility, the chains of polymer will be packed more loosely around the particles. The mobility of the chains will then be increased around the particles, and the particles are

acting as a plasticizer for the polymer. In the case of a good compatibility, the chains might be packed more densely, or their mobility reduced around the surface of the particle. This results in high modulus of the polymer, and sometime an increase of the glass transition temperature. This was reported for example in the case of reinforcement of rubbers by clay.

1.4 Interaction with polymeric matrix

Nanoparticles can reinforce or plasticize a polymer, depending on the interaction between the surface of the filler and the polymer. In some cases, an increase or decrease of the glass transition temperature (Tg) is observed. This shift can be from a few Celsius degrees to a dozen. In the case of amorphous thermoplastics, it can be explained by the good wetting of the polymer on the filler surface. The mobility of the chains is reduced near to the surface of the filler due to the higher density of chains, or the attractive forces with the surface. In the case of thermosets, the introduction of the filler can change the crosslinking density, parameter tightly correlated with the Tg. A lot of research was done concerning the reinforcement of rubber by clay particles. Clay is an inexpensive material that has a layered structure. Only one dimension is on a nanoscale: the thickness. Clay exhibited another nano-reinforcement effect, by changing the properties of the surrounding polymeric matrix. It was shown that a thin layer of polymer directly in contact with the clay surface had a higher young modulus. This is due to the higher density of polymeric chains near the clay surface, and the interactions between the filler and the polymer chains. The chains near the surface of the filler are then losing their mobility, increasing the Young's Modulus. In some cases this effect even led to the observation of a different glass transition. Similarly to clay, recent interest has been given to layered double hydroxides: it consists of a family of metal hydroxides, with two metal ions with a different valence. They are referred as anionic clays, because the layers are positively charged, and anions are intercalated instead of cations in the case of clay.

1.5 Dispersion

One of the major challenges in nanocomposites is the dispersion of the nano-filler in the matrix. Often, the nanoparticles tend to agglomerate together, forming big chunks of several μm. Having a bad dispersion of the nanoparticles in the polymer is often a sign of a bad compatibility between the polymer and the filler surface. Moreover, having big agglomerates kills the purpose of the nano-composite. Several methods can be used to obtain a good dispersion:

- Ultrasounds can break the weak forces between the agglomerated particles in a liquid media.
- Soaking the particles in a solvent can lead to swelling the agglomerate, by diffusing solvent molecules in the space between the particles
- Mixing the particles with the polymer, inducing shear forces. Those shear forces can break the agglomerate, but if too high, they can as well damage primary particles, especially with a high aspect ratio.

This problem is particularly relevant in the case of layered particles, such as clays or double layered hydroxides. In its dry state, clay is composed of several hundred or thousands of layers tightly stacked together. Several mechanisms are possible to explain the separation of the layers. They can be soaked in a solvent, typically water. The molecules of water will diffuse between the sheets, entering from the edges. As more water is inserted between the layers, they will start to separate from each other, until they are completely dispersed in the water. This procedure can be assisted by ultrasounds, accelerating the separation of the layers. Instead of a solvent, the particles can also be soaked directly in the monomer, if it is liquid at the working conditions. Finally, if the monomer is too viscous, or when working with a polymer, it is possible to use mechanical mixing inducing high shear stress in the mixture. It is believed that the shear stress will peel the layers one by one. This is typically achieved via extrusion melting process, or three roll mill.

The quality of the dispersion can be assessed in different ways. For suspensions in liquids, it is possible to control the particle size distribution before and after dispersion. The particle size should decrease as the agglomerates are destroyed. It is also possible to check it via a rheology study. It depends if the nanofiller is acting as a plasticizer or is reinforcing the polymer. In both cases, when better dispersed, the viscosity will be shifted greatly compared to the one before dispersion. It is also possible to measure the dispersion on the final composite. Different imaging technics can be used to observe the homogeneity, orientation and structure of the final composite. Scanning electron microscopy (SEM) and transmission electron microscopy (TEM) can be used to observe the topography of the composite, Atomic force microscopy (AFM) can provide further information by mapping the mechanical properties of the composite. Wide angle X-ray scanning (WAXS) can provide information about the degree of separation of layered nanoparticles. If the layers are still stacked, it is

possible to measure the distance between them. A higher degree of dispersion should show increase the space between the layers, until they are totally separated.

1.6 Composites and nanocomposites

Composite and nanocomposite materials regroup a very large number of possible materials. In this section, only a part will be covered, discussing about composites based on a polymeric matrix. Before going further in the discussion, it is important to keep in mind that using nanoparticles is not the only way how to create nano-composites and nanostructures. There exist other in-situ ways using immiscible block copolymers, self-assembled molecules, diffusion/segregation of atoms in solids, and more…

Polymer based composites are usually composed of a homogeneous continuous polymeric matrix, filled with inorganic particles. The matrix should define the basic properties of the material: flexibility, weight, processability, price, and other properties. The particles are added to improve certain properties of the matrix: mechanical resistance, thermal behavior, electrical conductivity, water imperviousness, color, light reflection or absorption, resistance to ageing, and other special properties… A non-exhaustive list of used nano-fillers comprises: exfoliated clay, carbon nanotubes, fullerenes, graphene, metal-oxides and other inorganic solids.

In order to obtain a good composite, the matrix and the filler should act in symbiosis. This is particularly true in the case of mechanical reinforcement: for anisotropic materials, fibers of a stronger material are introduced and aligned in the matrix. However, if the two materials are not compatible, the fibers will slide against the polymer, and offer no mechanical reinforcement to the polymeric matrix, even weaken it.

In some cases of nanocomposite, an increase or decrease of the *Tg* is also observed. This shift can be from a few Celsius degrees to a dozen, and is absent or very little observed with traditional composites. This effect shows how nanostructures can influence the surrounding polymeric matrix. In the case of amorphous thermoplastics, it can be explained by the good wetting of the polymer on the filler surface. The mobility of the chains is reduced near to the surface of the filler due to the higher density of chains, or the attractive forces with the surface. In the case of thermosets, the introduction of the filler can additionally change the crosslinking density, parameter tightly correlated with the *Tg*. A lot of research was done concerning the reinforcement of rubber by clay particles. Clay is an inexpensive material that

has a layered structure. Only one dimension is on a nanoscale: the thickness. It was shown that a thin layer of polymer directly in contact with the clay surface had a higher young modulus. Similarly to clay, recent interest has been given to layered double hydroxides, because of their similar layered structure and ion exchange properties. They are referred as anionic clays, because the layers are positively charged, and anions are intercalated instead of cations in the case of clay.

However, adding a filler in a polymer is not the only way to create polymer nanocomposites. It is possible to create nanostructures using two immiscible polymers, or block copolymers that contains two immiscible kinds of units. In the case of block copolymers the mobility of the chains will limit the phase separation, creating rather small domains at a nanoscale. For immiscible polymer, the manufacturing process will allow to create nanophases, or layers.

There is a last possibility, which makes the bridge between using a blend of polymers and filler. A precursor of inorganic filler can be grapthed on the polymeric chain, leading to phase separation, followed by reaction of the precursor into its final state. If this step is followed by a pyrolysis, it will result in nano-particles usually covered by a carbon layer, or carbon based nano-particles.

1.7 Synthesis methods for nanoparticles in general

Synthesis methods of nanoparticles are mostly bottom-up technics, except for high energy milling. The advantage of bottom-up methods is the extended possibilities to control the shape of the nanostructures, whereas top-down technics yield rather spherical isotropic structures. Nanoparticles can be synthesized either in gas or liquid phase, or both for instance in the vapor-liquid-solid growth of silicon nanowires [4,6].

Some nanoparticles are already present in nature and can be extracted and purified [8,10]. Among them, clays, graphite, and other hydrotalcites naturally have a layered structure, where almost individual sheets can be exfoliated under the right conditions. They can be further modified to stabilize the individual sheets and prevent them from aggregating again. Such treatments include for instance the exchange of cations in clays to weaken the bonding strength between the layers, or the partial oxidation of graphene. Living organisms are known to create numerous nanostructures with a very high selectivity (Figure 3). A few examples are highly adhesive fingers of gecko, or insects, allowing them to walk on ceilings, without losing the adhesion power over time [12]. The lotus leave presents incredible hydrophobicity, which is due to its surface chemical composition but also some nano-features, trapping air on the leaf surface [14].

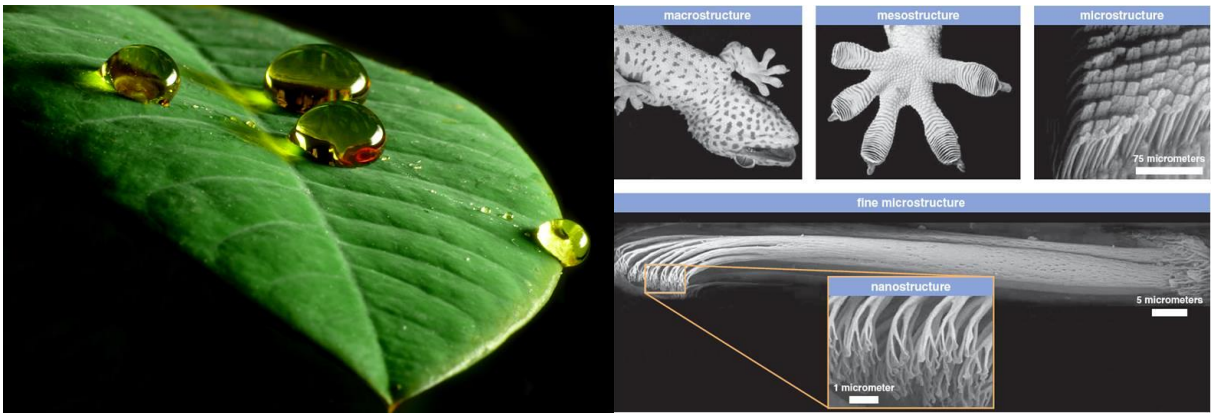

Figure 3: Two examples of naturally occuring nanostructures

To synthesize nanoparticles in gas or air phase, several methods are available: evaporation of aerosol of material or precursor. It is then transported generally to a target substrate, and is then deposited via decomposition, reaction or condensation to yield the final material. Among the methods available are : chemical vapor deposition [16], spray pyrolysis [4,5], laser ablation [6,7], plasma assisted methods, electrospinning. Those methods usually require higher temperatures, controlled atmosphere, and are namely suitable for the growth of nanoparticles and nanostructures with a specific crystalline orientation on a substrate. This is particularly interesting for electronics, photonics, energy harvesting from light and external forces via piezzoelectric effect [8]. Electrospinning however stands out from the other methods since it requires no higher temperature or a closed controlled atmosphere. It is more suitable for the synthesis of polymeric nanofibers, fabrics and mats [9,10].

In solution, the methods are usually called sol-gel methods, since they originate from a solution and yield a gel or colloidal suspension. For the production of metal oxides, a metal precursor is hydrolyzed or hydroxylated by the use of temperature or a base. The precipitation method can be assisted by ultrasonic treatment, the use of high temperature, high pressure, and various additives to influence the growth/nucleation rate ratio. Ultrasounds can help to reduce the final size of the nanoparticles and reduce aggregation, but might lead to fracture of the particle, resulting in lower aspect ratio of the particles. Synthesis in an autoclave allows reaching high temperatures and pressure, which improves greatly the size distribution. Ultrasounds can promote the nucleation of solids by creating local extreme conditions of temperature and pressure. It also keeps the reaction media well agitated, limiting the chance for aggregation. Both those technics play on the increased creation and stabilization of nuclei, critical point in the condensation of solid matter. The solvent can be water, alcohols, polyols, or reverse micro-emulsions. The use of polyols recently showed good results for a wide range of metal oxides. Using micro-emulsions limit the size of the particles to the cell size: each water micelle is acting as an independent micro-reactor (Figure 4).

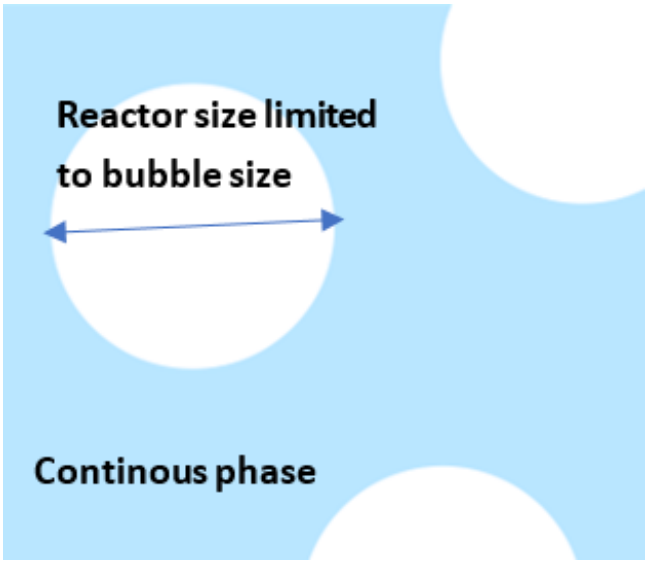

Figure 4: Confinement of the reaction in a microemulsion

Still from solutions, electrospinning is a popular method to produce polymeric nanofibers. In this process, a solution of polymer is passed through a needle charged with a given voltage. The polymeric solution is then ejected towards a target having a electrical potential different from the needle. A fiber is formed during the flight to the target, as the solvent evaporates. The applied voltage, concentration of the solution and other parameters influence the fibers diameter. With this technic, it is possible to create mats, or oriented layers of fibers. It is also possible to dope the fibers with some nanoparticles such as titanium dioxide and silver, for antibacterial purposes (Figure 5).

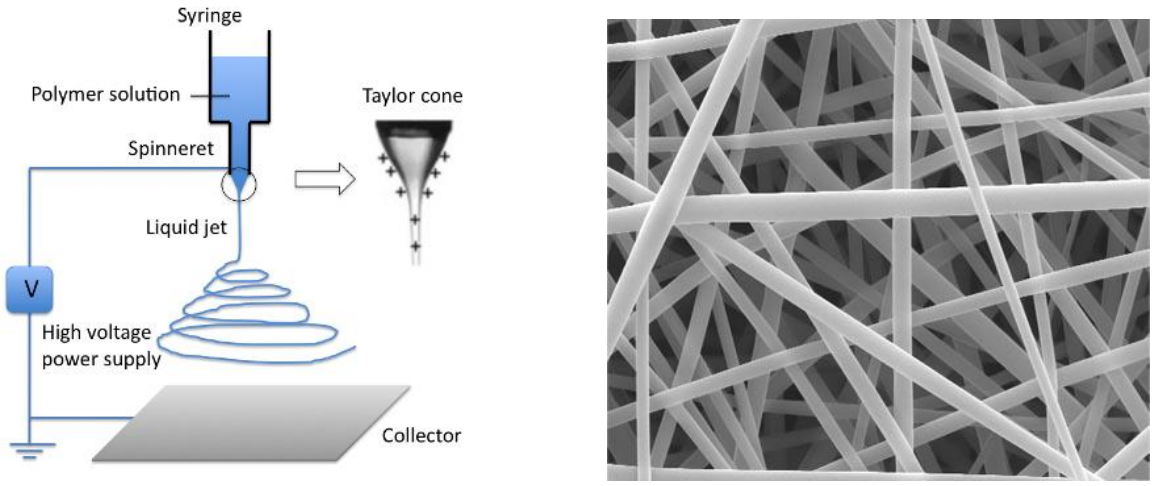

Figure 5: Electrospinning setup, and example of obtained morphology

The synthesis of nanoparticles can also be templated. Methods such as dip-pen AFM (Figure 6), e-beam lithography, nano-identation, and self-arranged alumina tubes can be used to influence the nucleation and growth of nanoparticles. A pattern can be created using seeds

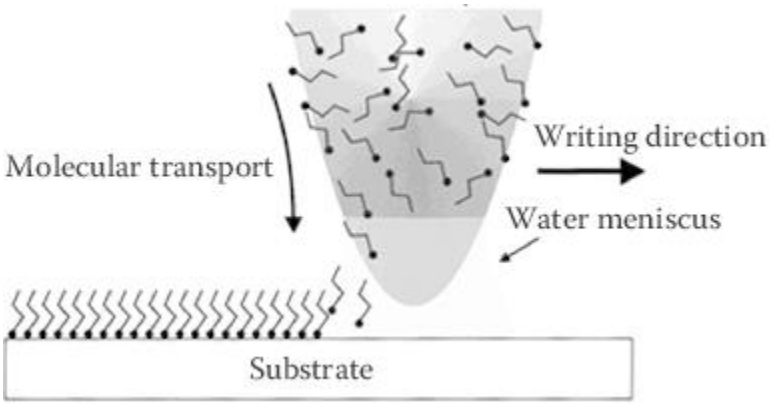

Figure 6: Principle of dip-pen AFM lithography

on the surface of a substrate, or deposition of specific molecules with an affinity towards the nanomaterial or its precursors. Particularly the dip-pen and e-beam lithography are interesting when the self arrangement of nanoparticles is limited, or when non-regular complex structures must be achieved, namely for electronics.

Challenges in the synthesis of nanoparticles are the control of the size, the size distribution, the purification and separation of nanoparticles. For synthesis in solution/suspensions, the small size of nanoparticles makes them difficult to separate from the solvent either by filtration or sedimentation. Standard filters can only keep big particles, and filters with micropores can be quickly clogged by particles about the size of their pores. Membranes can be used and are efficient mostly for solvent exchange, but to clean ionic species it is necessary to use ion exchange membranes. Even though metal and metal oxides have usually a higher density than the solvent, nanoparticles are subjected to Brownian movement and usually form stable suspensions. Centrifugation of the suspension can eventually help to sediment the particles, but is time consuming.

To control the size of the particles, their shape and size distribution, it is important to understand which mechanisms contribute to the formation of solids. In the case of amorphous materials, the growth is isotropic, and without templating, they will most likely form spherical particles. Crystals however have different surface energies depending on the exposed crystal plane. Some planes will be more stable than others and the crystal should grow perpendicularly to the planes with higher surface energy to prevent them from increasing their exposed surface. This is one of the reasons why crystals do not form spheres, supposed to be the most stable shape. Another example of anisotropy is dendritic growth, driven by some diffusion phenomenon. In the case of solidification from liquid, the heat released needs to be evacuated. The larger the surface, the faster the solid and its surrounding liquid are cooled and can further condensate. In the case of condensation of a material in a solvent or gas, it is the diffusion of the material to the solid surface which will favor the growth of dendrites sticking out of the bulk.

1.8 Synthesis methods for ZnO and nano ZnO production

The processes for ZnO synthesis can be classified in the following categories:

- precipitation from reactives in vapor phase, including: pyrometallurgical, chemical vapor deposition (CVD), pyrolysis spray, vapor-liquid-solid (VLS) growth

- reaction from dry form, namely mechanochemical process
- electrodeposition from solutions
- other wet precipitations without any oxido-reduction reaction, including: zinc salt precipitation, sol-gel method, solvothermal and hydrothermal, emulsion reaction confinement.

The pyrometallurgical process uses zinc in its metallic form, and oxidizes it under high temperatures. There are two main processes: French, and American. The first pyrometallurgical industrial process for ZnO production is the so-called French process, and was developed in 1840 by LeClaire. In this process, the starting metallic zinc is evaporated and carried in a flow of hot air. The vapors of zinc react with oxygen, precipitate in the flow of air, then are cooled and gathered in a bag. This process generally yields agglomerated particles of ZnO ranging from 0.1 to a few micrometers. The American direct process was developed later, and uses zinc ores and other zinc compounds in non-metallic form as a raw material source. The compounds are first heated and reduced by a burning bed of coke (carbon) to yield zinc vapor. It is then oxidized by oxygen in a flow of hot air, just like in the French process. The advantage of this process is the elimination of the purification step of zinc ore. On the other hand, the product of this reaction is a lower quality due to the presence of impurities from other compounds in the ore, and other metals.

Chemical Vapor Deposition is another method using precipitation from a vapor phase. Precursor of zinc is evaporated and carried by a flow of carrier gas in the deposition chamber, where it is deposited on a heated substrate. By-products of the deposition are usually volatile and evacuated with the flow of carrier gas. Many variants of the CVD technic exists, for instance in the presence of a plasma, or using an aerosol of the zinc precursor that is not volatile. The main advantage of the CVD is the possible to grow ZnO with a specific crystal orientation, referred as epitaxial growth [11,12].

Similarly to CVD, the vapour-liquid-solid method also uses the precipitation from a vapour phase. In this method, the zinc compound is first precipitated in a liquid phase. The liquid phase is composed of a melting or solvent agent, which can solute zinc to a certain concentration, forming an alloy. Common melting agents are composed of noble (Au and Ag) [5] or transition metals (Ni, Fe and Mo). As the liquid phase becomes saturated with zinc, zinc starts to crystallize under a pure solid form outside of the liquid phase. The whole system vapour-liquid is under equilibrium, and the solid is growing from the liquid phase. The liquid

phase is usually in the form of droplets, and the solid phase grows in the shape of rods, or towers, have the liquid droplet on the top of it [13,14]. The wire diameter depends strongly on the size of the alloy droplet. In many cases, gold was identified to be the ideal growth catalyst, as it promotes the formation of ZnO nanorods with 50–100 nm diameter and up to 10 μm length [15,16].

There are also some wet techniques which uses zinc salts as a precursor of ZnO. The zinc ions, usually in an oxidation state of +2, are precipitated with hydroxide, nitrate or carbonate anions to form an intermediate product. The intermediate precipitate is further calcinated at temperatures up to 800°C to decompose the unstable precursor into pure zinc oxide. Conversively, it is possible to prepare directly ZnO in a suspension form, without the need to calcinate the product, by carefully controlling the precipitation conditions and rendering the zinc precursor thermodynamically unstable. This allows to use lower temperature and avoid sintering during the calcination [17,18].

Another wet method is the hydrothermal precipitation of ZnO under high pressure. The method and reagent used are similar as for the classic wet precipitation, but the change of temperature and pressure modifies the kinetics, thermodynamic equilibriums and results in different morphologies, namely nanostructures. The temperature reached in this methods are typically up to 150-300^{o}C [19–21].

Finally electrodeposition can be used to deposit thin films of orientated crystalline ZnO [22–24].

There are generally two approaches to synthesize small structures: bottom-up, where discrete components are assembled in a bigger structure, or top-down where a structure is carved out of a bigger one, usually from a bulk material. The latter is less preferable for many reasons, but has a few advantages. The most common top-down methods are milling, and ion beam etching [25]. Milling is quite efficient and easy implemented for higher grain size, but becomes problematic when the target grain size is nanometric. This is because of the high energy involved in increasing the specific surface of the sample, and the necessity to have a smaller grinding gap, and the use of a solvent or wetting agent [26,27].

Wet precipitation or sol-gel method consists of a precipitation of zinc salt in solution. The size and distribution of nano-ZnO can be tuned by controlling the growth-nucleation rate. There are two strategies: being in a slow growth condition while using a seed material or

favoring the nucleation; or being in an equilibrium state between precipitation and dissolution. For that purpose, several means are known and researched: the use of temperature, pressure, surfactants… Some surfactants have different affinities with crystal planes of ZnO. In case of strong differences, the crystal might grow preferentially in some directions.

The wet precipitation of ZnO can also be assisted by ultrasonic treatment. It is particularly useful to reduce the crystallite size and their size distribution. Moreover, the ultrasounds created some micro-voids in the reaction media, via a mechanism named cavitation. This creates some local set of physical properties with extremely high pressure and or temperature, leading to different nucleation kinetics. However, the ultrasonic can damage structure with a high aspect ratio, such as sheets, rods, or needles [28,29].

1.9 Theory about ZnO formation from aqueous precipitation

There are several theories concerning the formation of ZnO from precipitation of Zn salts in aqueous media. There are different approaches, ranging from thermodynamic equilibrium of species in solution/suspension, to molecular dynamics and computional chemistry. It is admitted that several species might be formed as intermediates, such as zinc hydroxide, but also zinc hydroxide salts, depending on the composition of the reactive mixture. No oxido-reduction reaction is involved, since zinc stays in the same oxidation state as Zn^{2+}. Some research theorized that ZnO is crystalized from tetra coordinated Zn^{2+} with OH^-. The zinc hydroxide nuclei further dehydrate to leave the ZnO structure. It is therefore theorized that ZnO is not formed in one step, but that zinc hydroxide might be an intermediate. Zinc hydroxide is mostly amorphous and can be easily dissolved either with the addition of a base or acid in the solution. The kinetic of the dehydration of zinc hydroxide into ZnO is however still unclear.

1.10 About layered hydroxide salts and double hydroxide salts

Layered hydroxide salts (LHS) and layered double salts (LDH) also called anionic clays, have a layered structure derived from $Mg(OH)_2$, where OH^- are partially replaced by another anion. LDH and LHS can be used for many applications : catalysts [30–32], water polluant removal [33], separation of isomers [34–36], drug carriers [37–39], nanofillers [40,41], UV protection [42], mixed metal oxides precursors [43,44], flame retardants [45,46]...

LDH have the general formula $[M^{2+}_{1-x}\ M^{3+}_{x}\ (OH)_2]^{x+}\ A^{m-}_{x/m}\ .nH_2O$, where M^{2+} and M^{3+} represent two independent metal cations that can be identical or different. However, they

usually have comparable radius so that the trivalent cation can replace the bivalent without destabilizing the whole structure. Examples of divalent metal cations include Mg, Ni, Zn, Fe, Co, Mn, Cu, Li and trivalent metal cations Al, Fe, Cr (Table 1). A^{m-} represents an anion that can have different charges, usually NO_3^-, CO_3^{2-}, Cl^-, F^- or organic molecules bearing one of those anions or COO^-, SO_4^-, SO_3^-. LDH are compared to clays because of their similar structure, the possibility to exfoliate individual sheets, and the anion exchange ability. Several papers describe the intercalation of organic molecules in various LDH. For instance, a lot of attention was given to the LDH with formula $Mg_6Al_2(OH)_8CO_3.4H_2O$, also known as hydrotalcite. It was first believed to be formed of alternating layers of Mg and Al hydroxides, until it was proven to be composed of homogeneous layers containing both Mg^{2+} and Al^{3+} [47,48].

Table 1: Radius of metal cations used for LDH synthesis

M^{2+}	***Mg***	***Cu***	***Ni***	***Co***	***Zn***	***Fe***	***Mn***
Radius [nm]	0.65	0.69	0.72	0.74	0.74	0.76	0.80
M^{3+}	***Al***	***Fe***	***Cr***				
Radius [nm]	0.50	0.64	0.69				

However, less publication about LHS are found, especially concerning their functionalization and intercalation process. LHS have the general formula $M^{2+}(OH)^{2-}_{x}\ A^{m-}_{x/m}\ .nH_2O$, and unlike LDH, they contain only one type of metallic cation. The studied LHS, however, showed good anionic exchange capacity, exfoliation and intercalation of different molecules [49]. Among LHS, simonkolleite and other layered zinc hydroxide salts have been studied because of their interesting catalyst support [32], drug carrier [39], UV and visible light absorption [42], and corrosion inhibition properties [50].

Among LHS, simonkolleite (SK) has the formula $Zn_5(OH)_8Cl_2.H_2O$ [51] and was first reported in 1985 by Schmetzer et al. [52]. The two-dimensional layers of simonkolleite are formed of ZnO_6 octahedra interconnected with ZnO_3Cl tetrahedra, which is shown in Figure 7 (ab plane). Across the c axis, the layers are stacked into the 3d-structure. Additionally to the properties described previously, simonkolleite has raised a lot of interest for numerous applications, such as the preparation of photoluminescent aerogels [53], supercapacitors [54–56], polymeric filler, and gas sensors [57].

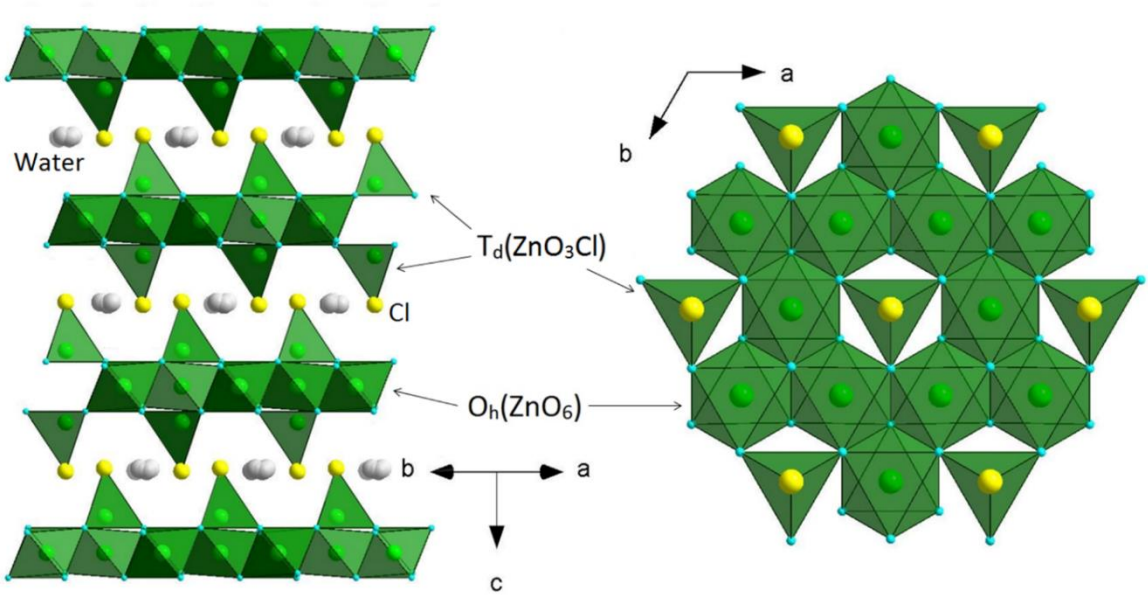

Figure 7: Arrangement of structural layers of simonkolleite across the axis c and two dimensional projection of the layers at plane ab.

1.11 Potential applications for simonkolleite

Simonkolleite has been less reported in the literature than ZnO, but showed nevertheless some promising properties for a few specific applications.

For instance, Khamlich et. al. prepared super capacitors based on Nickel-graphen foam. They deposited simonkolleite on the hybrid foam via microwave assisted hydrothermal precipitation. A higher capacity was observed than for the foam with only graphen or only simonkolleite [55].

Additionally, Sithole et. al. also explored the possibility the use simonkolleite as a H_2 sensor. The synthesis method was different, since they used different Zn salt and hexamethylenetetraamine as a surfactant and precipitating agent [57]. They measured the

change in electrical conductivity of the sample when exposed or not to H_2 in gaseous form. They observed a higher sensitivity and better response and recovery time for increased working temperatures.

Finally, Mohsin et. al. prepared a layered zinc hydroxide salt (LZH) using cinnamate as an anion [62]. The presented structure in their work is similar to the one of simonkolleite, as well as the platelets morphology. This led us to think that Cl^- could be replaced with larger molecules containing an anionic group, carboxylate in the case of cinnamate. They observe a good UV absorption of the hosted cinnamate molecule in the LZH platelets. This encapsulation method has several advantages: it can keep the water soluble molecule in a solid form and the host can protect the molecule against degradation.

Potential applications that were not reported to our knowledge in the literature further include: the mechanical reinforcement of polymers by sheets of nanoparticles; fire retardant properties due to the layered structure hindering the diffusion of oxygen in a material during combustion, and the release of water during the thermal decomposition of simonkolleite; depollution of water and soil by ion absorption of simonkolleite as a general layered zinc hydroxide; a precursor for zinc oxide preparation either by chemical or physical treatment.

1.12 Principles of measurements performed during this work

1.12.1 XRD of powder crystals

X-ray diffraction (XRD) of powders is a fast an efficient method to analyse mixture of crystalline phases. It relies on the facts that regular crystalline patterns will diffract electromagnetic waves constructively at given angles, as illustrated in Figure 8. The theory was developed mainly by Bragg and Laue, who gave their names to respectivley the

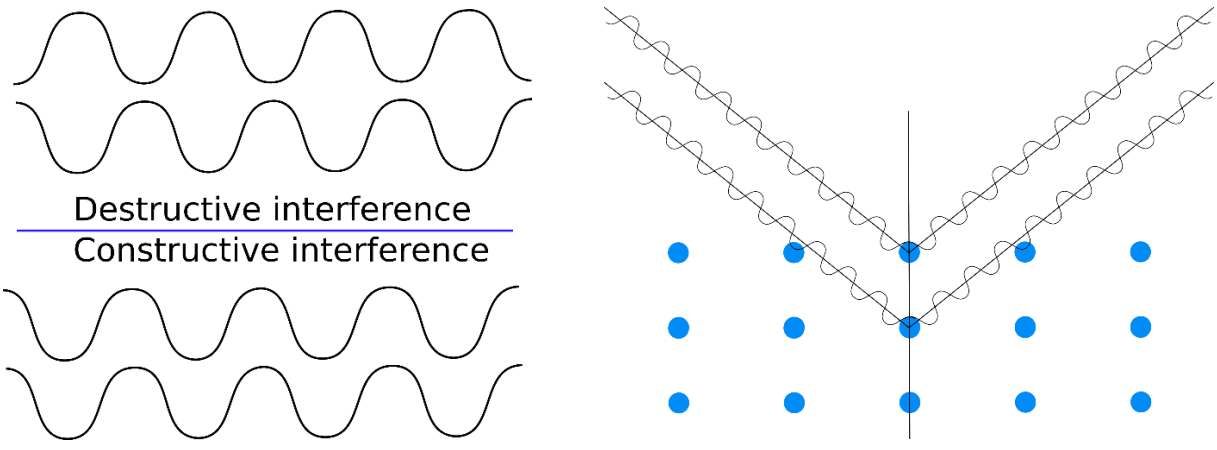

Figure 8: Representation of the physical phenomenon behind X-Ray diffraction of crystals

diffraction Bragg's law, and single crystal diffraction Laue patterns. An incoming coherent electromagnetic wave is diffracted in all direction by each atom. Depending on the exit angle of the electromagnetic wave and the distance between the atoms, there will be either constructive or destructive interference between the re-emitted electromagnetic waves. The relationship for constructive interference is given by the Bragg's law:

$$n.\lambda = 2.d.sin\theta \tag{7}$$

Where d is the distance between two atoms, λ the electromagnetic wavelength, and θ the incident angle.

Since the crystal structures are highly ordered, interferences will involve a large number of aligned atoms, under different angles. This results in well visible and resolved diffractions peaks. The wavelength of the electromagnetic wave is directly linked to the distance to be observed between the atoms in the crystal. This is why X-rays are used, as other types of electromagnetic waves will not be suitable for such magnitudes of length.

A same crystalline pattern will diffract the light at several angles, with intensities depends on the nature of the atoms (Figure 9). The analysis of a pattern can give us complete information on the crystalline structure and parameters. Furthermore, this technic can quantify the amount of a given phase in the sample. It can also analyse multi-phase samples, given that the diffraction peaks will be discriminated well enough. The advantage of this method is that

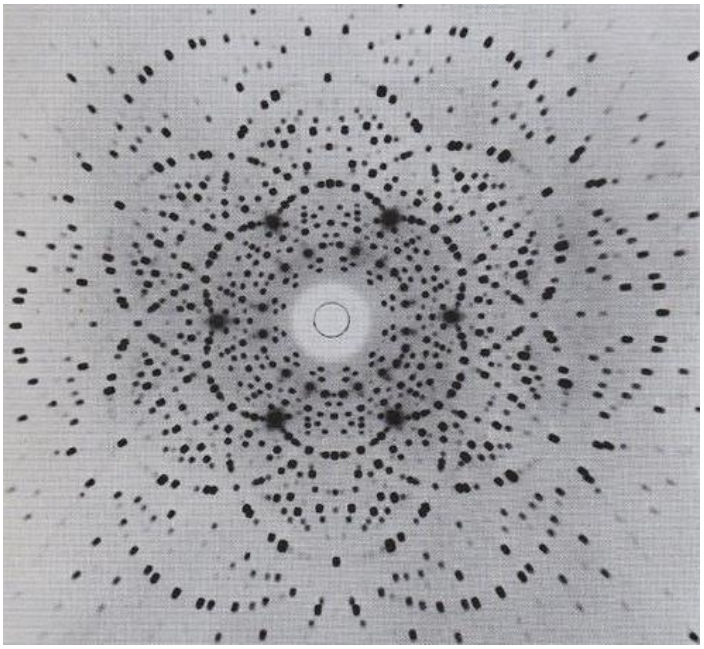

Figure 9: Diffraction pattern of a single beryl crystal

it gives more information than elemental composition, which is paramount in the case of a mixture of several phases, or when the crystalline structure of the compound is of interest. This is the case, for example, of TiO_2, where the photocatalytic activity will be different depending on the crystalline structure, while the chemical composition stays the same. The biggest disadvantage of this method is that it ignores totally amorphous phases, or irregular patterns. This can be problematic in case of phases with lots of defects, or low crystallinity.

1.12.2 Atomic absorption spectrometry

Atomic absorbtion spectrometry was used to analyse the absolute atomic content of Zn and Na in the synthesized samples. Atomic absorption spectrometry (AAS) measures the absorption of light at discreet wavelength of atoms in vapour phase. Each atom has very specific absorption-emission spectra, with very narrow bands of absorption. Practically, a lamp made of the element to be measured is emitting a spectrum that should be absorbed only by this element. The element to be measured can be in solution or even solid, and will be vaporized and reduce/oxidized to its ground oxidation state. The vaporization is usually realized either by a flame, or an electrically heated graphite tube. This method can detect traces in the range of few ppm, and is usually used for the detection of metals.

1.12.3 Particle size distribution measurement by the laser diffraction method

Particle size measurement by laser diffraction is an undirect method to measure a particle size distribution. It first measures the diffraction pattern of a laser beam by a dilluted suspension of the sample to be measured. The measured pattern is then fitted with a calculated theoretical diffraction pattern. The theoretical pattern is the addition of the individual patterns of monodispersed spherical particles, also calculated. The theoretical composite pattern is adjusted by iteration by changing the theoretical particle size distribution, until the theoretical and measured pattern match optimally.

The individual diffraction patterns of monodispersed particles are calculated beforehand and stored in the computer memory. Those patterns can be calculated via two different methods: Fraunhofer and Mie.

The Fraunhofer theory was used in the past for practical reasons since it requires less computing power than the Mie theory. It takes into account only the scattering due to the diffraction of light by edges. Two edges acts like secondary sources of light, and creates diffraction patterns via destructive and constructive interferences. It is accurate for large

particles as the scattering by diffraction is dominant, but is limited for particles smaller than 20-50 μm. The scattering pattern for a monodisperse particle can be expressed by the following equation:

$$I(\theta) \propto \left[\frac{J_1(\alpha.sin\theta)}{\alpha.sin\theta}\right]^2 \quad (8)$$

Where J_1 is a Bessel function, $\alpha = \pi D/\lambda$, D being the particle diameter, λ the light wavelength, and θ is the angle of diffraction, and $I(\theta)$ the diffracted intensity.

The Mie theory relies on the resolution of Maxwell schemes and is therefore more accurate since it solves a global problem, and takes all kinds of light interactions into account. The problem is written in polar coordinate to fit to the geometry and simplify the expression of the boundary conditions. The mathematics behind the resolution of this problem are quite complex, but the solution can be summurize as:

$$I(m,\alpha,\theta) \propto S_1(m,\alpha,\theta)^2 + S_2(m,\alpha,\theta)^2 \quad (9)$$

$$S_1(m,\alpha,\theta) = \sum_{n=1}^{\infty} \frac{2n+1}{n(n+1)} [a_n(m,\alpha).\pi_n(\theta) + b_n(m,\alpha).\tau_n(\theta)] \quad (10)$$

$$S_2(m,\alpha,\theta) = \sum_{n=1}^{\infty} \frac{2n+1}{n(n+1)} [a_n(m,\alpha).\tau_n(\theta) + b_n(m,\alpha).\pi_n(\theta)] \quad (11)$$

where $I(m,\alpha,\theta)$ is the scattered light intensity, θ is the scattering angle, $m = n_p/n_m$, n_p is the ratio of the refractive index of the particles and n_m is the refractive index of the dispersion media, $\alpha = \pi D/\lambda$, D being the particle diameter, λ the light wavelength. The functions a_n, b_n, π_n, and τ_n will not detailed here, as they have complex forms. The Mie solution takes more computing power since the functions a_n, b_n, π_n, and τ_n are calculated by an infinite sum of series. The numerical solution accuracy will depend on how many terms of each sum will be included in the calculation.

As a conclusion, Fraunhofer is a simplified version of the Mie theory, where both solutions can be only numerically approximated. In the case of big particles, for a given computing time, the Fraunhofer theory can give more accurate results than the Mie theory, so both theories should be considered for practical purposes. Moreover, Fraunhofer does not need to know the optical parameters of the particle being measured, which can be advantageous in the case of mixtures.

1.12.4 Differential scanning calorimetry

Differential scanning calorimetry (DSC) is a powerful method to analyse various thermal transitions. DSC can be used to measure the latent heat of chemical reaction, or phase transitions. Examples or their use are evaluating the melting point of substances, their purity, glass transition of polymers, curing kinetics of polymers, and degree of curing of polymers. Additionally, it was theorized by Schick and Merzlyakov [58] that it is possible to estimate the thermal conductivity of homogeneous materials using a special heating program, and special sample preparation, as well as proper calibration of the apparatus. This method has been used by several research groups, but is still very experimental, and will not be discussed in this thesis.

1.12.5 Atomic force microscopy

Atomic force microscopy is suitable for scanning nanostructures. It has a great vertical resolution, sub-nanometric, but a poorer horizontal resolution. The principle of the measurement is based on the interatomic interactions between a probing tip and the sample surface. The interatomic forces will start to be significant when the distance between the tip and the surface is in the order of a few nanometers. The tip is located on a metal strip and is oscillating up and down, driven by piezoelectric effect, and the displacement is measured via the deflection of a laser.

1.12.6 Scanning electron microscopy

Scanning electron microscopy (SEM) works in a complementary way to optical microscope: a ray of electrons is focused on the surface of the sample. Unlike optical microscope, the ray is then diffracted, absorbed and reemitted. Because of the diffraction, image cannot be obtained and this is why the apparatus is scanning the surface instead of taking an instant picture. The electrons are caught and separated depending on their flying speed, or kinetic energy. Based on their energy, there can be deduced whether they simply bounce back from the surface, or had some inelastic collision with atoms. In some models, it is possible to deduce the nature of the atom the electrons interacted with, and their concentration in function of the sample depth. SEM is suitable for inorganic materials, but not so much for organic materials, as they are insulating and can be degraded by the highly energetic electron stream. The problem with insulating materials is the accumulation of electrons on the sample surface and the increasing repulsion of incoming electrons overtime. Practically, the observer will receive brighter and brighter scans after few seconds.

1.12.7 Dynamic mechanical analysis

Dynamic mechanical analysis (DMA) is a method for measuring mechanical behavior of materials under a sinusoidal or generally periodic stress. This technique is particularly useful to measure viscoelastic behavior since it can measure both a modulus and a phase or damping term. The modulus is measured from the intensity of periodic strain measured, and the phase is measured from the delay between the applied stress and the measured strain. It is particularly interesting to measure the material response at different temperature, and different rates or oscillation frequency (usually ranging between less than 1Hz and several MHz). The response of the material tested at different oscillation frequency and temperature is very sensitive to the chemical and physical structure of the polymer. In particular, DMA is one of the most sensitive method to detect the glass transition and secondary transitions of polymers, as well as their crystalline structure.

2. Experimental part

2.1 Chemicals

The chemicals used were $ZnCl_2$ dried at 105°C, NaOH, and n-butanol all purchased from PENTA, Czech Republic.

The diglycidylether bisphenol A was purchased from Spolchemie under the trade name CHSE530, and the diamino polyether was purchased from Huntsman under the trade name Jeffamine D400. Both reactive were used without any further purification.

2.2 Instruments and devices

In this section, will be presented a few methods that were used to measure and characterize some products. Thoses methods were used to characterize both the chemical and physical aspects of the produced samples.

2.2.1 XRD of powder crystals

Practically, the synthesized samples were evaluated by XRD) analysis of polycrystalline powders using a diffractometer D8 Advance, monochromatic CuKα radiation and a scintillation detector, Bruker, GB (step scanning over 2θ range from 10 to 80^o with a step size of 0.02^o and 3s counting time at each step) and a diffractometer Rigaku Miniflex 600 (continuous scanning over 2θ range from 10 to 80^o, scanning speed – 5-10 2θ degrees per min), at the Joint Laboratory of Solid State Chemistry, University of Pardubice. Reference intensity ratio (RIR) method with Rietveld refinement was used to determine the content of simonkolleite and ZnO in the final products. The crystallite size of the powders was calculated on basis of Scherrer and Halder-Wagner methods. For the calculation, only well resolved XRD peaks were used.

2.2.2 Atomic absorption spectrometry

Atomic absorption spectrometry was used to analyse the absolute atomic content of Zn and Na in the synthesized samples at the Department of Inorganic Technology, University of Pardubice. The apparatus used was a AA 936 from GBC, Australia, equipped with a flame atomizer, fed with a mix of acetylene and air. The samples were dissolved prior to measurement in a solution of nitric acid in water at 0.5ml/L. The concentration of each element was determined by comparison with a calibration curve.

2.2.3 Particle size distribution measurement by the laser diffraction method

The particle size distribution of the samples was analysed using a Mastersizer 2000 from Malvern, at the Department of Inorganic Technology, University of Pardubice. The samples were dispersed 3 min in water by means of ultrasound prior to measurements in order to break the aggregates into primary particles. In the case where the dried samples did not wet properly with water, a few drops of sodium silicate aqueous solution were added. The samples were measured and the results analysed using the Mie theory and using the optical parameters of ZnO to simulate the refraction of the lasers by the particles.

2.2.4 Thermogravimetric analysis

Thermogravimetry was used as a fast screening method to analyse the products, as well as to study their thermal degradation behavior (Figure 10). This is particularly important in order to check the thermal stability of the product, to determine in which conditions it can be further processed for further application. The measurements were made on a TGA Q500 from TA, at Toseda s.r.o., Pardubice. Typically, a dozen of milligrams of dried product are loaded in a titanium pan, and the weight loss of the sample is monitored depending on the temperature and time. Typical conditions for this analysis were a heating ramp from room

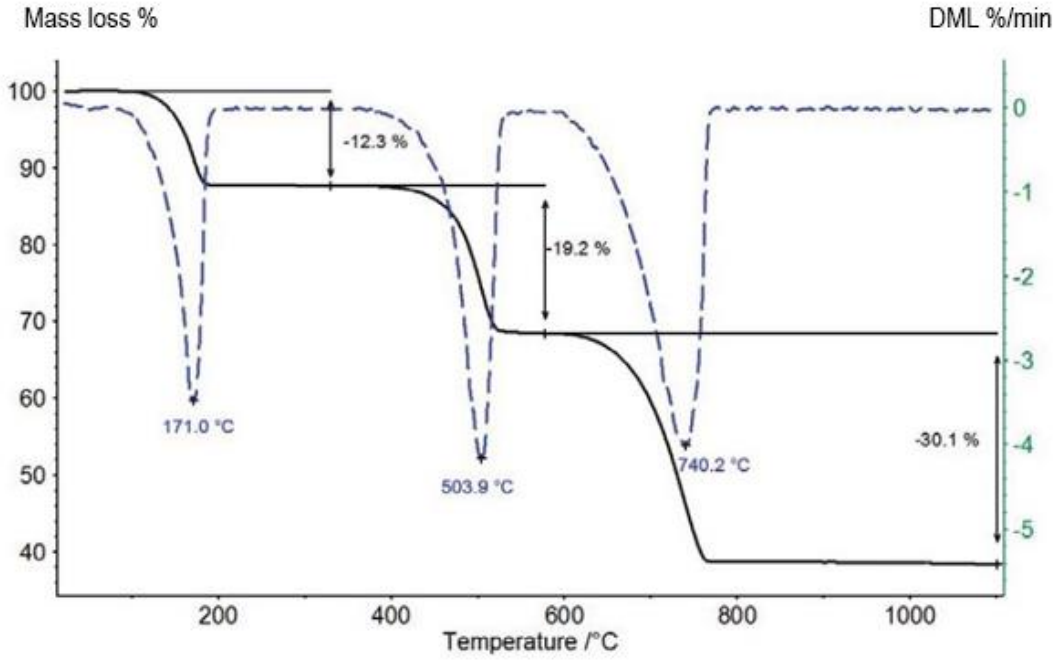

Figure 10: TGA of calcium oxalate in air

temperature to 600 or 1000 ^{o}C, with a constant heating rate of 10 ^{o}C/min, under a N_2 flow. Sometimes, an isotherm was added above 100 ^{o}C, to allow the product to be completely dry before proceeding further.

2.2.5 Atomic force microscopy

The AFM apparatus used was a Dimension icon from Brucker, at Toseda s.r.o., Pardubice. The scans were taken in tapping mode, with the PeakForce quantitative nano-mechanism mode activated, providing information on both the topography of the sample, the hardness of the material, and the attractive force between the tip and the measured sample.

2.2.6 Scanning electron microscopy

In our case, SEM scans were performed on the dried samples to analyse their morphology on a TM3030 plus electron microscope from Hitachi, at Toseda s.r.o., Pardubice. Dried powder was applied on the target without any grinding or other pre-treatment. The observation conditions were an acceleration voltage of 15 kV and the final image was the combination of both scattered and back-scattered electrons scans .

2.2.7 Dynamic mechanical analysis

Dynamic mechanical measurements were performed on a Discovery Hybrid Rheometer HR3 apparatus from TA, at Toseda s.r.o., Pardubice. The samples were cut in rectangular strips of variable geometry and were measured under a oscillating torsion mode under a constant heating rate of 2 ^{o}C/min. The glass transition temperature was determined as the temperature where the tan δ reaches its maximum. The sample was under a constant linear tension of 10N and an oscillation rate of 1 Hz, with a torque amplitude of 400 μN.m.

2.2.8 BET specific surface measurement

Measurements of the specific surface area of dried powders were performed using surface area and pore size analyser NOVA 1200e, Quantachrome Instruments, USA, at the Department of Inorganic Technology, University of Pardubice. Surface area was calculated using Multipoint BET adsorption approach. Measurements were performed at -196.15 ^{o}C in 9mm manifold using N_2 and He as adsorptive and non-adsorptive gases respectively; the samples weight were between 2.4-3.6 g. Seven relative pressure points were measured in the range of 0.03-0.25 P/P_0 under the following equilibrium conditions: pressure tolerance 0.1 mmHg, equilibration time 90 sec, equilibration timeout 240 sec. At least four P/P_0 points were

used to build multi-point Brunauer–Emmett–Teller plot. Prior to the measurement, the samples were degassed using vacuum for 24 h at room temperature.

2.3 Procedures

2.3.1 Synthesis of simonkolleite and ZnO

2.3.1.1 Precipitation of $ZnCl_2$ in presence of H_2O_2

Typically, a solution of 3.6 g of dried $ZnCl_2$ into 200 ml of deionized water is prepared. The $ZnCl_2$ solution was then introduced in a glass reactor equipped with a mechanical stirrer and a pH-meter. In the meantime, a mixture of 10 ml of ammonia NH_3 into 10 ml of deionized water was prepared. Then the solution of ammonia was slowly added drop by drop in the reactor at room temperature under mechanical stirring, until the solution reached a pH of 7.5. Typically, this value of pH is reached after the addition of about 6 ml of NH_3 solution.

Immediately after the pH was stabilized, the precipitate was washed over nanofiltration filter with deionized water. The precipitate was washed with a total of 1 L, divided in 5 times. After washing the filtrate was tested with $AgNO_3$, then some water was added to obtain a 200 ml suspension as before starting the washing.

Finally, a reflux heating reaction setup was prepared, and the washed suspension was put inside. Then 67 ml of H_2O_2 was injected at once into the reactor. The reactor was then sealed and started to be heated until a reflux was observed (Figure 11). The reaction was

Figure 11: Bubbles formation during the reaction of $Zn(OH)_2$ with peroxide

carried out for 3 days under reflux, then the precipitate was washed again over nanofiltration filter with 1L of water, divided in five times. The final product was then dried overnight at ambient atmosphere, gently crushed into powder and bottled up.

2.3.1.2 Precipitation of $ZnCl_2$ in presence of NaOH or KOH

The second synthesis method was inspired from the previous work of Ullah et al. [60]. They present a simple precipitation method, followed by aging of the precipitate. The raw materials used were $ZnCl_2$ and NaOH. In a typical experiment, a solution of 0.5 mol/L of NaOH into distilled water was prepared and 50 ml was heated to 45°C at least 30 min under stirring to stabilize the reactor temperature. Then 30 ml of 0.6 mol/L $ZnCl_2$ solution into distilled water was injected in the reactor containing NaOH solution. A white precipitate appeared instantly from the first drop added. The reaction was carried out at 45°C for 2 hours under vigorous mechanical stirring and the reactor was sealed to avoid water evaporation.

At the end of the reaction, the precipitate was kept and washed with distilled water, by vacuum filtration over a paper filter. The quality of the washing process was assessed by testing the presence of Cl^- ions in the filtrate by $AgNO_3$. Once clean, the slurry was dried at ambient atmosphere overnight, then gently crushed into fine powder and bottled up.

2.3.2 Study of precipitation mechanism of simonkolleite/ZnO

In order to study the precipitation mechanism of simonkolleite/ZnO, a series of experiments were made with different synthesis parameters.

2.3.2.1 Addition of $ZnCl_2$

In a first serie, 200 ml of a solution of 0.5 mol/L of NaOH into distilled water was prepared, then heated at 55 ^oC under magnetic stirring. A second solution of 2.5 mol/L of $ZnCl_2$ into water was prepared, and was added drop by drop into the NaOH solution under stirring. The total amount of $ZnCl_2$ added varied from 20 to 400 ml. Once the addition of $ZnCl_2$ solution was completed, the mixture was kept under stirring at 55 ^oC for 90 min, after what the samples were filtrated, washed several times with deionized water, dried at room temperature and bottled up.

2.3.2.2 Influence of excess Cl^- ions

In a typical experiment 200 ml of a solution of 0.5 mol/L of NaOH in distilled water was prepared. Then 0.1 mol of NaCl was introduced in the NaOH solution and the resulting

solution was heated at 55ºC under magnetic stirring. At the same time, 20 ml of a second solution of 2.5 mol/L of $ZnCl_2$ in distilled water was prepared. Once the temperature of the NaOH and NaCl was stabilized, the solution of $ZnCl_2$ was added drop by drop, still under magnetic stirring. Once the addition of $ZnCl_2$ solution was completed, the mixture was kept under stirring at 55 ºC for 90 min, after what the samples were filtrated, washed several times with distilled water, dried at room temperature and bottled up.

2.3.2.3 Addition of NaOH

In another series of experiments 200 ml of a 0.1 mol/L $ZnCl_2$ solution in distilled water was prepared. It was heated at 55 ºC under magnetic stirring. A solution of NaOH at 0.5 mol/L in distilled water was prepared and added drop by drop under stirring in the $ZnCl_2$ solution at 55 ºC. The amount of added NaOH varied from 26.7 to 80 ml. Once the addition of NaOH solution was completed, the mixture was kept under stirring at 55 ºC for 90 min, after what the samples were filtrated, washed several times with distilled water, dried at room temperature and bottled up.

2.3.2.4 Influence of maturation time

Additionally, in an extra experiment 200 ml of a solution of 0.5 mol/L of NaOH in distilled water was prepared and heated at 55 ºC under magnetic stirring. At the same time, 10 ml of 2.5 mol/L solution of $ZnCl_2$ in distilled water was prepared. Once the temperature of the NaOH and NaCl was stabilized, the solution of $ZnCl_2$ was added drop by drop, still under magnetic stirring. Once the addition of $ZnCl_2$ solution was completed, the sample was filtrated, washed several times with a solution of 0.5 mol/L of NaOH in distilled water, then with pure distilled water, dried at room temperature and bottled up.

Additionally, in an extra series of experiments 200 ml of a solution of 0.5 mol/L of NaOH in distilled water was prepared and heated at 55 ºC under magnetic stirring. At the same time, 40 ml of a solution of 2.5 mol/L of $ZnCl_2$ in distilled water was prepared. Once the temperature of the NaOH and NaCl was stabilized, the solution of $ZnCl_2$ was added drop by drop, still under magnetic stirring. Once the addition of $ZnCl_2$ solution was completed, the mixture was kept under stirring at 55 ºC for a period of time ranging from 0 to 90 min. Then the samples were filtrated, washed several times with a solution of 0.5 mol/L of NaOH in distilled water, then with pure distilled water, dried at room temperature and bottled up.

2.3.3 Study of Influence of n-butanol addition on simonkolleite dispersion

A first set of experiments was made by dispersing 0.5 g of dried samples of pure simonkolleite in 100 g of a mixture of water/n-butanol. The mass ratio between n-butanol and water varied from 0.2 to 0.01. The suspension was dispersed by ultrasonic treatment several times until the suspension was visibly uniform. Then the suspensions were let to rest minimally 24 h before observation.

In a second set of experiments, 7.77 g of KOH was dissolved in 100 ml of deionized water and a variable amount of n-butanol was added, ranging from 0 to 24 g. This solution was stirred and heated at 55 ^{o}C until the temperature stabilizes. A second solution of a variable amount of $ZnCl_2$ ranging from 6.74 to 18.87 g in 20 ml of deionized water was prepared, then injected at once into the reactor still under stirring. The reaction was allowed to maturate for 2 hours at 55 ^{o}C under stirring, then it was washed over a paper filter if the precipitate did not go through, or by sedimentation in a centrifuge in the opposite case. Washing by centrifugation can be tedious in the case of large volumes, but is necessary when the particles are too small to be filtered by paper. The suspensions were washed minimally 5 times with deionized water, then dried overnight at ambient air, gently crushed into powder and bottled up.

2.3.4 Synthesis of ZnO from thermal degradation of simonkolleite

ZnO was produced via calcination of pure simonkolleite at 600 ^{o}C in air, during 3h. The samples of simonkolleite were used in powder form without any further preparation, put in a crucible and laid in the oven. The powder layer had a few mm in thickness only, to allow a uniform contact with air to the whole sample.

2.3.4.1 Photocatalytic activity of the prepared ZnO

The photocatalytic activity of the calcinated simonkolleite was measured and compared against standard ZnO purchased from Aldrich and another sample of ZnO prepared via precipitation with a OH: Zn ratio of 2.2, with the addition of 5% of n-butanol in water. Methyl orange was used as an indicator of the degradation activity, measurement of the relative intensity of its absorption peak at 470 nm as an indication of its remaining concentration in the solution was carried out.

In each measurement, 0.5 g of dry powder sample was weighted and added to 0.5 L of a methylene orange solution at 20 mg/L concentration. The suspension was constantly

stirred by the means of magnetic agitation and circulated between a reservoir and the reactor with the UV lamp. The whole reaction was carried out at room temperature, and absorption spectra were measured from 400 to 700 nm with a 1 min interval.

2.3.5 Simonkolleite as anticorrosive agent

Simonkolleite was immersed in solutions of phosphates with different concentrations for different times. In a typical experiment, 500 mg of simonkolleite was immersed in 50 ml of solution, in order to have a suspension with 1 % of solid content.

In a first experiment, 500 mg of pure simonkolleite was immersed in 50 ml of a solution of H_3PO_4 with a concentration of 72 mmol/L. The whole mixture was kept in a sealed flask and gently agitated for a minute by hand. After 1 hour it was filtered and washed with distilled water, then dried overnight at room temperature, gently crushed into powder and bottled up.

In a second series of experiments, 500 mg of pure simonkolleite was immersed in 50 ml or 100 ml of a solution of $(NH_4)H_2PO_4$ with a concentration of 72 mmol/L. The whole mixture was kept in a sealed flask and gently agitated for a minute by hand, then dispersed in an ultrasonic bath for a period of 5 to 60 min. The suspension was further let to rest during 30 min to 3 weeks, after what it was filtered and washed with distilled water, then dried overnight at room temperature, gently crushed into powder and bottled up.

2.4 Preparation of composites

In a typical composite preparation, dried powder of simonkolleite was weighted and added to 50 g of Jeffamine D400. The weight of added simonkolleite varied between 1.31 to 14.36 g. The particles were soaked for at least 24 h at room temperature in the amine at rest, then dispersed three times by ultrasonic treatment by five minutes intervals. Then 25 g of the amine mixture with particles was mixed by hand with an amount of epoxy reactive varying between 30.79 to 38.62 g. The amount of epoxy was calculated in order to obtain an equimolar ratio between epoxy groups and amine hydrogens. The mixture was then outgassed under vacuum to remove bubbles, then casted in a metallic form and cured at 80 ^{o}C for 24h.

Additionally, a composite was prepared with amine functionalized simonkolleite. In a first step, 2.04 g of amine groups functionalized simonkolleite particles was dispersed in 15 g of Jeffamine D400 via ultrasonic treatment. The dispersion was carried on until the suspension was visibly uniform. Then 10 g of Jeffamine/Simonkolleite mix was mixed with

13.95 g of CHSE530. The mixture was then outgassed under vacuum to remove bubbles, then casted in a metallic form and cured at 80 ºC for 24 h.

Finally, a neat system was prepared by mixing 25 g of Jeffamine D400 with 37.74 g of CHS EPOXY 530. The mixture was homogenized by hand, outgassed under vacuum to remove bubbles, then casted in a metallic form and cured at 80 ºC for 24 h.

3. Results and discussion

Among all the possible methods for the synthesis of nano-ZnO and simonkollkeite, a simple wet precipitation was selected, as it requires no special equipment such as a CVD chamber, ultrasonic reactors, pressure reactors, microwave emitter, plasma chamber… Moreover, it was decided to work at low temperatures and avoid using solvents and therefore not to use templating microemulsions. Finally, it was attempted to avoid using surfactants, as they are difficult to wash away and might remain in the final product. Especially polymeric surfactants can interact strongly when the particles are introduced in a polymeric matrix.

3.1 Precipitation of $ZnCl_2$ in presence of H_2O_2

A first attempt to create ZnO was made following a procedure inspired from the literature [59]. This method consists of two step including the precipitation of $ZnCl_2$ with ammonia under controlled pH, followed by the reaction of the intermediate product with hydrogen peroxide.

According to the litterature, it was expected to obtain $Zn(OH)_2$ as a product of the controlled precipitation of $ZnCl_2$ with NH_3. In the second step, oxygen released from decomposing H_2O_2 is supposed to replace the OH^- coordinated groups in $Zn(OH)_2$ to form ZnO. However, XRD analysis revealed a major presence of ZnO_2, meaning that H_2O_2 most likely further oxidized Zn^{2+} into Zn^{4+} (Figure 12). Traces of what could be simonkolleite were

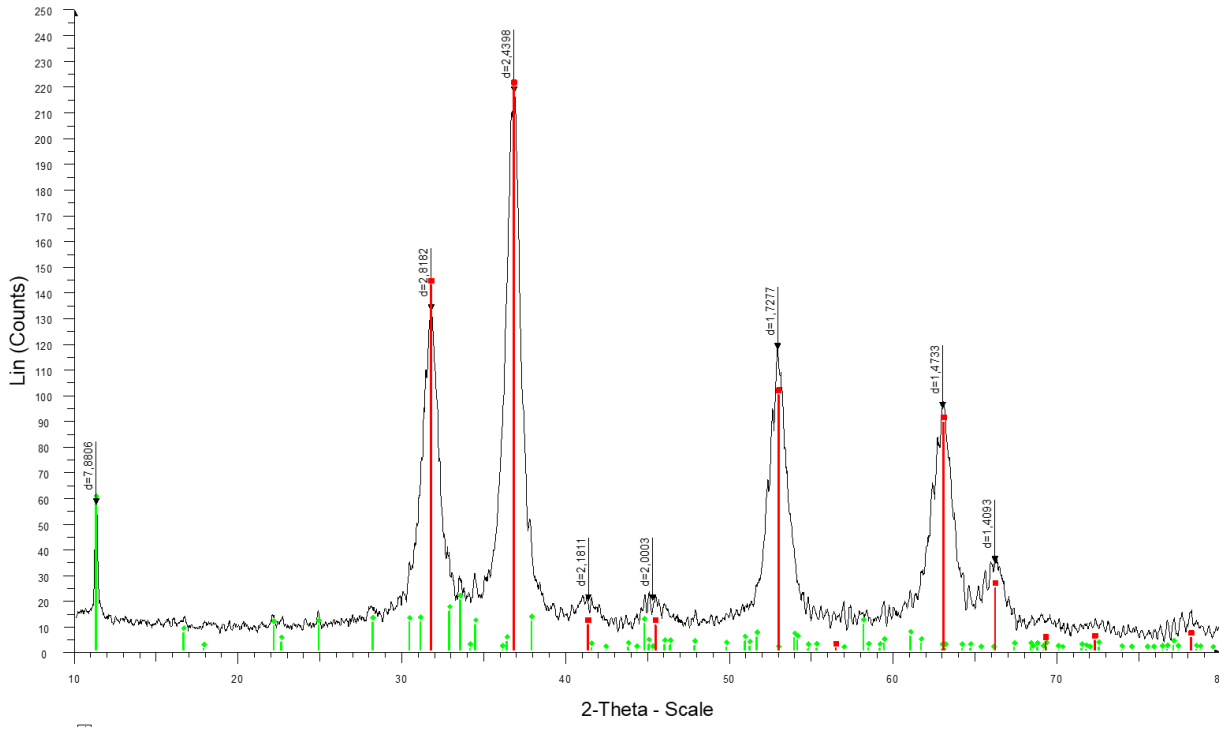

Figure 12: XRD analysis of the sample, where red lines correspond to ZnO_2 standard and green lines to simonkolleite

found, based on the position of one peak, the others being hidden by noise. The quantity of simonkollteite was estimated to be of 4 % in mass, based on the peak intensity. TGA analysis further showed that ZnO_2 degrades around 280 °C. A mass loss of 1.8 % occurs below 100 °C, most likely remaining water since the sample was not dried at temperatures higher than room temperature. Despites its potential as oxygen donor for several applications, ZnO_2 is not of interest for our study, and this synthesis method was not explored further, because of the oxidizing potential of H_2O_2.

3.2 Precipitation of $ZnCl_2$ in presence of NaOH or KOH

The second synthesis method was inspired from the previous work of Ullah et al. [60]. They present a simple precipitation method, followed by aging of the precipitate.

However, with these experimental conditions, instead of the expected ZnO, the layered zinc hydroxide compound simonkolleite was obtained, which has the theoretical formulae $Zn_5(OH)_8Cl_2.H_2O$. The nature of the product was determined by the combination of several analysis described below.

The XRD analysis showed that the product contains a major phase matching the pattern of simonkolleite (Figure 13). There was no other crystalline phase identified by XRD, but there still might be other amorphous phases present, especially $Zn(OH)_2$. The chemical composition of the sample was further tested, to check if there is any deviation from the

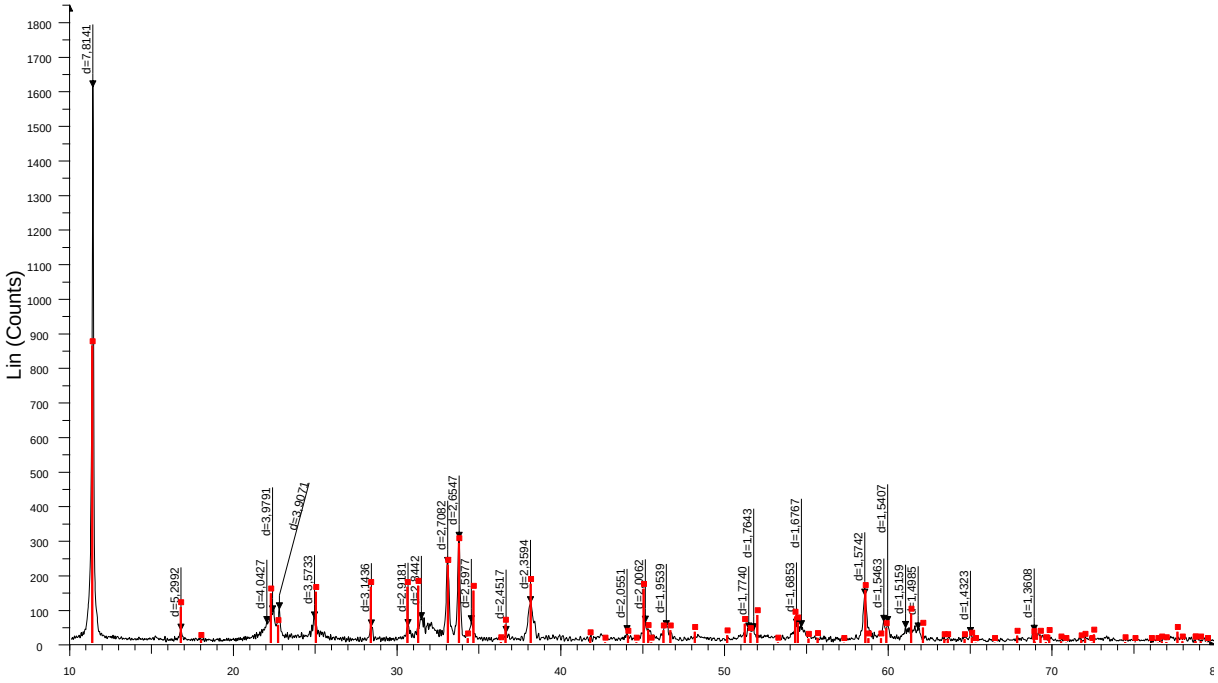

Figure 13: XRD crystallography of the sample overlayed with simonkolleite pattern

simonkolleite theoretical composition (Table 2). Zn^{2+} and Na^{+} were tested by atomic absorption spectrometry, OH^{-} was tested by indirect alkalimetric titration, Cl^{-} by ion chromatography, and H_2O by gravimetry after drying the samples at 110 °C. The results show traces of Na^{+}, which is probably associated to Cl^{-} to form NaCl, accounting for 0.29 % of the total mass. After deduction of the NaCl, the comparison of the composition and the stoichiometry of simonkolleite, it was found that Zn^{2+} is in limiting quantity and that there is an excedent of OH^{-} and Cl^{-}. It was also observed that the global measured composition does not respect the neutrality of charges. By assuming the presence of some $Zn(OH)_2$, it means the sample have an even bigger excess of Cl^{-}.

Table 2: Chemical analysis of the synthesized samples

Atomic content	% Zn	% OH	% Cl	% H_2O	% Na
Average	57.8	25.1	13.7	2.2	0.12
Standard deviation	0.86	0.49	0.24	0.98	0.005
$Zn_5(OH)_8Cl_2.H_2O$	59,24	24,65	12,85	3,26	0,00

Moreover, the thermogravimetric analysis showed two mass losses at 176 and 466 °C (Figure 14), corresponding to the theoretical mass losses of simonkolleite, described more in details in section 3.5 of this thesis. The combination of those three different analysis allow us

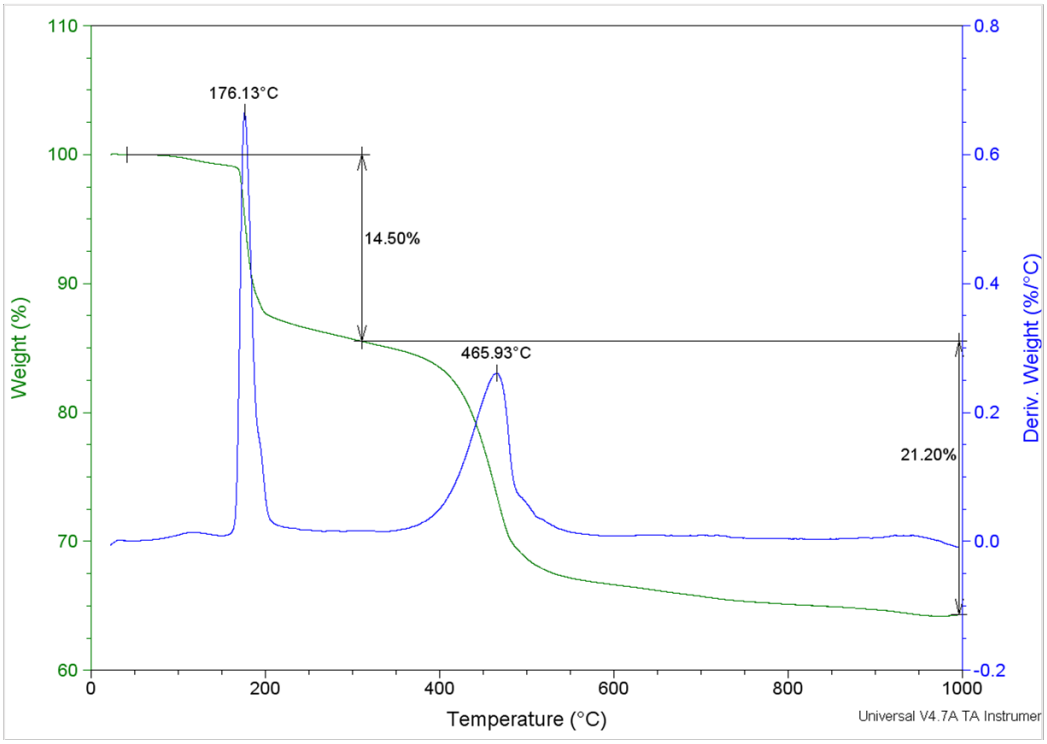

Figure 14: TGA profile of the sample, displaying two major mass losses

to conclude that the samples contain pure simonkolleite, except for traces of NaCl.

The morphology of the particles was studied by the means of AFM scanning. Some sheets of irregular shape are observed, but of comparable thickness, as illustrated on Figure 15. The observed particles had a diameter ranging from 50 to 400 nm, and a thickness of 2 to 5 nm. Furthermore, a lot of aggregates were observed by optical microscope, but were too big to be observed by AFM.

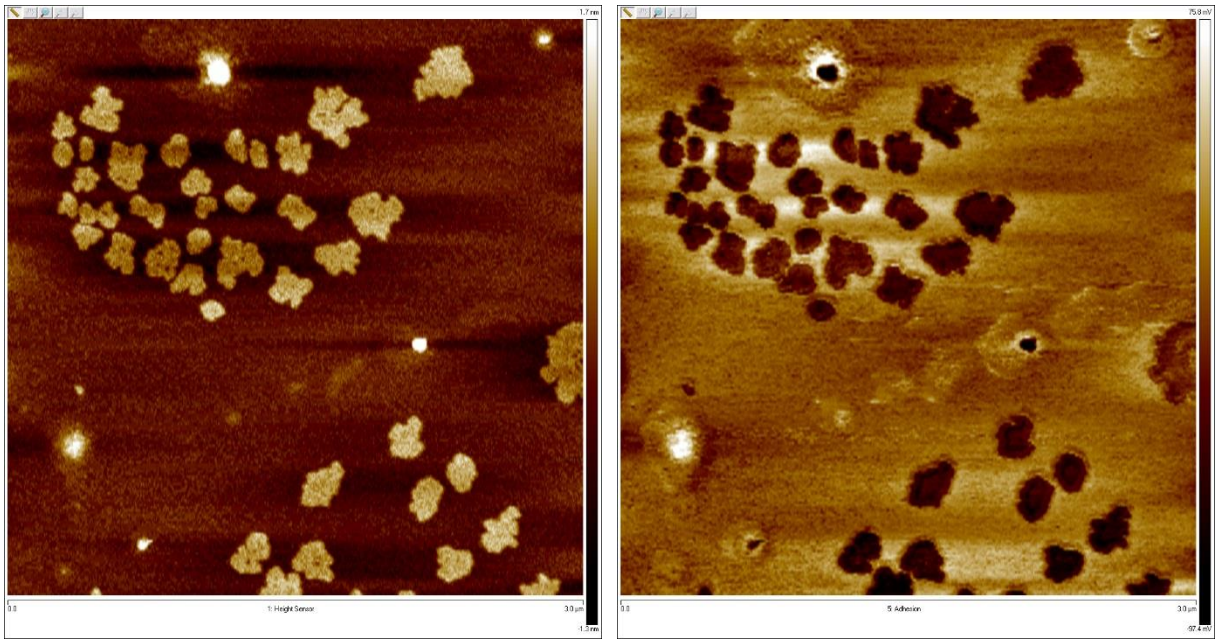

Figure 15: AFM scans of simonkolleite particles on a mica plate. Topographic map on the left, and adhesion map on the right

3.3 Study of precipitation mechanism of simonkolleite/ZnO

Although in the method described in section 3.2 pure simonkolleite was obtained, it was found out that the precipitation of $ZnCl_2$ with NaOH yielded either simonkolleite or ZnO depending on the synthesis conditions. In this section, the influence of the OH:Zn molar ratio, addition method and concentration of Cl^- anions on the product nature and morphology will be described. Based on the study of the pH curves, kinetic studies and thermodynamic equilibrium values, a global formation mechanism is proposed to explain the influence of all the synthesis conditions on the product nature and morphology.

3.3.1 Addition of $ZnCl_2$

In the series of experiments n°1 to 11, the $ZnCl_2$ solution was added into the NaOH solution, starting from high pH and infinite OH:Zn molar ratio, and going towards lower values of pH and OH:Zn molar ratio. An immediate precipitation was observed from the first added drop, and the pH is stabilized instantly upon addition of one solution in the other. At the beginning of the addition, the pH decreased very slowly, until the system went through a pH equivalence point at a OH:Zn molar ratio of 2.1, accompanied with a large pH drop from 12 to 6. After the equivalence, the pH continued to decrease very slowly with further addition of $ZnCl_2$. A typical curve of pH change during synthesis is shown in (Figure 16) based on experiment n°4 conditions (OH:Zn = 0.75). The pH equivalence point of all experiments of the series (n°1-11), and the concentration range were almost identical, because the initial concentration of NaOH as well as concentration of added $ZnCl_2$ solution were the same. The difference between the experiments consisted only in the amount of added $ZnCl_2$, which in all cases was above the amount required to reach the equivalence point.The dependence of pH on the concentration of $ZnCl_2$ in the matrix solution for the same experiment (n°4) is presented in Figure 16.

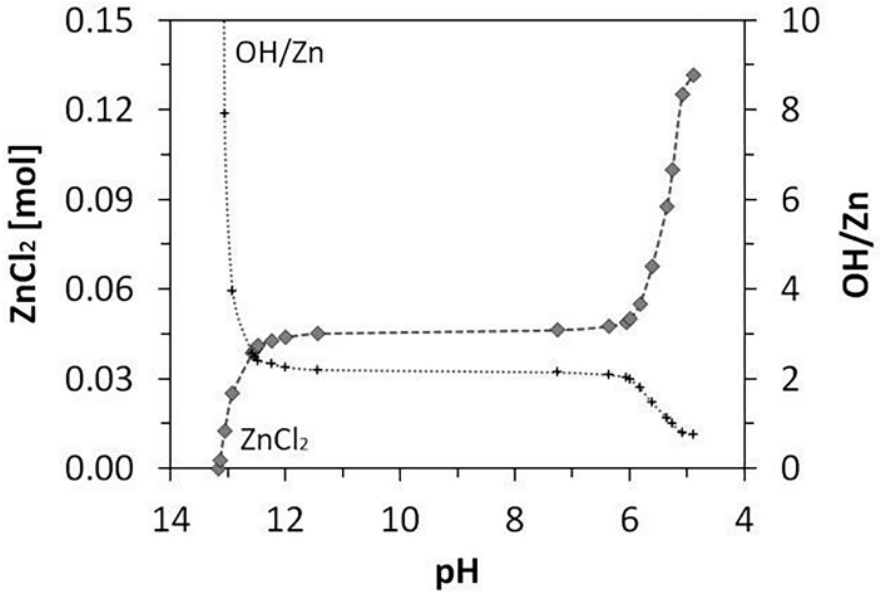

Figure 16: Effect of added amount of $ZnCl_2$ and OH:Zn ratio in the matrix solution on its pH, experiment n°4 (OH:Zn=0.75; initial amount of NaOH is 0.1 mol, V = 200 ml)

To support the analysis of the processes which take place in the reaction mixtures during addition, equilibrium diagrams were used for Zn^{2+} fractions which are presented in Figure 17. The diagrams represent the thermodynamically stable Zinc (II) phases (both the solid phases and soluble species) depending on the pH in a $ZnCl_2$-H_2O system at 25 ^oC (calculated on basis of equilibria and thermodynamic data using Medusa-Hydra chemical equilibrium software). The equilibrium diagrams are presented for 5 different concentration points marked at the main graph. According to the equilibrium diagrams, both ZnO and $Zn(OH)_2$ solids are thermodynamically stable at given concentrations over a similar pH range. The pH edge of the stability range of this solid was shifted from 7 to 9 when the $ZnCl_2$ concentration was increased from 0.00062 to 0.521 mol/L. Simonkolleite solid phase, $Zn_5(OH)_8Cl_2{\cdot}H_2O$, becomes stable at a concentration $C(ZnCl_2) \geq 0.007$ ($10^{-2.15}$) mol/L. Concerning the soluble species, zinc hydroxide complexes, $Zn(OH)^+$, $Zn(OH)_3^-$ and $Zn(OH)_4^{2-}$, are stable only at lower $ZnCl_2$ concentrations: the first one – at pH range 5-9, while two others – at very basic pH (>12). The Zn^{2+} and other chloride complexes are stable at pH < 7; the H_2O molecules in coordination sphere of Zn^{2+} ion were not specified at the diagrams for simplicity reasons.

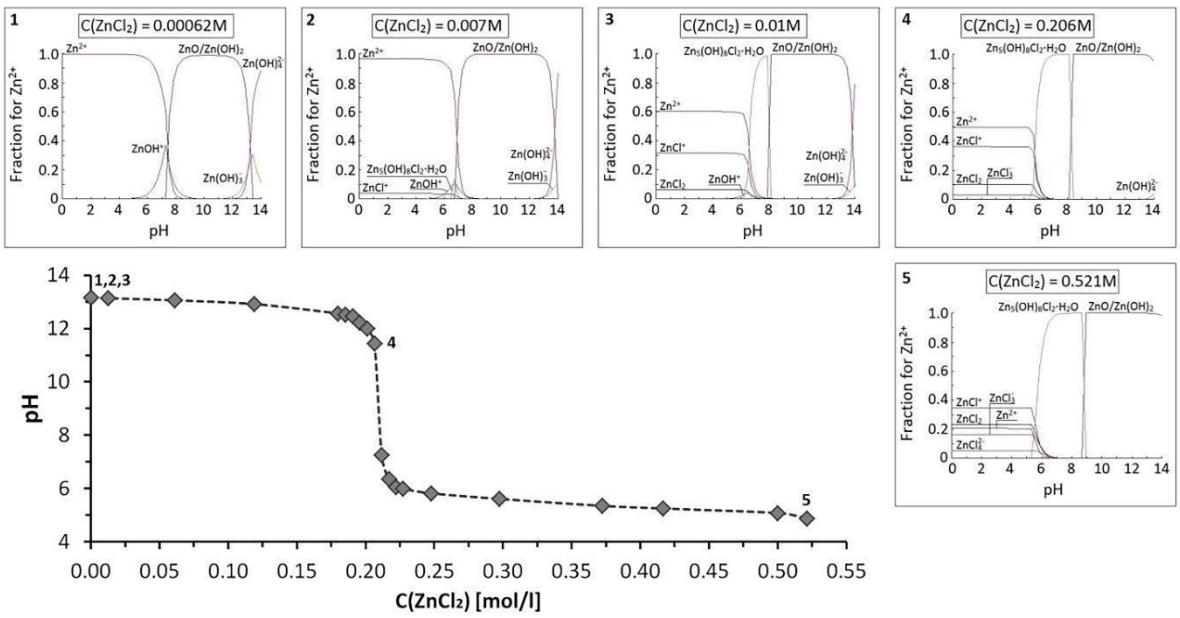

Figure 17: pH change during synthesis of sample 4 (OH:Zn=0.75) and equilibrium diagrams for Zn^{2+} fraction at 5 different points at 25 ºC. The main graph represents dependence of pH on concentration of $ZnCl_2$ in the matrix solution

Considering our system, the observed pH decrease during synthesis could be achieved via two different mechanisms: either by consumption of OH^- during the formation of the insoluble solid hydroxide/hydroxide chloride or, neutralisation by the H^+ ions released during the formation of ZnO. The simplified reactions corresponding to these mechanisms are presented below in schemes 9, 10 and 11.

$$Zn^{2+} + 2\ OH^- = Zn(OH)_2 \quad (12)$$

$$5\ Zn^{2+} + 8\ OH^- + 2\ Cl^- + H_2O = Zn_5(OH)_8Cl_2 \cdot H_2O \quad (13)$$

$$Zn^{2+} + H_2O = ZnO + 2\ H^+ \quad (14)$$

According to the equilibrium diagrams in Figure 17, starting from high pH, either ZnO or $Zn(OH)_2$ should have been formed (schemes 9 and 11), while simonkolleite could have been formed only when the pH is low enough. From the schemes (9) and (11) it is visible that the equivalence for both the formation of $Zn(OH)_2$ and ZnO should occur for OH:Zn molar ratio = 2. From the scheme (10) it is visible that the equivalence for the formation of simonkolleite should occur at a molar ratio OH:Zn = 1.6. However, instead of two equivalence points as should be expected, the pH measurements during the addition showed only one at 2.1. In both mechanisms no further OH^- was consumed for the formation of simonkolleite beyond the first equivalence point. Therefore, the equivalence point that was observed should correspond either to the consumption of OH^- for the formation of $Zn(OH)_2$ (Scheme 9) or to neutralisation during the formation of ZnO (Scheme 11). Moreover, instead of being formed directly from the dissolved species (Scheme 10), simonkolleite should be formed from the reaction products ($Zn(OH)_2$ or ZnO), following a mechanism that does not involve any pH change (Scheme 12 and 13).

$$4\ Zn(OH)_2 + ZnCl_2 + H_2O = Zn_5(OH)_8Cl_2.H_2O \quad (15)$$

$$4\ ZnO + ZnCl_2 + 5\ H_2O = Zn_5(OH)_8Cl_2.H_2O \quad (16)$$

In the case of $Zn(OH)_2$ formation, if only $Zn(OH)_2$ was formed, an equivalence point at OH : Zn molar ratio of 2 would be observed. Since it is at 2.1, it was deduced there is an equilibrium between $Zn(OH)_2$, $Zn(OH)_3^-$, and $Zn(OH)_4^{2-}$ (Scheme 14).

$$20ZnCl_2 + 42(OH)^- = (18+x)Zn(OH)_2 + (2-2x)Zn(OH)_3^- + xZn(OH)_4^{2-} + 40Cl^- \quad (17)$$

It is worth to note that according to the equilibrium diagrams (Figure 17-4), $Zn(OH)_3^-$, and $Zn(OH)_4^{2-}$ are stable only at high pH, while with pH decrease they should transform into ZnO or $Zn(OH)_2$ (Scheme 15, 16, 17, and 18). At the same time, $Zn(OH)_2$ could also dehydrate into ZnO during the synthesis (Scheme 19). Therefore, when approaching the equivalence point, the concentration of $Zn(OH)_3^-$, and $Zn(OH)_4^{2-}$ should become negligible, while the main phases present in the mixture should be $Zn(OH)_2$ and/or ZnO.

$$Zn(OH)_4^{2-} + 2\ H^+ = Zn(OH)_2 + 2\ H_2O \quad (18)$$

$$Zn(OH)_4^{2-} + 2\ H^+ = ZnO + 3\ H_2O \quad (19)$$

$$Zn(OH)_3^- + H^+ = Zn(OH)_2 + H_2O \quad (20)$$

$$Zn(OH)_3^- + H^+ = ZnO + 2\ H_2O \quad (21)$$

$$Zn(OH)_2 = ZnO + H_2O \quad (22)$$

The second mechanism, which may lead to decrease of pH, is neutralisation in result of the direct formation of ZnO by hydrolysis (Scheme 11). In this case, the formation of H^+ ions should lead to neutralisation of the solution. According to the reaction (Scheme 11), formation of one ZnO produces two H^+ ions, thus the pH equivalence point should be reached with OH : Zn= 2, which is also very close to the observed value (OH : Zn= 2.1). The slight difference to the stoichiometry can again be explained by the formation of $Zn(OH)_3^-$, and $Zn(OH)_4^{2-}$. The whole mechanism can be represented by the general scheme 20, where x is comprised between 0 and 1.

$$20ZnCl_2 + 42(OH)^- = (18+x)ZnO + (2-2x)Zn(OH)_3^- + xZn(OH)_4^{2-} + 40Cl^- + (18+x)H_2O \quad (23)$$

In general, according to the equilibrium diagrams and the observed pH change of the solution, the formation of simonkolleite phase can be described as follows. After addition of the first drop of $ZnCl_2$ (0.05 ml) to highly basic NaOH solution, besides the formation of ZnO or $Zn(OH)_2$, two soluble zinc hydroxide complexes $Zn(OH)_4^{2-}$ and $Zn(OH)_3^-$ are also formed (Figure 17-1). Further increase of $ZnCl_2$ concentration in the solution leads to the formation of only ZnO or $Zn(OH)_2$, which, according to the equilibrium diagram (Figure 17-3), are the only thermodynamically stable compounds at this concentration and pH. The formation of ZnO or $Zn(OH)_2$ should lead to neutralisation of the solution. The equivalence point

corresponds to pH 9 and is associated with a sharp fall in pH from 12 to 6. The fact, that equivalence point corresponded to pH higher than 7 can be explained with the limited stability of $Zn(OH)_2$ and ZnO at lower pH. In particular, when pH became low enough, the reactions leading to pH increase may take place (Schemes 21 and 22) that prevented further sharp falling of the pH in the system.

$$Zn(OH)_2 + 2\ H^+ = Zn^{2+} + 2\ H_2O \quad (24)$$

$$ZnO + 2\ H^+ = Zn^{2+} + H_2O \quad (25)$$

In order to prove this suggestion, another experiment has been performed. For a separate sample the $ZnCl_2$ solution was added in the amount a little bit less than required to reach the equivalence point and, thereafter, a very acidic HCl solution (C(HCl) = 0.5 mol/l, similar to the initial concentration of NaOH) was added instead of $ZnCl_2$ solution. The experiment was aimed to reveal how the acid will influence the equilibrium in the system. Although it was expected that by addition of HCl the equivalence point will be reached almost immediately and a sharp fall of pH will take place, it did not happen. Instead, the pH remained stable (around 12.2) and it fell only after the addition of 80ml of HCl solution. Thus, in our opinion, the result can be explained by the consumption of H^+ ions via the dissolution of precipitation products ($Zn(OH)_2$ or ZnO) according to the above described reactions (Schemes 21 and 22) that prevented the pH drop.

When continuing to add more $ZnCl_2$, past a OH:Zn molar ratio of 2, simonkolleite started to form without changing the pH from either $Zn(OH)_2$ or ZnO (Scheme 12 and 13). A similar reaction between ZnO and $Zn(NO_3)_2$, has already been described in literature [61], but since it was unclear whether $ZnCl_2$ reacted with dehydrated ZnO or $Zn(OH)_2$, it was impossible to conclude which of the reactions occurred during our synthesis method. In both cases, the pH continued to decrease very slowly on the account of the addition of $ZnCl_2$ solution, which is acidic. To ensure that the reaction was accomplished, the mixtures were aged during 90 min under constant stirring. The final conditions that were reached after complete addition of $ZnCl_2$ solution for experiment n°4 corresponded to equilibrium diagram 5 in Figure 17. The final pH value for this experiment was below 5 and, according to the equilibrium diagram, only the soluble Zn^{2+} species are thermodynamically stable in $ZnCl_2$-H_2O system at this pH pointing out that the solid should gradually dissolve. This was the same situation for other experiments where the OH:Zn molar ratio was below 1 (n°1-5).

Therefore, it was expected that the yield of simonkolleite phase in these experiments should have in general gradually decreased. However, a decrease in the yield was observed only for the samples n°1 and 2, which was especially low for the sample n°1 with Zn/OH = 0.1, where the most acidic final pH was reached. It was connected not with sample dissolution, but with partial loss of the solid sample during filtration due to penetration of low crystal size fracture through the filtration paper. Moreover, according to SEM analysis, lower OH : Zn molar ratio also resulted in slightly thinner crystal plates. At the same time, the pH of the system during stirring also almost did not changed. In view of these facts, it was concluded that the system had reached some kind of dynamic equilibrium between the dissolution of simonkolleite crystals and their recrystallization. Also, because the pH in this series of experiments was only slightly lower than the stability range of simonkolleite phase, the process of dissolution could be very slow. This result is quite interesting because via correlation of OH:Zn molar ratio in the system, it is possible to manipulate the equilibrium in the system and slightly influence the thickness of the crystal plates formed.

3.3.2 Influence of maturation time

In order to study the kinetic of the formation of simonkolleite in more details as well as to clarify which compound is formed at the intermediate step ($Zn(OH)_2$ or ZnO), a series of additional experiments was performed. In particular, the addition of $ZnCl_2$ solution (experiment n°5, OH : Zn = 1) was stopped at different stages and the resulting solid was filtrated, washed, dried and studied with XRD analysis. To this purpose, the products of 5 different reaction steps were studied:

- step 1: the reaction was stopped after addition of 10 ml of 2.5 mol/L $ZnCl_2$ solution (reached OH:Zn molar ratio at this point was 4, pH of the suspension was close to 13); the solid was washed using 2 different liquids (NaOH solution with pH =10 and distilled H_2O with pH = 6);
- step 2: the reaction was stopped immediately after addition of all the $ZnCl_2$ solution required to reach OH:Zn molar ratio 1 (42 ml of 2.5 mol/L solution), the pH of the suspension was 5.3;
- step 3: the reaction was stopped 30 min after addition of all the $ZnCl_2$ solution;
- step 4: the reaction was stopped 60 min after addition of all the $ZnCl_2$ solution;
- step 5: the reaction was stopped 90 min after addition of all the $ZnCl_2$ solution.

The results of XRD analysis of the obtained samples are presented in Figure 18, and indicate that even in the case when the equilibrium point was not reached (step1), simonkolleite phase started to form during washing of the sample with slightly acidic water. The content of simonkolleite phase in this sample after washing constituted ~1.31(2) %. As the main product at step1, low crystalline ZnO was detected (crystallite size ~10 nm). After the whole $ZnCl_2$ solution was added and the pH decreased (steps 2-5), simonkolleite became immediately the only phase observed with XRD analysis pointing out that the kinetic of its formation was very fast. With continuous stirring, the crystallinity of the samples significantly improved (the crystallite size gradually increased from 13-15 nm to 50-60 nm). Although the results of the experiment imply that ZnO was the intermediate product and the formation of simonkolleite took place according to scheme 13, ZnO may also be formed from $Zn(OH)_2$ during drying stage, rendering detection of $Zn(OH)_2$ impossible when the conditions are altered. Therefore, definite confirmation that ZnO is the only intermediate product of the studied reaction could be obtained only in result of in situ studies.

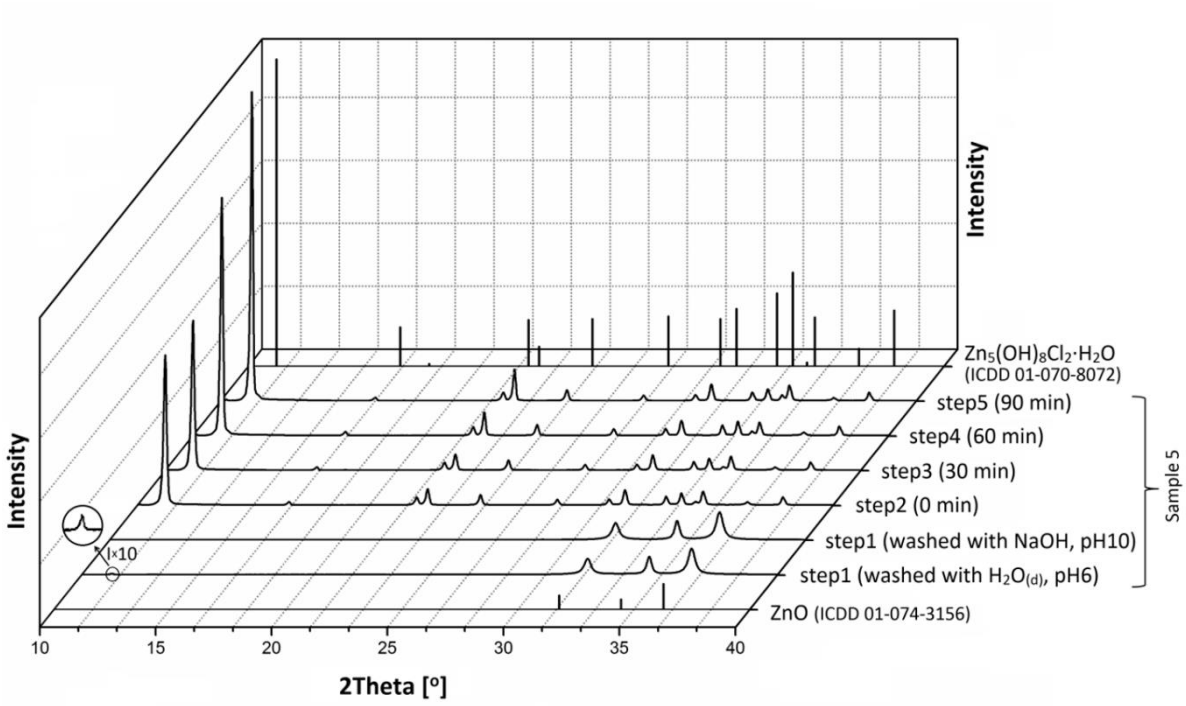

Figure 18: Results of XRD analysis of sample 5 (OH : Zn = 1) at different reaction stages; diffraction patterns of ZnO and $Zn_5(OH)_8Cl_2 \cdot H_2O$ (database PDF-2)

3.3.3 Influence of excess Cl^- ions

In order to gain more information on the reaction of the formation of simonkolleite, the impact of Cl^- ions and their ability to shift the equilibrium towards the formation of simonkolleite phase was also studied. In particular, since simonkolleite and $Zn(OH)_2$ have a similar crystal structure, $Zn(OH)_2$ could be converted to simonkolleite via partial replacement of OH^- into Cl^- following the scheme 23. Or, alternatively, $Zn_5(OH)_8Cl_2 \cdot H_2O$ can be also formed from ZnO according to scheme 24.

$$5\ Zn(OH)_2 + 2\ Cl^- + H_2O = Zn_5(OH)_8Cl_2 \cdot H_2O + 2\ OH^- \quad (26)$$

$$5\ ZnO + 2\ Cl^- + 6H_2O = Zn_5(OH)_8Cl_2 \cdot H_2O + 2\ OH^- \quad (27)$$

Concerning our experiment, the concentration of Cl^- in the system was increased via addition of a NaCl solution (experiment n° 12). In this experiment, the OH:Zn molar ratio was the same as in experiment n° 11 (which resulted in the formation of a ZnO and $Zn_5(OH)_8Cl_2 \cdot H_2O$ mixture), but the amount of Cl^- is similar to the experiment n° 5, which resulted in the formation of pure $Zn_5(OH)_8Cl_2 \cdot H_2O$. Since a mixture 8 % richer in simonkolleite was obtained than for experiment n° 11, it was concluded that adding Cl^- favoured a little bit the formation of simonkolleite, but not as significantly as the presence of both Zn^{2+} and Cl^- ions.

3.3.4 Addition of NaOH

In order to find out how the order of the added solution would affect the precipitated product, 3 points were chosen with OH:Zn molar ratio 0.5, 1 and 1.5. For all these points, a pure simonkolleite phase was obtained in case of addition of $ZnCl_2$ into NaOH. Similarly to the previous case, an immediate precipitation was observed during the addition of NaOH solution into $ZnCl_2$ solution. The initial pH of the solutions was quite acidic (4.23-4.36), and it increased and stabilized instantly upon addition of one solution in the other. However, the character of pH change was totally different than in previous case: with addition of NaOH, the pH increased quite quickly to 4.85-4.92 while above this point it increased much slower. The curves of pH change during synthesis for all 3 experiments (n° 13-15) are shown in Figure 19.

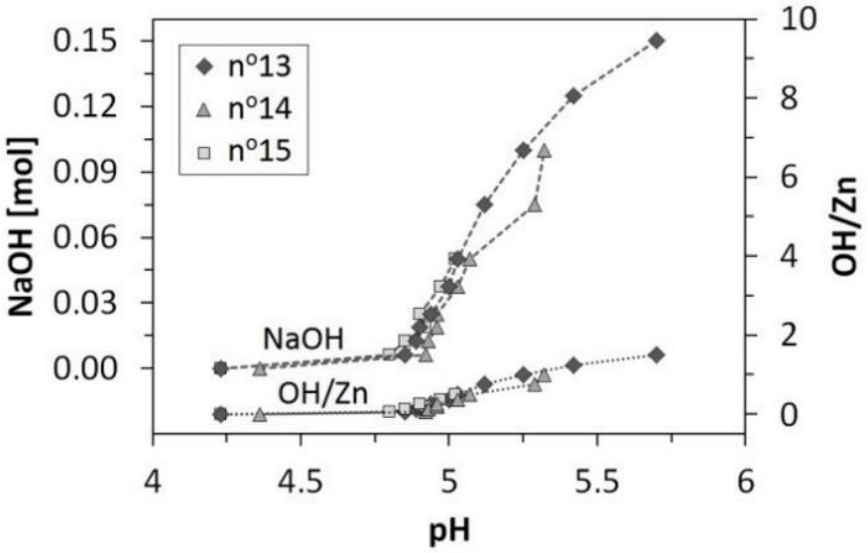

Figure 19: Effect of the added amount of NaOH and OH:Zn molar ratio in the matrix solution on its pH, experiments n° 13-15 (OH:Zn=0.5-1.5; initial amount of $ZnCl_2$ is 0.1 mol, V = 200 ml))

With the addition of NaOH the initial concentration of $ZnCl_2$ in the matrix solution decreased from 0.5 mol/L to 0.385-0.455 mol/L depending on final OH : Zn molar ratio. In such case, the equilibrium diagram for Zn^{2+} fraction should be very similar to those presented in Figure 17, equilibrium diagram 5. Accordingly, simonkolleite phase should have appeared only at a pH above 6. However, in spite that the pH in these experiments was below 6, pure simonkolleite phase was obtained in all cases. With the increase of OH:Zn molar ratio, the product yield also significantly increased. It can be explained with higher final pH where the simonkolleite phase became more thermodynamically stable. For all studied experiments, the resulting powders consisted of very thin and small crystal plates pointing out less favourable

conditions for the formation of simonkolleite than in the case of addition of $ZnCl_2$ into NaOH solution.

Those results can be put in parallel with those obtained by Zhu et al. [53], where they used propylene oxide (PO) as a cation scavenger instead of NaOH, and DMF as a solvent. In this study, they added some water as a source of OH groups, and explained the formation mechanism by the formation of two complexes of Zn^{2+} corresponding to the octahedron and tetrahedron present in the SK structure. Although the reaction mechanism was different and the obtained structure was flower-like, they observe that the ratio between PO and Zn^{2+} had a major influence on the results.

3.3.5 Morphology of the samples

The dried samples morphology was observed by SEM and AFM. The AFM scans were of poor quality due to the presence of big aggregates, whereas SEM scans revealed the morphology of both aggregates and primary particles.

When adding $ZnCl_2$ into NaOH, no noticeable influence of the OH:Zn molar ratio was observed ranging from 0.1 to 1.5 (Table 3). Pure simonkolleite was obtained, having the shape of hexagonal platelets with dimensions varying between 1 to 10 μm in width and 0.1 to 1 μm in thickness.

Table 3: Composition and morphology of samples n°1 to n°12

Sample	***OH:Zn initial molar ratio [mol/mol]***	***Phase composition obtained by XRD RIR***	***Morphology***
1	0.1	SK 100 %	Small plates, 3-5 μm*0.1-0.3 μm
2	0.25	SK 100 %	Small plates, 1-3 μm*0.1-0.3 μm
3	0.5	SK 100 %	Small plates, 2-5 μm*0.1-0.3μm
4	0.75	SK 100 %	Small plates, 3.5-4.5 μm*0.2-0.4 μm
5	1	SK 100 %	Small plates, 4-5 μm*0.2-0.4 μm
6	1.1	SK 100 %	Small plates, 3-7 μm*0.1-0.3 μm
7	1.2	SK 100 %	Regular big plates, 10-5μm*0.5-1 μm
8	1.4	SK 100 %	Small plates, 4-8 μm*0.1-0.4 μm
9	1.5	SK 100 %	Lots of thin plates, lower than 0.1 μm, 3-7 μm wide
10	1.6	SK 75 %	Plates 3-8 μm and some much smaller particles
11	2	SK 28 %	No visible plates, only big shapeless solids covered with very small particles
12[a]	2	SK 36 %	No visible plates, only big shapeless solids covered with very small particles

[a] 0.1 mol of NaCl is added to double amount of Cl^- ions in the reactive mixture

Lower OH:Zn molar ratio tended to yield thinner plates, with the exception of the molar ratio 1.5 which also yielded thin plates (Figure 20-a, b, c, e). Then for molar ratios from 1.6 to 2 a mixture of ZnO and simonkolleite was observed. Simonkolleite kept a hexagonal plates shape, and ZnO was either in the form of shapeless small particles on the surface of simonkolleite for the molar ratio 1.6, or in aggregated form for the molar ratio 2 (Figure 20-e, f).

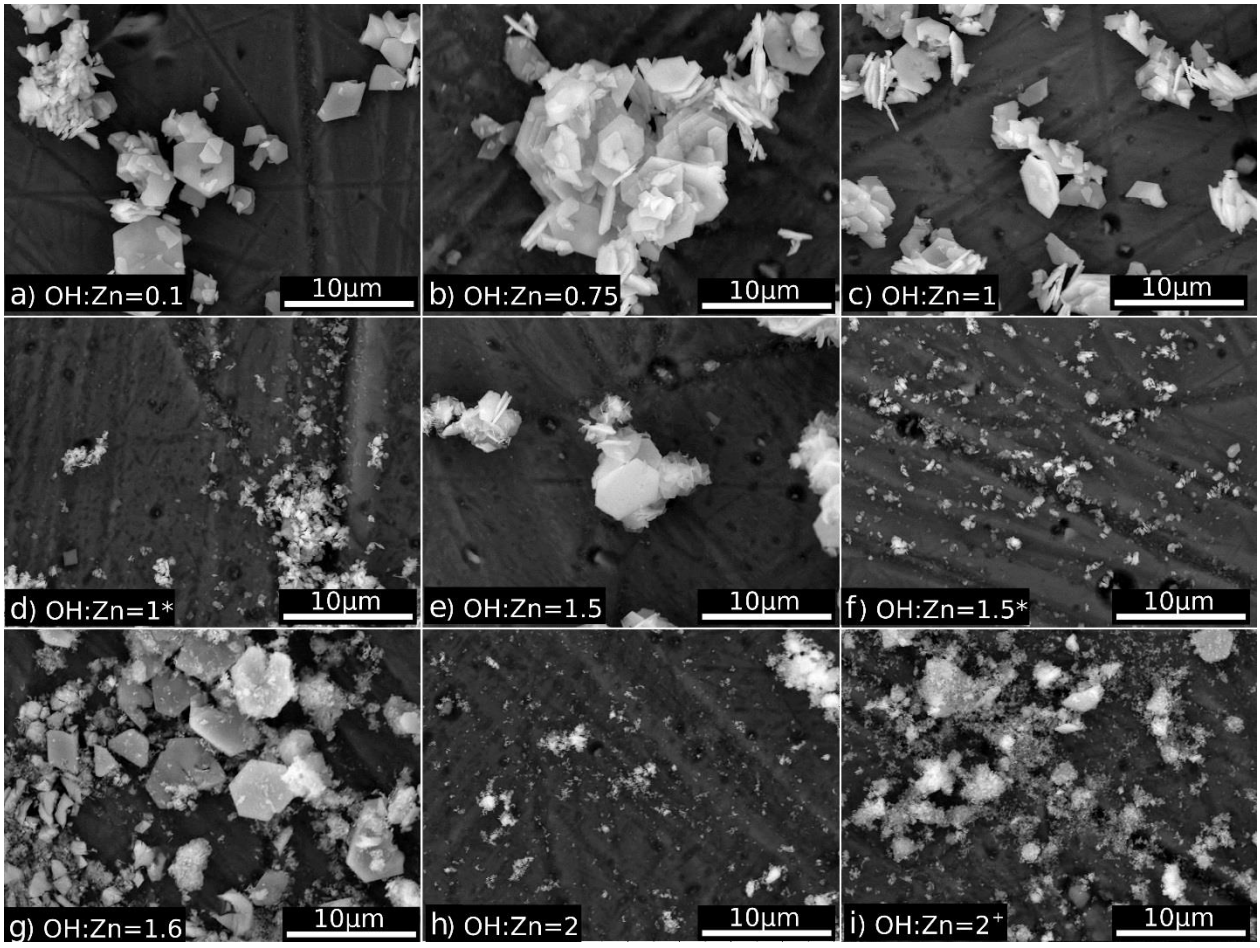

Figure 20: SEM scan of dried samples. a) sample 1, OH:Zn= 0.1;b)sample 4, OH:Zn= 0.75;c) sample 5, OH:Zn= 1; d) sample 14, OH:Zn= 1, reversed addition; e) sample 9, OH:Zn= 1.5; f) sample 15, OH:Zn= 1.5, reversed addition; g) sample 16, OH:Zn= 1.6; h) sample 11, OH:Zn= 2, addition of NaCl

By adding NaOH in $ZnCl_2$, the reaction started at a low pH, and the formation of pure simonkolleite was also observed in the OH:Zn molar ratio range of 0.5-1.5 (Table 4). However the morphology was totally different with much smaller plates than for the opposite addition method. Again, for the same addition method, the ratio had very little or no influence on the resulting morphology (Figure 20-b, d).

Table 4: Composition and morphology of samples n°13 to n°15

Experiment	*OH : Zn [mol/mol]*	*XRD phase composition*	*Size of the particles*
13	0.5	SK 100 %	0.5-0.6 µm
14	1	SK 100 %	0.6-0.9 µm
15	1.5	SK 100 %	0.5-0.8 µm

Additionally, surface area of the samples varied from 2.9 to 5.3 m^2g^{-1}. However, no regularity has been observed regarding synthesis conditions and crystal shape or size. At the same time, the measured result depended very much on degassing conditions prior to the measurement. It should be connected with removal of crystalline water and structure collapse under vacuum treatment above room temperature.

3.3.6 Global formation mechanism

As a conclusion, the synthesis mechanism of simonkolleite is favoured at slightly acidic pH, whereas the ZnO formation is being favoured by a higher initial OH:Zn molar ratio.

The study of the pH profile during the addition of $ZnCl_2$ into NaOH solution at 50 °C showed three things: the system reaches an equilibrium immediately, simonkolleite is formed through the reaction of either ZnO or $Zn(OH)_2$ intermediate products, and the intermediate product neutralizes HCl. The kinetic study showed that the intermediate product yields a major part of ZnO after drying, and a very small part of simonkolleite when neutralized before drying. Moreover, an increasing stirring time post-addition increases the crystallinity of the product. With the support of thermodynamic equilibrium diagrams it was concluded that ZnO and/or $Zn(OH)_2$ are the main intermediate products. Since the position of the equivalence is shifted to a OH:Zn molar ratio slightly higher than 2, it was deduced that there is also a small part of $Zn(OH)_3^-$ and/or $Zn(OH)_4^{2-}$ present in the intermediate product. Simonkolleite is further formed by the reaction between $ZnCl_2$ and the intermediate product, with no pH change involved. Despite its structure being close to that of $Zn(OH)_2$,

simonkolleite is not formed by partial replacement of OH^- by Cl^- anions, but the addition of Cl^- can slightly favour the formation of simonkolleite.

The influence of OH:Zn molar ratio on the morphology of simonkolleite is very faint. Thinner plates formation for lower OH:Zn molar ratios was observed, with the exception of the molar ratio 1.5 which also yields thin plates. The thickness of the plates is probably influenced by the final pH, regulated by an equilibrium between dissolution and reprecipitation of simonkolleite in slightly acidic conditions at 50 ºC.

On the other side, the addition order had a big influence on the morphology. Starting from low pH yielded much smaller plates than the opposite way. This could be due to different precipitation pathways for simonkolleite. Starting from low pH, $Zn(OH)_2$ would react immediately with the excess of $ZnCl_2$, but starting form high pH, $Zn(OH)_2$ would first dehydrate into ZnO before further reacting with $ZnCl_2$. In the latter case, the size and morphology of simonkolleite depends on the one of the intermediate product.

3.4 Influence of n-butanol addition

After clarifying the global formation mechanism of simonkolleite/ZnO under our synthesis method, the influence of 1-butanol on the formation and stabilization of simonkolleite/ZnO was studied. n-butanol is partially miscible with water because of its OH group, but not completely because of its short hydrocarbon chain. It evaporates easily at temperatures lower than 100 ºC, so any physically adsorbed molecule on simonkolleite surface can be removed easily.

N-butanol (BuOH) was tried to increase the stability of simonkolleite, and eventually ZnO suspensions. A first set of experiments was made by dispersing dried samples of pure simonkolleite in a mixture of water/n-butanol (Table 5). It was observed that for an increasing amount of n-butanol the settled phase is occupying a bigger and bigger volume, sign of a looser network in the sediment. However, above a threshold the particles start to be hydrophobic and stick to the glass wall (Figure 21, photo on the left). Finally, for a higher amount of n-butanol a phase separation was observed, where the sediment lay on the bottom of the top phase containing n-butanol. This illustrates how the affinity with n-butanol is stronger than the gravitational force.

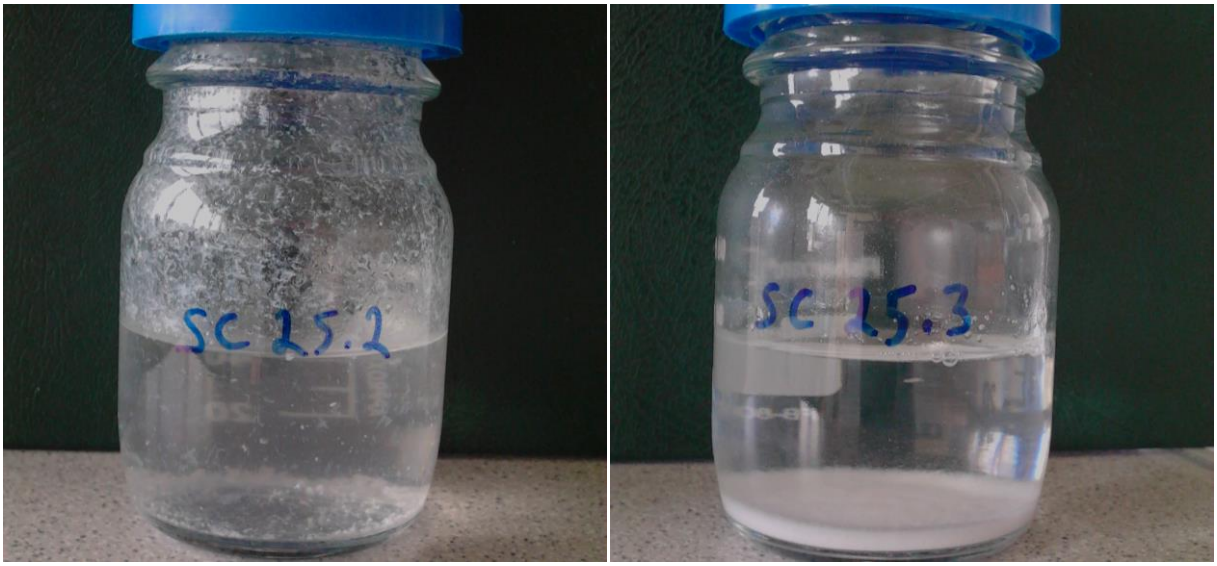

Figure 21: Dispersions of simonkolleite in water : BuOH = 0.1 on the left and 0.04 on the right

Table 5: Stabilization tests of simonkolleite in water/1-butanol

Sample	***n-butanol/H_2O***	***n-butanol/SK***	***Observation***
1	0.20	33,33	Two phases, the upper phase contains the particles, which sedimentates on the bottom of the upper phase.
2	0.10	18,18	Aggregation, the particles are sticking to the walls, no dispersion, but one phase.
3	0.04	7,69	One phase, sedimentation on the bottom.
4	0.02	3,93	One phase, sedimentation on the bottom, smaller than sample 3
5	0.01	2,10	One phase, sedimentation on the bottom, smaller than samples 3 and 4

To explain this phenomenon, it was theorized that simonkolleite is only mildly hydrophilic and that the hydrophobic tail of n-butanol reduces its energy by adsorption on simonkolleite surface with the OH group pending towards the water media (Figure 22). Once the surface is saturated with n-butanol, it is possible that the covered simonkolleite becomes hydrophobic and starts to stick to the glass walls. Moreover, when adding n-butanol, a second phase was created, where the suspension rather stays.

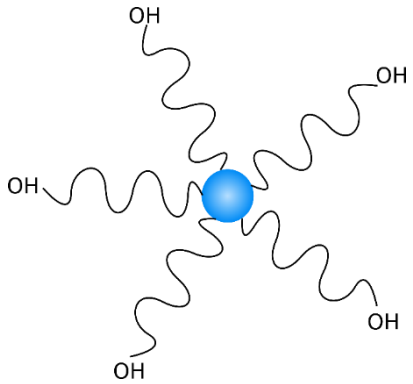

Figure 22: Illustration of BuOH adsorption on simonkolleite surface

The stabilization mode of n-butanol was not electrostatic, since the pH must be very high to remove the proton from the alcohol group. And since it has a short hydrocarbon tail, it was not a very efficient steric stabilizer as well. It did reduce the packing density of the sediment, its surface energy, and also can act as a growth inhibitor since it adsorbs on the surface of simonkolleite.

In a second set of experiments, the n-butanol was added in the reaction mixture to observe its influence on the morphology of simonkolleite and ZnO formation. The amount of n-butanol and $ZnCl_2$ varied to obtain different n-butanol:H_2O and Zn:OH ratios, as presented in the Table 6 below.

Table 6: Experiment plan of simonkolleite/ZnO synthesized with variable n-butanol:H_2O and Zn:OH ratio

		n-butanol/H_2O				
		0	0.05	0.1	0.15	0.2
Zn : OH	1 : 1	E 4.5.1 Pure SK	E4.5.5 Pure SK	E4.5.9 Pure SK	E4.5.13 Pure SK	E4.5.17 Pure SK
	1 : 1.4	E4.5.2 Pure SK	E4.5.6 Pure SK	E4.5.10 Pure SK	E4.5.14 Pure SK	E4.5.18 Pure SK
	1 : 2.2	E4.5.3 Pure ZnO	E4.5.7 Pure ZnO	E4.5.11 Pure ZnO	E4.5.15 Pure ZnO	E4.5.19 Pure ZnO
	1 : 2.8	E4.5.4 Pure ZnO	E4.5.8 Pure ZnO	E4.5.12 Pure ZnO	E4.5.16 Pure ZnO	E4.5.20 Pure ZnO

The butanol was expected to have rather an influence on the morphology of the products, therefore the samples were observed by SEM. To avoid destroying aggregates and have an idea of the dispersion degree of the particles, dried powder was simply deposited in metallic targets, without US treatment. The influence on simonkolleite and ZnO morphology was independently observed.

As illustrated in Figure 23, it was observed that an increasing amount of n-butanol will reduce the size of the simonkolleite plates, while the molar ratio Zn:OH has a very mild influence. This reduction of the particles size is not desirable since it reduces the aspect ratio of the plates. Concerning the quality of the dispersion, all the prepared samples sedimented in the water, but did not start to show any hydrophobic behaviour, or migrate to the n-butanol phase.

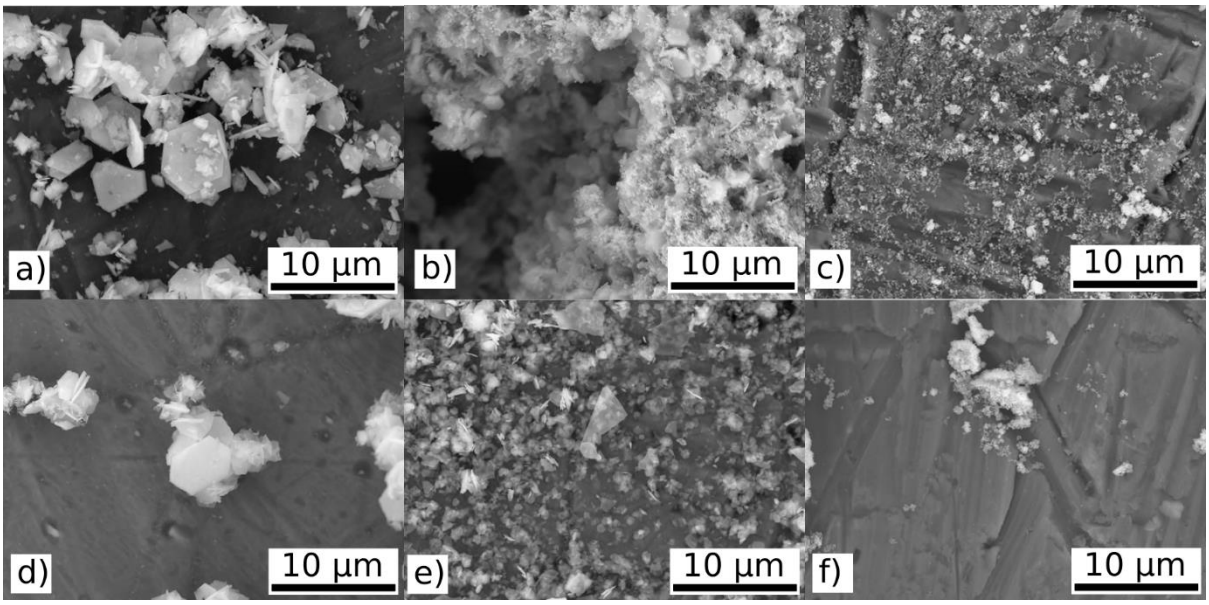

Figure 23: SEM scans of simonkolleite synthesized in presence of BuOH. A) sample 1; b) sample 9; c) sample 17; d) sample 2; e) sample 10; f) sample 18

In the case where a lower Zn:OH molar ratio was used, the formation of ZnO as a major product was observed (Figure 24). Interestingly, a mixture of two different morphologies was observed: some platelets with an hexagonal shape, and some aggregates of very small primary particles. The size and shape of the primary particles cannot be determined on the SEM scans since their size is lower than the resolution power on apparatus. Additionally, the addition of an increasing amount of n-butanol did not prevent the aggregation of the primary ZnO particles.

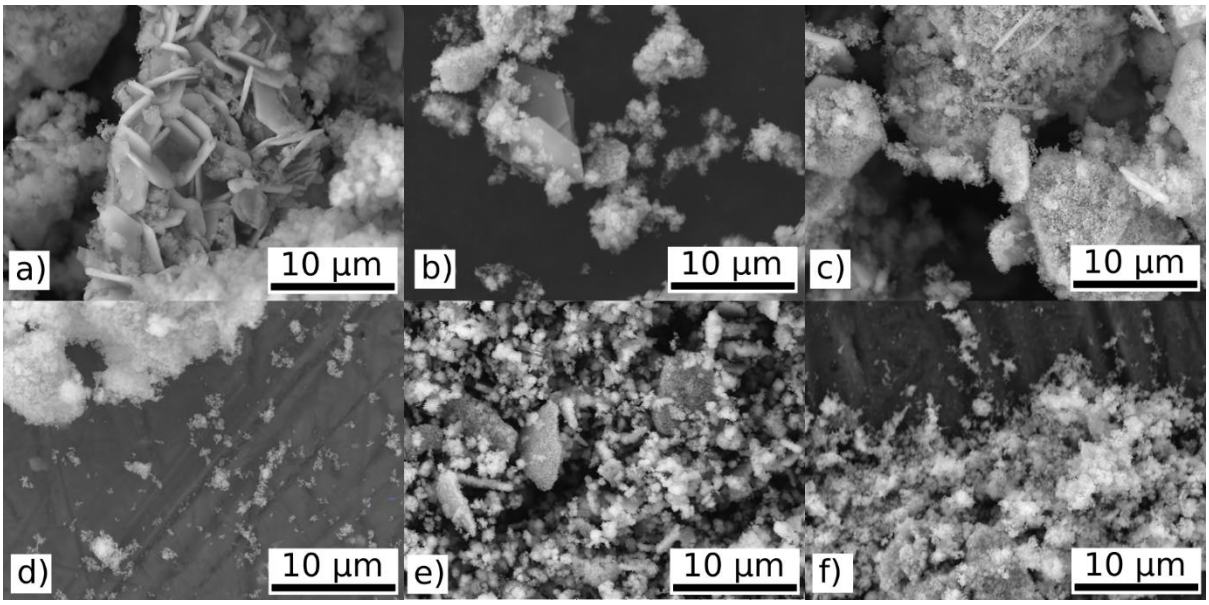

Figure 24: SEM scans of ZnO synthesized in presence of BuOH. A) sample3; b) sample 11; c) sample 19; d) sample 4; e) sample 12; f) sample 20

Since their size was already very small without any n-butanol addition, no further reduction in size was observed for the primary particles. No clear influence was observed on the platelets as well. Therefore, the role of n-butanol as a growth inhibitor during the precipitation of ZnO under used experimental conditions was not proved. Moreover, as in the case of simonkolleite, it is not an efficient dispersion stabilizer, as the primary particles in all experiments were visibly strongly aggregated.

The results from PSD however do not reflect the difference of morphology observed via SEM. The curves are bimodals and the average size varies between 11 and 315 µm, with no correlation with the observations from SEM. The presence of a bimodal curve can be explained by the partial dispersion of primary particles, while a lot of aggregates remain in the suspension. Further, the theory behind the PSD measurements relies on the diffraction of light

by spherical particles. Additionally, the optical parameters used for the analysis were the ones on ZnO, which are probably slightly innacurate in the case of simonkolleite.

As a conclusion, n-butanol clearely shows some affinity with simonkolleite and effectively acts as a growth inhibitor. A clear decrease in plate diameter with an increasing concentration of n-butanol was observed. However, adding n-butanol during the synthesis of simonkolleite did not significantly improve the final suspension stability. This confirms the poor potential of n-butanol as a surfactant. Concerning ZnO synthesis, since the ZnO primary particles are already very small without the use of n-butanol, the only improvement could have been the reduction of the aggregation degree. This was not achieved since n-butanol is a poor suspension stabilizer. In the end, no influence of n-butanol on ZnO synthesis under those synthesis conditions was observed.

3.5 Thermal degradation of simonkolleite

Simonkolleite has a limited thermal stability, degrades at temperatures higher than 170 ^{o}C in a series of reactions and yield ultimately ZnO, which is stable at temperatures higher than 1000 ^{o}C. Instead of a final product, simonkolleite can be seen as an intermediate to produce ZnO via thermal treatment. Ideally the ZnO would keep the same platelet morphology as the simonkolleite precursor, but could have some defects in its crystallographic structure. Those defects might be caused by some remaining Cl^-, that might negatively or positively affects the final properties of the ZnO. In a first section, the degradation mechanism of simonkolleite and possibilities of TGA to quantify pure and modified simonkolleite are discussed. In a second part, the properties of the ZnO resulting from thermal degradation of simonkolleite will be discussed.

3.5.1 Mechanism of simonkolleite degradation

Simonkolleite has a low thermal resistance with a first thermal degradation at 170 ^{o}C. Simonkolleite undergoes three phase transformations, described in the literature [63].

$$Zn_5(OH)_8Cl_2.H_2O \rightarrow 3ZnO + 2\beta\text{-}Zn(OH)Cl + 4H_2O \quad (28)$$

This reaction occurs at 170°C.

$$2\beta\text{-}Zn(OH)Cl \rightarrow ZnO + ZnCl_2.0{,}25H_2O + 0{,}75H_2O \quad (29)$$

This second reaction occurs at 220-230 °C

$$ZnCl_2.0{,}25H_2O \rightarrow 0{,}25\ ZnO + 0{,}5HCl + 0{,}75\ ZnCl_2 \quad (30)$$

This third reaction happens also at 230C, and the weight loss is 21,82 %. Although the reaction occurs at 230 °C, the $ZnCl_2$ is evaporated slowly around 450 °C, still below its boiling point : 756 °C.

However, some studies showed than in presence of extra water vapor, more $ZnCl_2$ can hydrolyse into ZnO in the third step. It can be represented by the modified scheme:

$$ZnCl_2.xH_2O \rightarrow x\ ZnO + 2x\ HCl + (1\text{-}x)\ ZnCl_2 \quad (31)$$

The water may come from either partial dehydration during the second step, or extra water from the surrounding gas phase.

The mass losses associated to this mechanism should occur at three different temperatures :

1. Around 170 ^{o}C, 4 mol of water are lost, correponding to 13,06 %
2. Around 230 ^{o}C, (1-x) mol of H_2O and 2x mol of HCl are lost, where x is the degree of $ZnCl_2$ hydrolysis. Water used for the hydrolysis can only come from the original simonkolleite since dry N_2 was used. The associated mass loss is 3,26 % + x.9,95 %, where x is the degree of $ZnCl_2$ hydrolysis. The value of x is between 0 and 1.
3. Around 450 ^{o}C, (1-x) mol of $ZnCl_2$ are lost. The associated mass loss is (1-x), 24,70 %.

Experimentally, the samples were measured at a heating rate of 10 ^{o}C/min, under a flow of dry N_2. Two or maximally three steps with non-horizontal plateau in between were observed. For this reason it is difficult to determine the exact mass loss attributed to each step. In order to determine more accurately the mass loss associated with each step, a method of peak fitting was developed. Three methods on how to determine the mass loss associated with each temperature are presented and compared in the next three sub-sections.

3.5.1.1 Mass loss determined at fixed temperature intervals

The first method is the fastest and simplest. A temperature between two theoretical mass losses was arbitrary chosen and the current mass loss was taken. This method is quite unprecise since there is no horizontal plateau between the thermal degradations. The values will therefore strongly depend on the position where the mass is taken. The median temperatures between the theoretical mass losses were taken:

- 25 ^{o}C original weight.
- 200 ^{o}C between 170 and 230 ^{o}C.
- 340 ^{o}C between 230 and 450 ^{o}C.
- 600 ^{o}C it is assumed that all decomposition products are evaporated, except for ZnO.

3.5.1.2 Temperature intervals defined according to the derivative

The second method uses the derivative of the mass loss over time. This first put into evidence the inflections points where the mass loss is the fastest, and the curve drop is sharper. Additionally, short of having horizontal plateau, indicating where the mass loss is the slowest. The weight at those places, where the derivative is minimum, is taken and the mass loss temperature is defined as the place where the derivative is at its local maximum. Experimentally, three or four peaks are observed, corresponding to the three mass losses plus a loss of water adsorbed on the sample. The two-three first peaks overlap, which explain why no horizontal plateau is observed. Then the last peak is well separated from the three first, but the derivative does not go down to 0 in between. On the Figure 25, it is visible that it is quite difficult to see the three mass losses on the TGA curve, but it appears more clearly on the derivative curve.

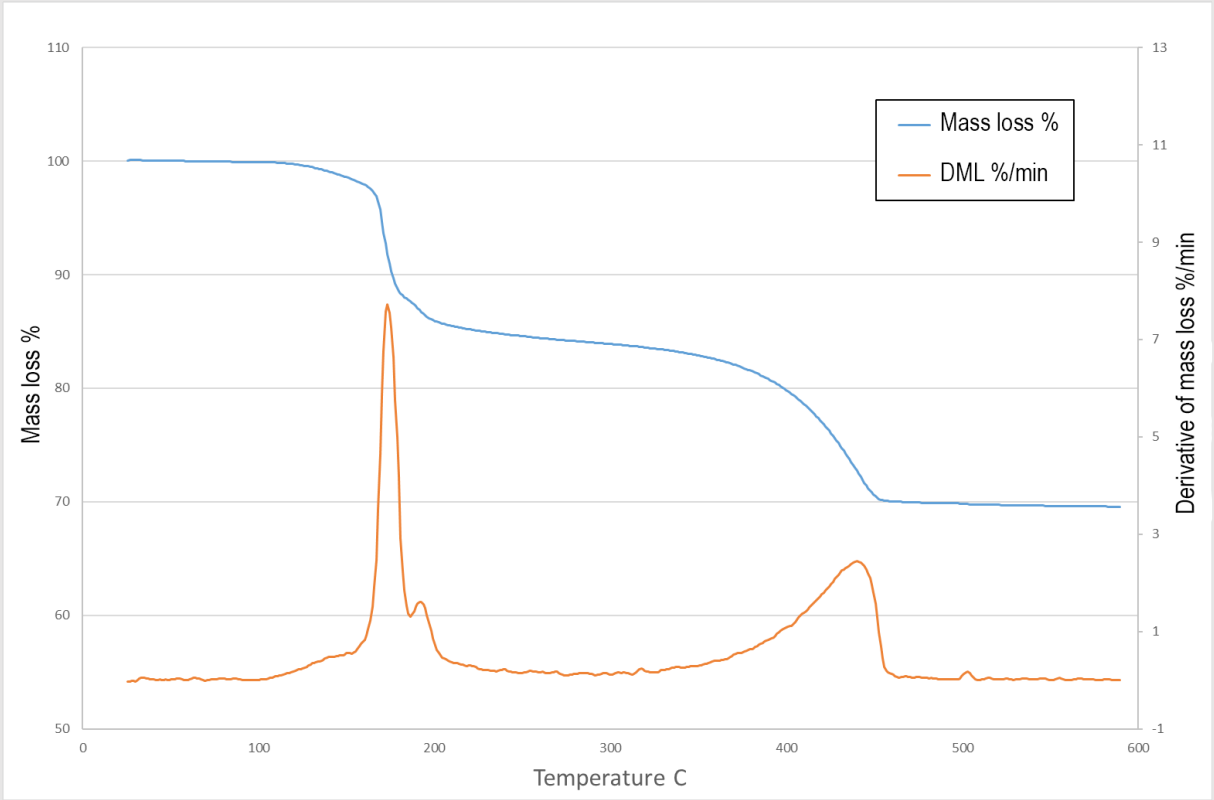

Figure 25: TGA measurement of a pure simonkolleite sample, showing the mass loss and its derivative over time

3.5.1.3 Fitting of the derivative profile with gaussian peaks

The third method extends the second one, where the overlapping derivative peaks are separated. Gaussian peaks (equation 29) were fitted to the experimental derivative curve to deconvolute them. Practically the peaks are asymmetric, meaning that all the width is different above and below the center position of the peak. The solver will have therefore four variable parameters for each peak: position, height, width, and asymmetry. To speed up the resolution process, the user can manually input the position of each peak and an arbitrary height. The solver first optimizes the height, width and asymmetry, and then fine tune the solution by optimizing all four parameters. Then the peaks are integrated to get the mass loss associated with each separate peak. If there is a mistake between the simulated integral and the real overall mass loss, the remaining mass loss is distributed between each peak proportionally to their width.

$$g(x) = a.exp\left(-\frac{(x-b)^2}{2c^2}\right) \quad (32)$$

On the Figure 26, is presented the resulting fitting curve with a total of four Gaussian peaks. Left and right limits have to be defined because the curve does not go to 0, and the peaks would not be able to fit on an extended range. In this case the fitting limits were 50 and 240 °C.

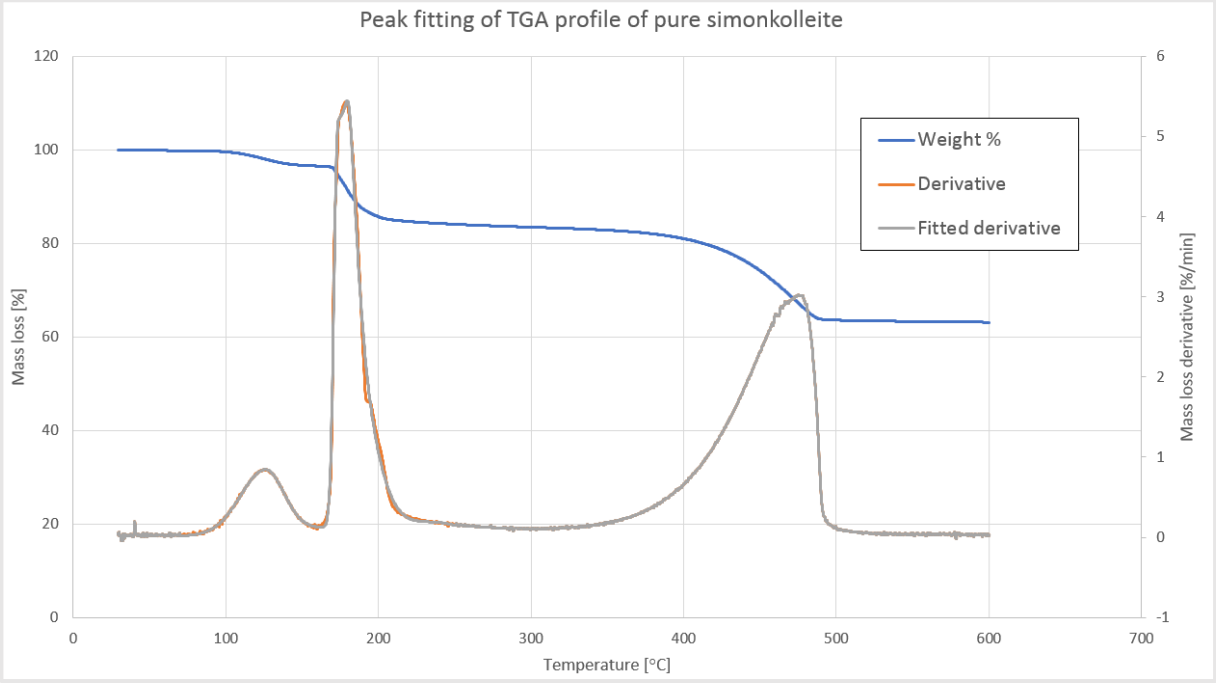

Figure 26: Peak fitting results of a pure simonkolleite sample TGA profile

As an example, the results of the peak fitting for a sample of pure simonkolleite synthesized with a OH:Zn molar ratio of 1.4, without any n-butanol, are shown in Table 7. It is important to note that the mass loss was derived by the time, but the curve was draw and fitted against the temperature, since it has more sense visually. This can be done only because the heating rate is constant, otherwise the peaks position and width should be in minutes instead of ºC.From the example, a mass loss is visibly occuring at 126 ºC, probably due to adsorbed water release and/or crystalline water removal. Moreover, the first mass loss is at a slightly higher temperature than 170 ºC, and is composed of two peaks at 174 and 182 ºC, probably to better fit the imperfect shape of the raw data. Finally, the second mass loss might be represented by the peak at 234 ºC. However, this peak is quite wide and might simply compensate for an imperfect baseline.

Table 7: Peak fitting resulting parameters for pure simonkolleite

Parameters	***Peak1***	***Peak2***	***Peak3***	***Peak4***
Position [ºC]	126	174	182	234
Height [%/min]	0.78	4.98	1.94	0.19
Width [C]	16.2	2.6	3.4	73.0
Asymmetry	0.75	3.27	4.14	0.31
Integral [%]	2.77	6.85	4.21	1.91
Total mass loss between 50 and 300 ºC		15.74 %		

On the base of this example, the derivative curve of pure simonkolleite obtained under different synthesis conditions, plus few samples of simonkolleite and ZnO mixtures, were fitted. Not three but four different mass losses were defined: the three associated to the theoretical ones, plus the mass loss occuring at temperature lower than 170 ^{o}C. The mass loss around 450 ^{o}C is taken as the total mass loss between the upper fitting limit and the final remaining mass. This allows to reduce the number of peaks to fit, since the last peak is very well separated from the others. The mass losses at 170 ^{o}C and 230 ^{o}C are calculated from the integral of the fitted peaks. Finally, the mass loss before 170 ^{o}C is taken as the mass loss at the upper fitting limit, minus the mass loss at 170 and 230 ^{o}C, and plus eventually a fitted peak if there is a clear one. The results of all the tested samples under different OH:Zn molar ratio synthesis conditions are presented in Table 8.

Table 8: Mass losses of different samples according to the third method

Sample	***OH:Zn ratio***	***Mass loss < 170 ^{o}C***	***Mass loss at 170 ^{o}C***	***Mass loss at 230 ^{o}C***	***Mass loss at 450 ^{o}C***
SK6	1,6	0,86	6,60	8,23	8,13
SK7	1,5	2,37	10,12	3,13	13,37
SK8	1,4	2,13	10,58	2,55	15,17
SK9	1	2,33	10,77	2,38	18,84
SK3	1,4	1,63	11,16	2,37	13,52
SK13	1,2	0,93	12,64	1,55	20,33
SK14	1,1	2,31	10,98	2,54	19,22
SK15	0,75	2,24	11,37	1,42	21,93
SK16	0,25	2,91	11,04	0,72	19,48
SK17	0,1	2,64	10,79	1,16	21,61
SK19	1	3,17	11,90	1,29	19,65
SK20	1,5	2,89	11,27	0,99	19,39
SK21	2	2,49	3,28	5,39	4,56
SK22	2	1,34	3,17	4,77	4,03
SK23	1	2,37	11,92	1,47	19,15

It was tried to correlate the mass losses to the simonkolleite content, or the synthesis conditions. In the Figure 27 the mass loss before 170 ºC seems to be constant regardless of the OH:Zn ratio and of the SK content. The mass loss at 230 ºC varies in function of OH:Zn ratio, but is not proportional to the SK content, since it increases with decreasing SK content. Both the mass losses at 170 and 450 ºC seem to decrease with the SK content. When calculating the mass loss ratio over the simonkolleite content, it was observed that only the mass loss at 170ºC is proportional to the simonkolleite content for different samples.

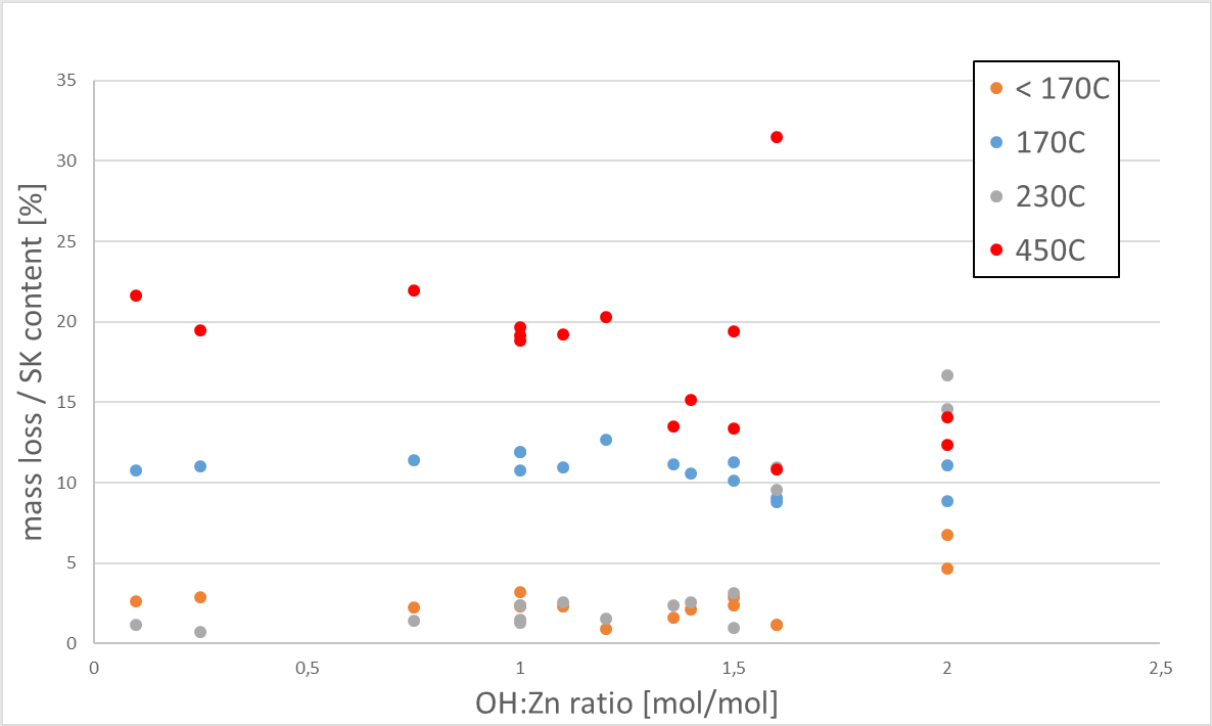

Figure 27: Ratio of the Mass loss at different temperature by SK content

The average values and the standard deviation for the 15 measured samples are presented in Table 9. The mass loss before 170 °C should not happen theoretically so it was not expected to be correlated to the simonkolleite amount. However, the mass losses at 230 °C and 450 °C depend on both the content of simonkolleite and the degree of hydrolysis. Despite the same measuring conditions, different results were obtained, tending to show that the synthesis conditions influenced slightly the thermal degradation process, and therefore the $ZnCl_2$ hydrolysis degree. The mass loss at 170 °C is proportional to the content of simonkolleite, but the standard deviation is quite high, leading to an error of 10 % of the total value. Thermogravimetry could be used as a way to determine the simonkolleite content when the precision does not have to be higher than 10 %.

Table 9: Ratio of mass loss at different temperature per simonkolleite content

Temperature [C]	< 170 °C	170 °C	230 °C	450 °C
Average [%]	2,60	10,77	4,58	18,15
Standard deviation [%]	1,43	1,10	5,23	4,99
Theoretical mass loss [%]	0	13,06	3,26-13,21	0-24,70

It was found out that the mass loss is lower than the theoretical one. A hypothesis was formulated that the simonkolleite is partially dehydrated at a lower temperature than 170 °C and loses partially its crystalline water, in addition to water adsorbed on the sample. The mass loss not from the original sample was calculated, but taking the weight after the mass loss below 170 °C. A corrected value of 11,0 ± 1,1 % was obtained. The amount of adsorbed water on simonkolleite will vary from sample to sample depending on the surface area and atmospheric conditions. However, the fraction of crystalline water removed at temperatures below 170 °C was calculated according to the equation 30, where *x* is the degree of hydration, MH_2O is the molar mass of H_2O, MSK is the molar mass of simonkolleite, f_{SK} is the mass content of simonkolleite in the sample, m<170C the relative mass loss below 170 °C expressed in %, and m170C the relative mass loss at 170 °C expressed in %.

$$\frac{(4-x).MH_2O}{MSK-x.MH_2O}.f_{SK} = \frac{m_{170C}}{100\%-m_{<170C}} \quad (33)$$

Solving the equation gives us a dehydration fraction *x* = 71 %. This value was calculated from the average of the mass loss, but might actually be different from sample to sample, which might explain why the mass loss at 170 °C is proportional to the simonkolleite content ± 10 %. Theoretically, from a dehydration *x* between 0 and 1, a mass loss lies in the

range of 10,13-13,06 %, which correspond to 11,6 ± 1,5 %. Corrected experimental data fit exactly in those limits.

Additionally, it is possible also estimate the amount of $ZnCl_2$ hydrolysis from the mass losses at 230 and 450 ºC. The hydrolysis degree was calculated from three different ways: the mass loss at 230 ºC (equation 31), the mass loss at 450 ºC (equation 32), or the addition of both (equation 33).

$$m_{230C} = \frac{(1-x).MH_2O+2x.MHCl}{MSK}.f_{SK} \Rightarrow x = \frac{m_{230C}.MSK/f_{SK}-MH_2O}{2.MHCl-MH_2O} \quad (34)$$

$$m_{450C} = \frac{(1-x).MZnCl_2}{MSK}.f_{SK} \Rightarrow x = 1 - \frac{m_{450C}}{f_{SK}}.\frac{MSK}{MZnCl_2} \quad (35)$$

$$m_{230C} + m_{450C} = \frac{(1-x).(MH_2O+MZnCl_2)+2x.MHCl}{MSK}.f_{SK}$$

$$x = \frac{(m_{230C}+m_{450C}).MSK/f_{SK}-MH_2O-MZnCl_2}{2MHCl-MH_2O-MZnCl_2} \quad (36)$$

The calculation results are presented in the Figure 28. Indeed, using the mass loss at 230 ºC leads to negative numbers, or even higher then 100 %, which is physically impossible.

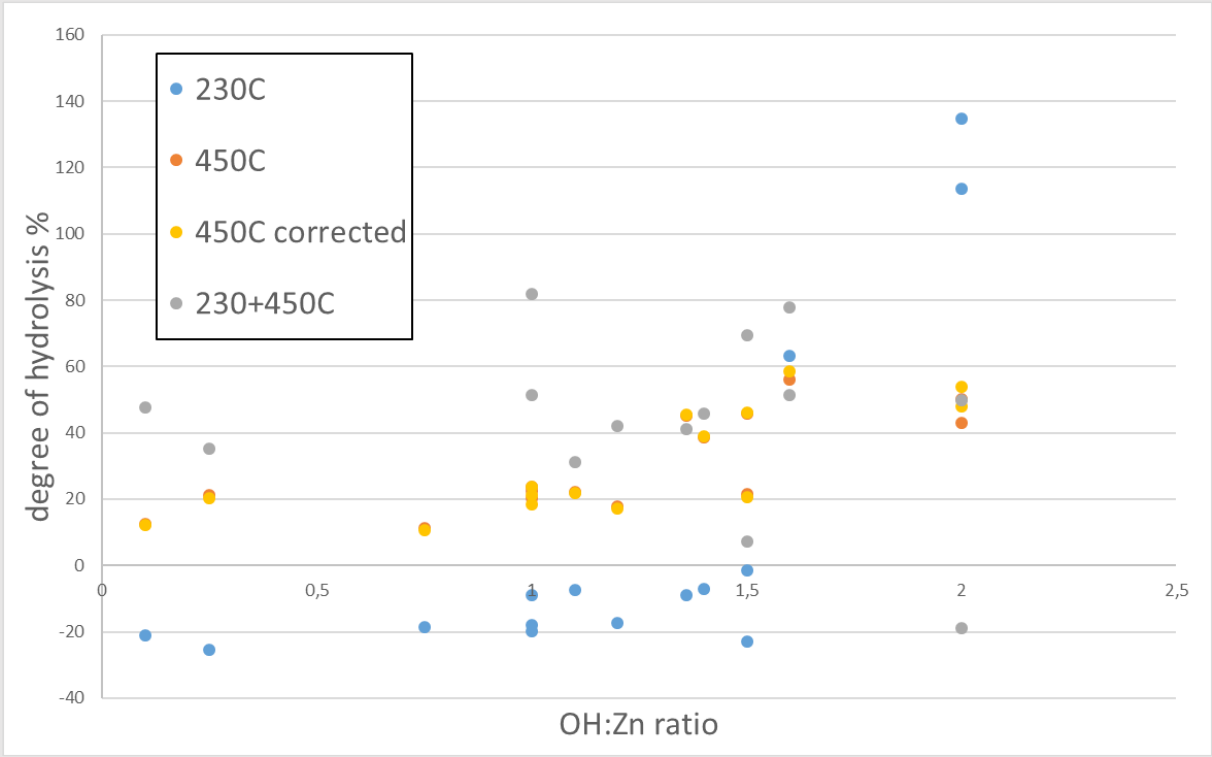

Figure 28: Calculated hydrolysis degree of $ZnCl_2$ during simonkolleite thermal degradation

The results using both mass losses are located between 0 and 100 %, except for one negative value. But because of the influence of the mass loss at 230 °C, they are not so reliable to estimate the hydrolysis degree. The results from the mass loss at 450 °C are more realistic, with values between 25 and 50 % of hydrolysis. To increase the accuracy of the calculations, it was proposed to compensate for the unknown amount of water adsorbed on the sample like previously in the case of the mass loss at 170 °C. It is considered that after 170 °C, the only products of simonkolleite decomposition remaining are Zn(OH)Cl, and ZnO. It is possible to rewrite the equations 31-33, in function of the remaining mass after the mass loss at 170 °C (equations 34-36). The corrected values are very close to the uncorrected ones, and only the hydrolysis calculated from the 450 °C mass loss are plausible.

$$m_{230C} = \frac{(1-x).MH_2O+2x.MHCl}{2MZHC+3MZnO}.f_{SK}.(100\% - m_{<170C} - m_{170C})$$

$$x = \frac{\frac{m_{230C}.(2MZHC+3MZnO)}{f_{SK}.(100-m_{<170C}-m_{170C})} - MH_2O}{2.MHCl-MH_2O} \quad (37)$$

$$m_{450C} = \frac{(1-x).MZnCl_2}{2MZHC+3MZnO}.f_{SK}.(100\% - m_{<170C} - m_{170C})$$

$$x = 1 - \frac{m_{450C}}{f_{SK}.(100\%-m_{<170C}-m_{170C})}.\frac{2MZHC+3MZnO}{MZnCl_2} \quad (38)$$

$$m_{230C} + m_{450C} = \frac{(1-x).(MH_2O+MZnCl_2)+2x.MHCl}{2MZHC+3MZnO}.f_{SK}.(100\% - m_{<170C} - m_{170C})$$

$$x = \frac{\frac{(m_{230C}+m_{450C}).(2MZHC+3MZnO)}{f_{SK}.(100\%-m_{<170C}-m_{170C})} - MH_2O - MZnCl_2}{2MHCl-MH_2O-MZnCl_2} \quad (39)$$

The results from the mass loss at 450 °C show that the degree of hydrolysis is around 18 ± 5 % for a OH:Zn ratio lower or equal to 1.2.

3.5.2 Synthesis of ZnO from thermal degradation of simonkolleite

Despite the absence of N_2 atmosphere, a similar decomposition mechanism was expected, with perhaps some extra oxidation of $ZnCl_2$ with atmospheric oxygen. After reaction, the product was observed by SEM (Figure 29). The layer structure was expected to remain, however the product consisted of aggregated spherical particles. This is probably due to a large change of volume, since not only water, but also $ZnCl_2$ is eliminated during the process. The aggregates are strongly linked and cannot be properly dispersed even under ultrasonic treatment, as shown on the Figure 29. Compared to ZnO obtained via direct precipitation, the calcinated product has a slightly yellow color, that might be due to defects in the ZnO structure (Figure 30). Possible deffects in the structure can be Cl^- ions or vacancies in the crystal lattice introducing new energy levels. However the XRD analysis showed no new absportion bands from the ZnO pattern.

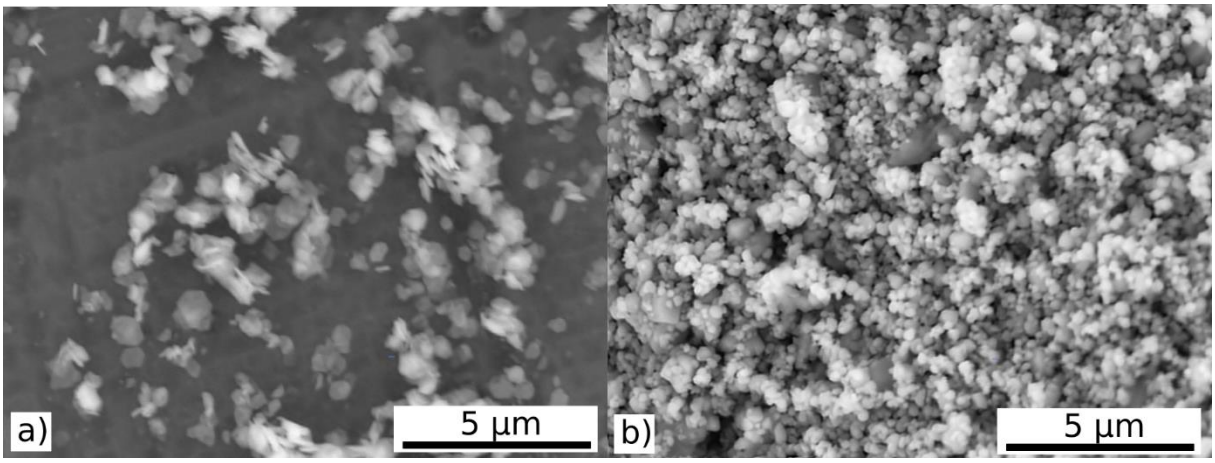

Figure 29: SEM scans of simonkolleite: a) before calcination; b) after calcination

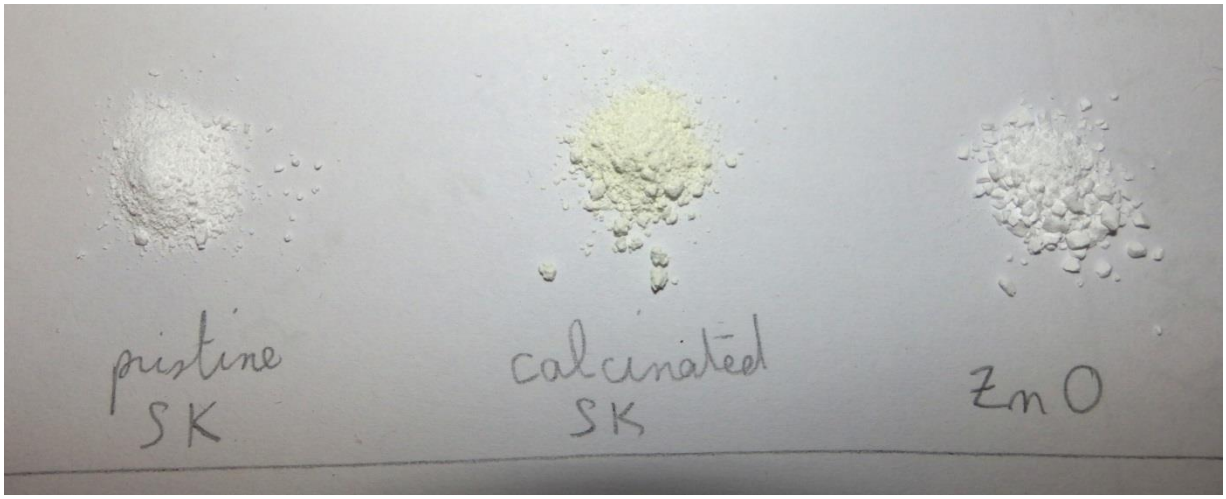

Figure 30: Visual aspect of simonkolleite (left), calcinated simonkolleite (middle), and ZnO (right)

3.5.2.1 Photocatalytic activity of the prepared ZnO

The concentration of methylene orange was assumed to be proportional to the intensity of the absorption peak at 490nm, after substraction of the baseline. As a result, curves displaying the relative concentration of methyl orange against reaction time were obtained (Figure 31).

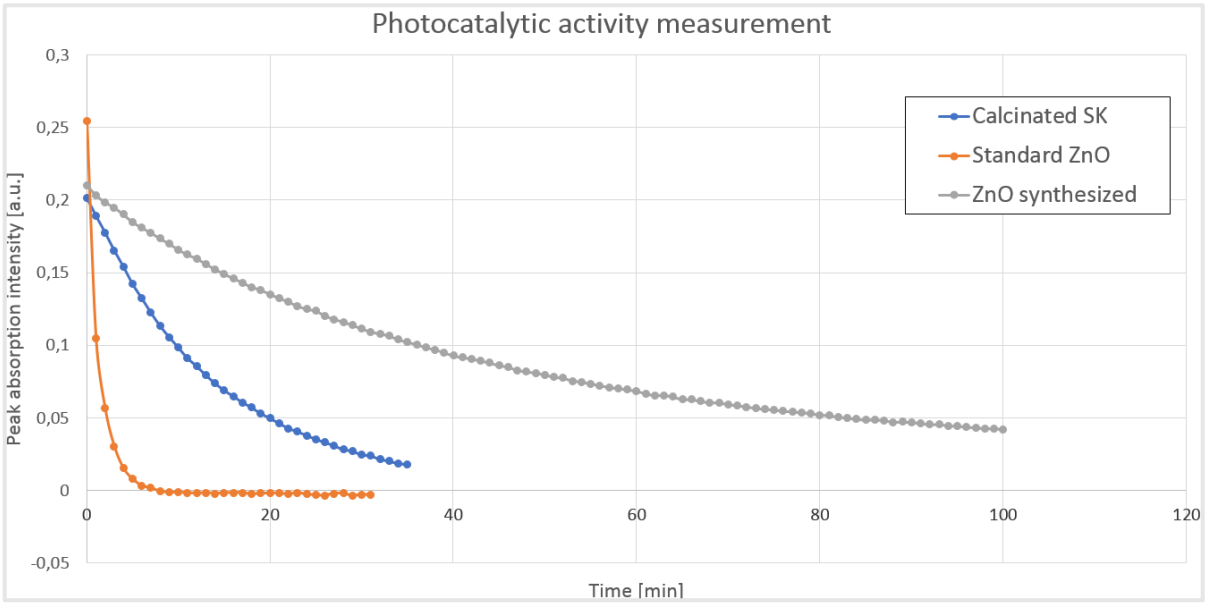

Figure 31: Intensity of methylene orange absorption peak against photodegradation reaction time

To assess the kinetic parameters and compare quantitatively the kinetic of degradation of each sample, the obtain data is fitted to a kinetic model. Assuming that the degradation mechanism is not autocatalyzed, and then it should take the following form:

$$-\frac{dx}{dt} = x^n . A . exp\left(\frac{-Ea}{RT}\right) \quad (40)$$

Where x is the intensity of the absorption peak at 490nm, n is the order of the reaction, Ea is the activation energy, R, the gas constant, and T the absolute temperature of the reaction mixture. A is a constant including both the pre-exponential kinetic factor and the proportional factor between the methylene orange and the absorption peak intensity.

It is further assumed that the temperature was stable over time, as the experiment was performed at room temperature, and the heat generated by the UV lamp can be neglected. The right part of scheme can therefore be simplified with a constant B:

$$-\frac{dx}{dt} = x^n . B \quad (41)$$

After integration over time, the scheme becomes:

$$\frac{1}{n-1}\left[x_f^{1-n} - x_i^{1-n}\right] = B.t \quad (42)$$

The remaining kinetic scheme contains two unknowns, that can be determined using excel solver by minimizing the sum of squared differences between the measured and calculated reaction time for each measured point. The results are summarized in Table 10.

Table 10: Comparative kinetic parameters of photodegradation reaction

Sample	***Calcinated SK***	***Synthesized ZnO***	***ZnO standard***
B	$7.17*10^{-2}$	$2.52*10^{-2}$	$7.23*10^{-1}$
N	1.03	1.00	1.51
R^2	0.9997	0.997	0.9997

As a result, the degradation was much slower for our two samples than for the standard ZnO. Since the ZnO catalyst is heterogenous, the kinetic of degradation is directly proportional to the specific surface. The decrease in catalytic activity can therefore be explained by the strong aggregation during the thermal degradation of simonkolleite, which led to a lower specific surface. However, it was observed that simonkolleite after calcination has a higher catalytic activity than the directly synthesized ZnO. This might be due to the presence of defects in the crystal, allowing to absorb light at different energy levels, or stabilizing the radicals on the ZnO surface created during the absorption of photons.

However, the results were not promising enough to justify pursuing the research in this direction. To improve the photocatalytic activity further, the particles should be individual to offer a higher specific surface.

3.6 Simonkolleite as anticorrosive agent

Additionally, it was attempted to exchange the Cl^- with ions, in the perspective to give anticorrosion properties to simonkolleite. Indeed, simonkolleite has a layered structure which can act as a barrier against the diffusion of corrosion promoters such as Cl^-, H_2O to the surface of the metal, as illustrated in Figure 32. Moreover, since PO_4^{3-} is known to provide good anticorrosion properties, it was theorized that its retention in simonkolleite would prolong its effect over time. Especially as Cl^- would start to diffuse in the coating, simonkolleite would have the ability to absorb them and release PO_4^{3-}, which could continue to migrate to the surface of the metal. The advantage of using simonkolleite instead of zinc phosphate is the layered structure, that add barrier effect and ion adsorption properties of simonkolleite. Theoretically, a partial replacement of Cl^- by PO_4^{3-} should not alter the layered structure of simonkolleite.

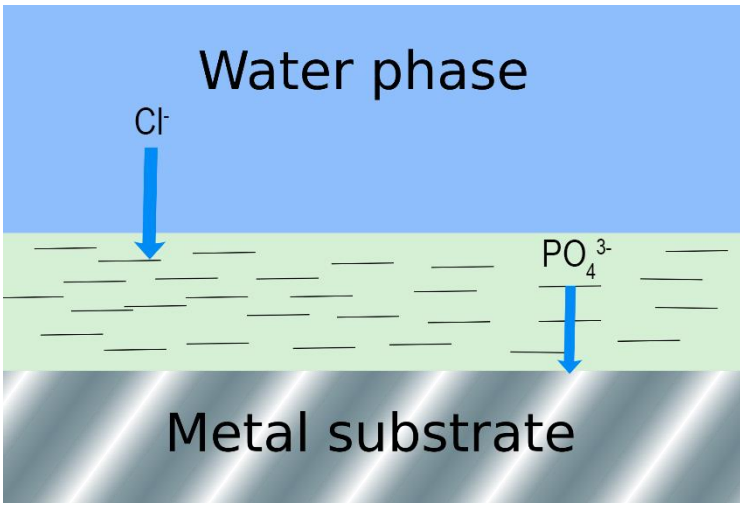

Figure 32: Illustration of anti-corrosion concept of phosphate modified simonkolleite

Simonkolleite was immersed in solutions of phosphates with different concentrations and different times. The samples of simonkolleite were soaked during periods of time ranging from 1 h to 3 weeks, with ultrasonic pretreatment. After the soaking period was over, the samples were filtered over paper, washed with distilled water and dried. They were tested by XRD to check the crystallographic structure was still intact.

However, the replacement of Cl^- by PO_4^{3-} resulted in a modification of the simonkolleite structure. the apparition of an unreferenced crystalline phase was observed for soaking times up to 24h, and the apparition of a second unreferenced phase plus $Zn_3(PO_4)_2.4H_2O$ for a soaking time of three weeks. RIR quantitative method was used to estimate the amount of the unknown phase synthesized. However, in the absence of any reference data, the values are only relative and do not inform us about the real content of each phase (Table 11).

Table 11: Summarize of experiment conditions for simonkolleite soaking on phosphate solution

Sample	***Soaking time***	***Pretreatment***	***SK peak intensity***	***Unknown phase peak intensity***	***Ratio***
1	1 h	5 min US	130.2	187.59	1.44
2	30 min	30 min US	134.85	267.06	1.98
3	1 h	1 h US	114.69	249.96	2.15
4	6 h	5 min US	100.77	209.69	2.08
5	24 h	5 min US	94.81	229.13	2.42
6$^+$	6 h	5 min US	22.94	282.15	12.30
7*	3 weeks	5 min US	/	/	/

+ a double amount of solution was added
* only $Zn_3(PO_4)_2.4H_2O$ and a second unknown phase are obtained

When comparing the samples 1 and 2, it seems that a longer ultrasonic treatment increases the conversion, while the total soaking time remains the same. However, when comparing the samples 2 and 3, it appears the conversion reaches a plateau, with a ratio of peak intensity of approximatively 2. When comparing samples 1, 4 and 5, a slow increase of the conversion is observed, with a peak intensity ratio increasing from 1.4 to 2.4. However, the conversion is quite slow, and is limited in time, since a totally different phase is formed after three weeks, as shown in sample 7. Additionally, one experiment was performed with a double amount of phosphate solution, while keeping a constant concentration (sample 6). When comparing it with the sample 4, the peak intensity ratio increased from 2 to 12.

This shows that an increase of the total amount of phosphate has a stronger influence than the reaction time, or the ultrasonic treatment on the conversion degree.

Additionally, SEM scans of the samples containing the unreferenced phase to check its morphology were performed (Figure 33). The samples presented some remaining plates corresponding to simonkolleite, along with some long square based sticks, constituting the unknown phase. The simonkolleite platelets appear to lose their regular shape, having holes bumpy surface. Also the fact that the unknown phase didn't keep the plate shape renders it improper for the anti-corrosive intended use, since they will lose their barrier effect, and probably their ion exchange capacity.

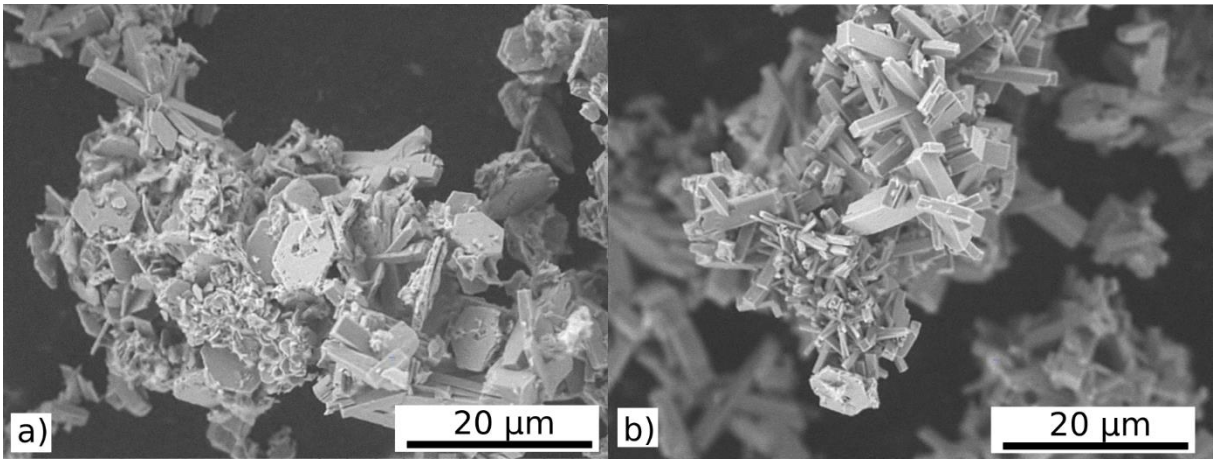

Figure 33: SEM scans of sample 1 (a), and sample 2 (b), showing two coexisting different morphologies

3.7 Preparation of composites

The last of the potential applications for simonkolleite is the property improvement of polymers. A diglycidylether of bisphenol A epoxy system was chosen for this study, cross-linked with a diamino polyether hardener (Figure 34).

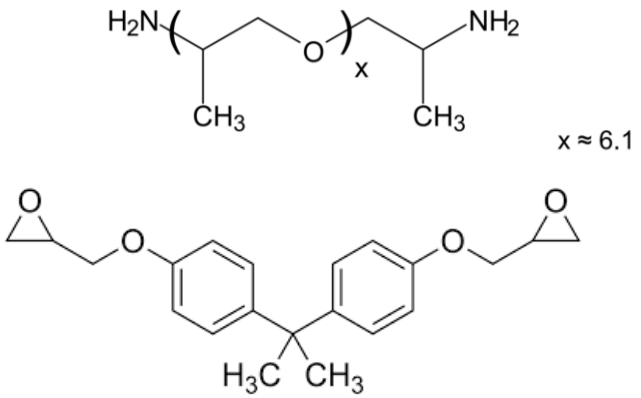

Figure 34: Chemical structure of used monomers

In a typical composite preparation, the particles are first dried and redispersed in the amine reactive rather than the epoxy because it is more hydrophilic and therefore has a better affinity with simonkolleite. However, sedimentation of the particles in the amine reactive was observed within a few hours to a few days at room temperature.

To ensure an optimal interface between the matrix and the nanoparticles, the simonkolleite particles were modified by Toseda to obtain reactive amine groups on the nanoparticle surface. The amount of amine groups per gram of particles was estimated by TGA, by quantifying the amount of simonkolleite, according to the method described previously in section 3.5.1. The TGA analysis of modified simonkolleite showed one sharp transition around 170 °C, corresponding to the first simonkolleite transition, then the second transition is overlapping with the decomposition of the surface modifier (Figure 35). Residual solvent is evaporated above 100 °C, corresponding to 4.15 % mass loss. The mass loss around 170 °C corresponds to 9.03 % of the product remaining after solvent removal. Since the experimental first mass loss of Simonkolleite is 11.0 %, is was deduced there is 82 % of Simonkolleite in the dry product, and 18 % of modifier. The equivalent weight of the modifier per active primary amine given by Toseda is 130.74 g/mol of NH_2. The particles after modification therefore have an equivalent weight of 726.33 g/mol of NH_2.

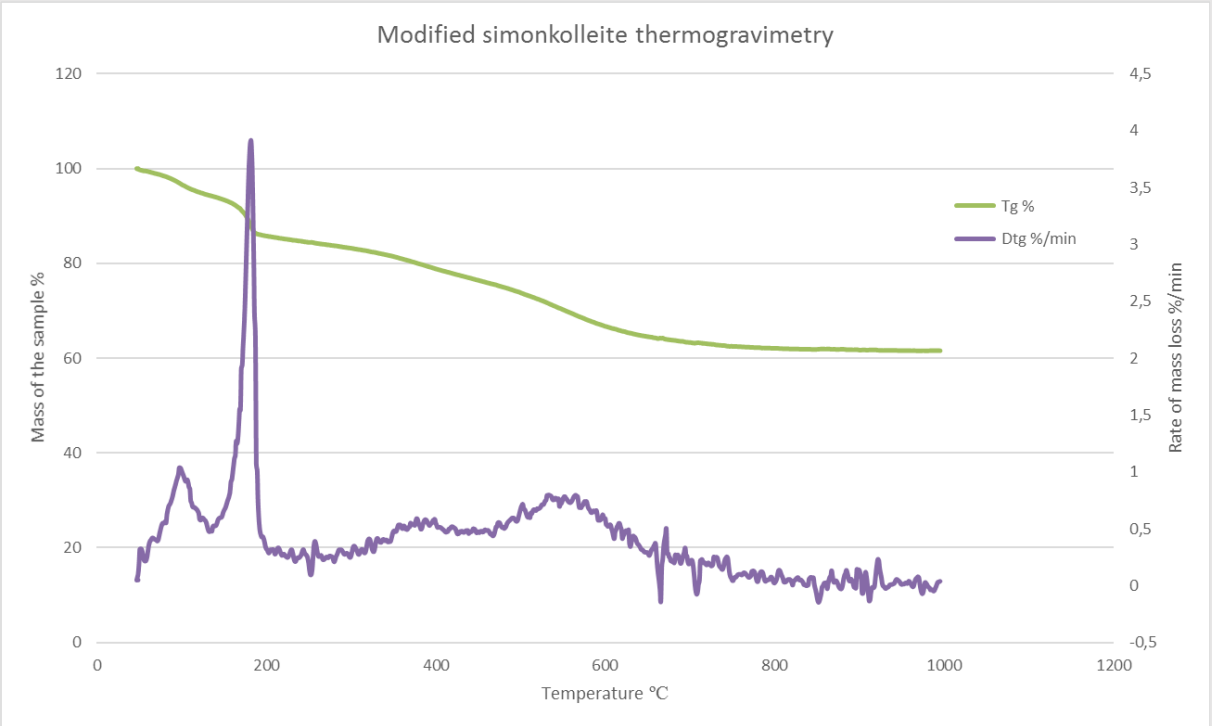

Figure 35: Thermogravimetry of simonkolleite functionalized with amines

Composite sheets of modified simonkolleite in an epoxy matrix were then prepared. The matrix was composed of CHSE 530 and Jeffamine D400, and the amount of modified simonkolleite was 5% in weight. The resulting samples are both transparent, although the sample with simonkolleite is slightly coloured (Figure 36). Despite the degassing, the presence of bubbles in the composite was observed, which may affect adversely the mechanical performances, more particularly the strength of the material. The composite with unmodified simonkolleite was opaque, owing to a bad dispersion, whereas the composite with modified simonkolleite was transparent. However, SEM scans of the fractured composite with modified simonkolleite showed a non-homogeneous repartition of the particles in the system (Figure 37). XRD was performed on the composite as well, but the pattern was not as clear as the one obtained from pure simonkolleite sample.

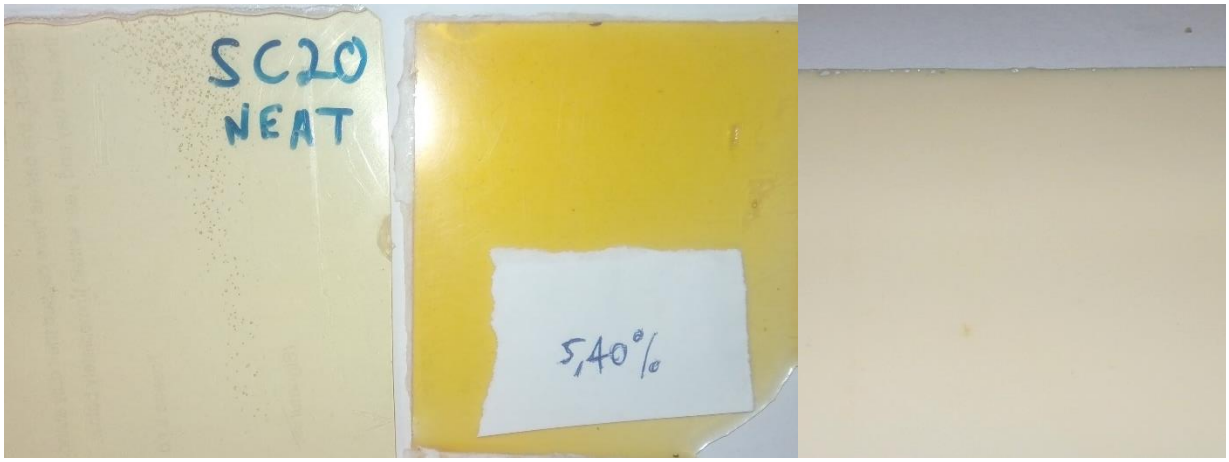

Figure 36: Comparison of the neat system (left), the composite loaded with 5% weight content of modified simonkolleite (middle), and the composite with 5% of unmodified simonkolleite (right)

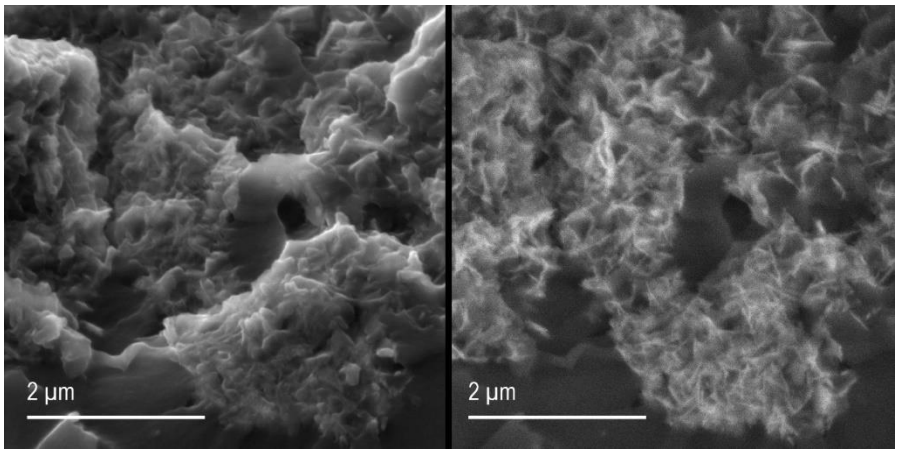

Figure 37: SEM scans of fractured composite with modifed simonkolleite in SE mode on the left and BSE mode on the right.

Several mathematical models such as, Kerner, Nielsen, Halpin-Tsai, and Mori-Tanaka were developed to estimate the modulus of composites based on different kinds of nano-particles and their orientation. Spherical nanoparticles provide the weakest reinforcement, whereas sheets, nanofibers and nanotubes provides a stronger reinforcement, that may be strongly anisotropic if the nanoparticles are aligned in one direction. The mechanical properties improvement of the composite filled by simonkolleite can be estimated by the use of two different methods: Halpin-Tsai, and Lewis-Nielsen.

Halpin-Tsai estimates the composite modulus according to the following equation:

$$E = \frac{1+\xi\eta V_f}{1-\eta V_f} E_m \tag{43}$$

where E is the composite modulus, V_f the volume fraction of the filler, E_m the modulus of the neat polymer, η and ξ are two constants.

η can be estimated by the following equation:

$$\eta = \frac{E_p/E_m - 1}{E_p/E_m + \xi} \tag{44}$$

where Ep is the modulus of the filler

ξ is a shape factor and depends on the orientation of the filler relative to the applied strain.

- ξ = 2 ,when the loading is perpendicular to the particles orientation,
- ξ = 2*a/b otherwise, where a/b is the aspect ratio of the filler particles.

In our case, the volume fraction of simonkolleite is 1.72%, we estimate its modulus to be similar to ZnO, and therefore 40 GPa [71]. The aspect ratio of simonkolleite is approximately 30. The shear modulus of the neat polymer is 4.29 MPa according to DMA measurements. The shear modulus estimated from the Halpin-Tsai theory should vary between 4.52 and 9.58 MPa in rubber state, depending on the orientation of the simonkolleite particles.

Alternatively, Lewis-Nielsen theory estimates the modulus of composite according to the following equation:

$$E = \frac{1+(k_E-1)\beta V_f}{1-\mu\beta V_f} E_m \quad (45)$$

Where E is the modulus of the composite, V_f the volume fraction of the filler, E_m the modulus of the neat polymer, k_E the Einstein constant, μ and β two constants.

k_E depends on the interfacial adhesion between the polymer and the filler. In the case of a good adhesion we will take a value of 2.2, and 0.9 in the case of a bad adhesion.

β can be calculated from the following equation:

$$\beta = \frac{E_p/E_m - 1}{E_p/E_m + k_E - 1} \quad (46)$$

where E_p is the filler modulus.

Finally, μ can be calculated from the following equation:

$$\mu = 1 + \frac{1+V_f}{V_{max}}\left[V_f V_{max} + (1 - V_{max})(1 - V_f)\right] \quad (47)$$

where V_{max} is the maximum filler volume fraction attainable.

In our case, the volume fraction of simonkolleite is 1.72%, we estimate its modulus to be similar to ZnO, and therefore 40 GPa [71]. The shear modulus of the neat polymer is 4.29 MPa according to DMA measurements. The maximum volume of filler attainable for the geometry of the simonkolleite particles is 0.68 [72]. The shear modulus estimated from the Lewis-Nielsen theory should vary between 4.39 and 4.49 MPa in rubber state, depending on the interfacial adhesion between simonkolleite and the polymer.

DMA measurements were performed on rectangular samples, from room temperature to 100°C (Figure 38). Both shear storage and shear loss modulus were measured during the temperature ramp. Results show very similar storage modulus in glassy state, very similar glass transition temperature, but an increase of 70% storage modulus in the rubber state for the composite with modified simonkolleite (Table 12). Even at low simonkolleite loading content, a significant increase of the mechanical performances was observed. This result was compared with computed values from both Halpin-Tsai and Lewis-Nielsen theories. Halpin-Tsai yielded a wider range of values : 4.52 to 9.58 MPa, than Lewis-Nielsen : 4.39 to 4.49 MPa. The actual results are located close to the middle of the range calculated from Halpin-Tsai, but is outside of the range calculated by Lewis-Nielsen theory. The glass transition was however not significantly shifted.

Table 12: DMA results of a composite with 5% modified simonkolleite and a neat system

	Pristine matrix	***Composite with simonkolleite***
Storage modulus in glassy state	1.11 GPa	1.14 GPa
Glass transition	61 °C	63 °C
Storage modulus in rubber state	4.29 MPa	7.30 MPa
Theoretical modulus according to Halpin-Tsai		4.52 to 9.58 MPa
Theoretical modulus according to Lewis-Nielsen		4.39 to 4.49 MPa

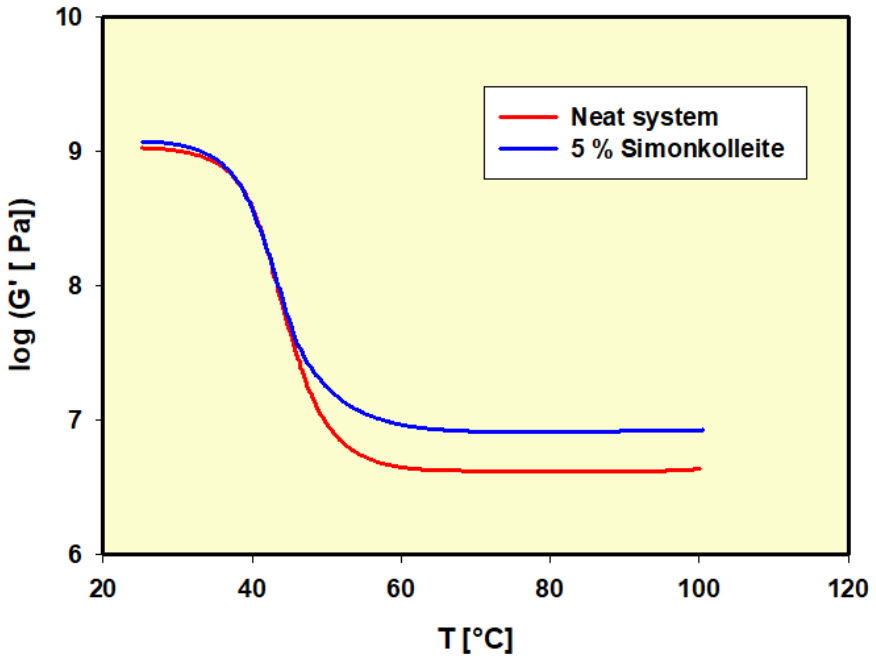

Figure 36: DMA plot of the storage modulus against the temperature of the composite and neat systems

The barrier effect of simonkolleite nanoparticles against solvent intake was further investigated. To this purpose, square samples of the two systems were cut and let to soak in toluene while monitoring the weight changes of the samples along time. The geometry of the samples was both 20 mm*20 mm*2 mm to eliminate any effects of the geometry on the results After three days of soaking in toluene, both samples lost their structural integrity.

It was found out, that the mass increase is proportional to the square root of the time for both systems. The intake was found to be 28 % slower for the composite system than the neat system. This is to be expected since simonkolleite has a sheet structure and is imprevious to toluene. It is also possible that the sheets oriented themselves in a coplanar orientation with the mold walls during pouring of the uncured mixture (Figure 37).

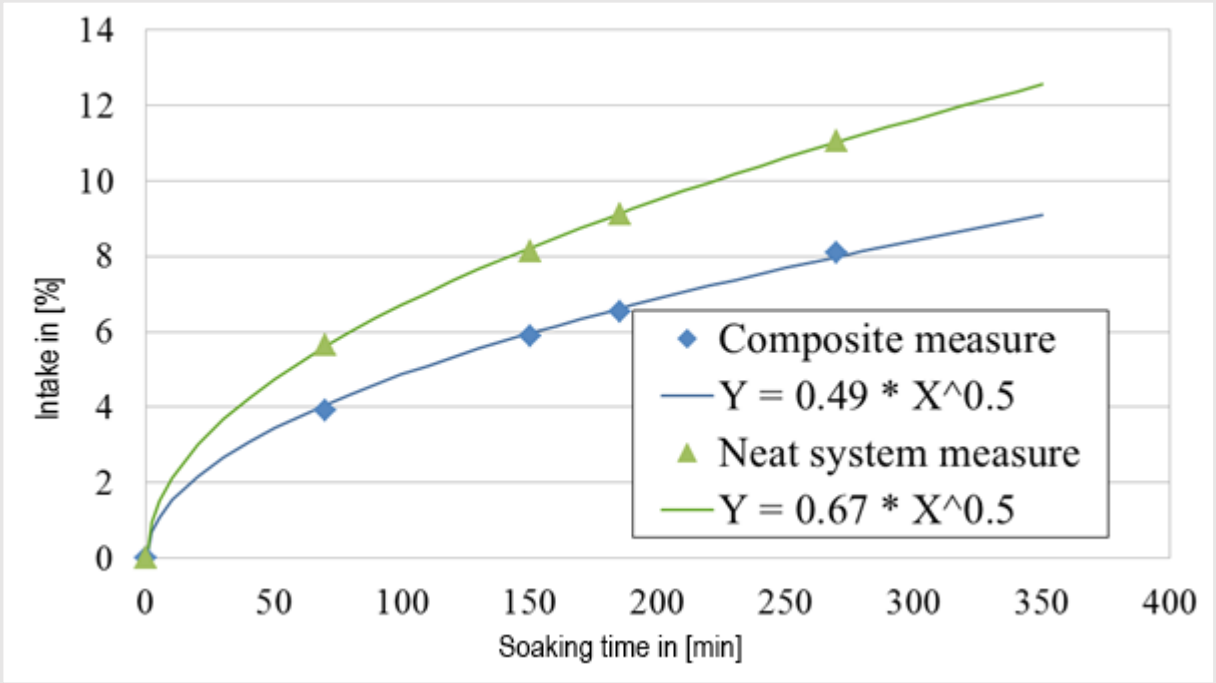

Figure 37: Mass changes of pristine polymer and composite vs. time

The modification of simonkolleite by chemically bounded amine terminated molecules improved the dispersion quality and prevented sedimentation of the particles in the composite. Mechanical performances of the polymer were improved even at low loading of nanoparticles, and the barrier properties of simonkolleite against solvent were demonstrated.

4. Conclusion

The main goals of this thesis were at first to test two possible synthesis methods for the synthesis of ZnO and/or simonkolleite, both based on a precipitation of salts in aqueous media. Subsequently, the most promising method should be studied with the aim of more closely to understand the precipitation mechanism and to find out the influence of different synthesis parameters on the product. Further aim was to study the effect of n-butanol on simonkolleite and ZnO stabilization in aqueous suspension, both after and during the synthesis process. And finally, three potential applications were chosen to be explored for the synthesized products: ZnO as a photocatalyst, simonkolleite as an anticorrosive agent, and surface modified simonkolleite as a filler for a polymeric matrix.

Two synthesis methods were tested to produce ZnO, following a wet precipitation of $ZnCl_2$ salt. Both methods consist of precipitating Zn^{2+} ions with OH^-. In the first method, hydrogen peroxide was used as a source of oxygen, but the Zn^{2+} ions are also oxidized into Zn^{4+}, and yield ZnO_2 rather than ZnO. In the second method, no peroxide was used and OH^- ions were the main source of oxygen. The second method allows to yield both ZnO and simonkolleite.

The precipitation mechanism was studied and it was concluded that a higher molar ratio of OH:Zn favored the formation of ZnO, while the addition of Cl^- ions did have a faint influence on the nature of the product. The initial pH had a strong influence on the size of the simonkolleite particles, whereas the OH:Zn molar ratio had no strong effect on the size or shape of the product.

Butanol was found to improve slightly the dispersion stability of simonkolleite into water. It was theorized that the hydrophobic chains reduce their free energy by bonding to the simonkolleite surface and act as a stabilizer. However, since the chains are short and in the absence of electrostatic stabilization, the particles eventually aggregated and sedimented. The effect of butanol on both ZnO and simonkolleite morphology was studied in the concentration range where it stabilized the best simonkolleite dispersions. The effects were very faint, especially for ZnO where it did not prevent aggregation of the nanoparticles.

Further, three potential applications of simonkolleite were studied. The use of simonkolleite for the intercalation of other molecules was theorized, but in the case of the replacement of Cl^- with PO_4^{3-}, the structure of simonkolleite was destabilized, and the layered

shape was lost. Furthermore, the thermal conversion of simonkolleite into ZnO was also tested, but a strong aggregation occurred. The final ZnO did not retained the layered shape of the simonkolleite, but showed strong aggregates, which would be impossible to break down to individual particles unless using milling. The photocatalytic activity of the synthesized ZnO was tested, but it was lower than at standard ZnO commercially available. Finally, composites were prepared using surface modified simonkolleite particles. After dispersion of reactive mixture by US the cured samples showed transparency and a shear modulus 70% higher in rubber state.

The major outputs of this work are the understanding of simonkolleite/ZnO formation, and the control over the proportion of simonkolleite and ZnO in the final product by controlling the synthesis conditions. It was shown that simonkolleite has a potential in polymers for barrier effect, and might also behave well as a fire retardant, but was not tested. Although it does not possess the same properties as ZnO, simonkolleite was the most successful product in term of nano-structure, given the synthesis constraints.

Finally, some potential applications that were not explored in this work further include: fire retardant properties due to the layered structure hindering the diffusion of oxygen in a material during combustion, and the release of water during the thermal decomposition of simonkolleite; and the depollution of water and soil by ion absorption of simonkolleite as a general layered zinc hydroxide.

5. List of References

[1] Hough, D. B., and White, L. R.: *The calculation of hamaker constants from liftshitz theory with applications to wetting phenomena*. Adv. Colloid Interface Sci. (14) (1980) 3–41.

[2] Israelachvili, J. N.: *Intermolecular and surface forces*, in Intermol. Surf. Forces, 2nd ed., (1991), pp. 176–209.

[3] Bergström, L.: *Hamaker constants of inorganic materials*. Adv. Colloid Interface Sci. (70) (1997) 125–169.

[4] Kuo, C. Y., and Gau, C.: *Vapor–solid–solid growth of crystalline silicon nanowires using anodic aluminum oxide template*. Thin Solid Films (519) (2011) 3603–3607.

[5] Song, Y. L.: *Ultrasonic spray pyrolysis for nanoparticles*. J. Mater. Sci. (39) (2004) 3647–3657.

[6] Lew, K.-K., Reuther, C., et al.: *Template-directed vapor–liquid–solid growth of silicon nanowires*. J. Vac. Sci. Technol. B Microelectron. Nanom. Struct. (20) (2002).

[7] Zhang, S. C., Mulholland, G., et al.: *Synthesis of ZrO2 nanoparticles by spray pyrolysis.* J. Mater. Synth. Process. (1996).

[8] Strambeanu, N., Demetrovici, L., et al.: *Natural sources of nanoparticles*, in Nanoparticles' Promises Risks Charact. Manip. Potential Hazards to Humanit. Environ., (2015).

[9] Sasaki, T., Xiaoyan, Z., et al.: *Fabrication of iron oxide nanoparticles by pulsed-laser ablation*. Adv. Laser Ablation Mater. Symp. (1998).

[10] Sharma, V. K., Filip, J., et al.: *Natural inorganic nanoparticles – formation, fate, and toxicity in the environment*. Chem. Soc. Rev. (44) (2015) 8410–8423.

[11] Yang, G.: *Laser Ablation in Liquids: Principles and Applications in the Preparation of Nanomaterials*, in Laser Ablation Liq., (2012).

[12] Berengueres, J., Saito, S., et al.: *Structural properties of a scaled gecko foot-hair*. Bioinspir. Biomim. (2007) 1–8.

[13] Almusallam, A., Luo, Z., et al.: *Flexible piezoelectric nano-composite films for kinetic energy harvesting from textiles*. Nano Energy (2017).

[14] Wang, J., Chen, H., et al.: *Investigation on hydrophobicity of lotus leaf: Experiment and theory*. Plant Sci. (176) (2009) 687–695.

[15] Esmaeili, A., and Haseli, M.: *Electrospinning of thermoplastic carboxymethyl cellulose/poly(ethylene oxide) nanofibers for use in drug-release systems*. Mater. Sci. Eng. C (2017).

[16] Liu, R., Liu, M., et al.: *Preparation of highly flexible SiC nanowires by fluidized bed chemical vapor deposition*. Chem. Vap. Depos. (21) (2015) 196–203.

[17] Anka, F. H., and Balkus, K. J.: *Novel nanofiltration hollow fiber membrane produced via electrospinning*. Ind. Eng. Chem. Res. (2013).

[18] Dutta, A., and Basu, S.: *Modified CVD growth and characterization of ZnO thin films*. Mater. Chem. Phys. (34) (1993) 41–45.

[19] Chang, P.-C., Fan, Z., et al.: *Characterization ZnO Nanowires Synthesized by Vapor Trapping CVD Method*. Microsc. Microanal. (2004).

[20] Zhu, G., Zhou, Y., et al.: *Synthesis of vertically aligned ultra-long ZnO nanowires on heterogeneous substrates with catalyst at the root*. Nanotechnology (2012).

[21] Zhao, Q. X., Klason, P., et al.: *Growth of ZnO nanostructures by vapor-liquid-solid method*. Appl. Phys. A Mater. Sci. Process. (2007).

[22] Dai, Z. R., Pan, Z. W., et al.: *Novel nanostructures of functional oxides synthesized by thermal evaporation*. Adv. Funct. Mater. (2003).

[23] Özgür, Ü., Alivov, Y. I., et al.: *APPLIED PHYSICS REVIEWS A comprehensive review of ZnO materials and devices*. J. Appl. Phys. (2005).

[24] Rul, H., Mondelaers, D., et al.: *Water-based wet chemical synthesis of (doped) ZnO nanostructures*. J. Sol-Gel Sci. Technol. (2006).

[25] Oliveira, A. P. A., Hochepied, J. F., et al.: *Controlled precipitation of zinc oxide particles at room temperature*. Chem. Mater. (2003).

[26] Ashfold, M. N. R., Doherty, R. P., et al.: *The kinetics of the hydrothermal growth of ZnO nanostructures*. Thin Solid Films (515) (2007) 8679–8683.

[27] Sunandan, B., and Joydeep, D.: *Hydrothermal growth of ZnO nanostructures*. Sci. Technol. Adv. Mater. (2009).

[28] Demoisson, F., Piolet, R., et al.: *Hydrothermal growth of ZnO nanostructures in supercritical domain: Effect of the metal salt concentration (Zn(NO3)2) in alkali medium (KOH)*. J. Supercrit. Fluids (97) (2015) 268–274.

[29] Mahalingam, T., John, V. S., et al.: *Electrodeposition and characterization of transparent ZnO thin films*. Sol. Energy Mater. Sol. Cells (88) (2005) 227–235.

[30] Illy, B. N., Cruickshank, A. C., et al.: *Electrodeposition of ZnO layers for photovoltaic applications: controlling film thickness and orientation*. J. Mater. Chem. (2011).

[31] Ludwig, W., Ohm, W., et al.: *Electrodeposition parameters for ZnO nanorod arrays for photovoltaic applications*. Phys. Status Solidi Appl. Mater. Sci. (2013).

[32] Sun, K., Zeimpekis, I., et al.: *Low-cost top-down zinc oxide nanowire sensors through a highly transferable ion beam etching for healthcare applications*. Microelectron. Eng. (2016).

[33] Moribe, K., Ueda, K., et al.: *Nano-sized crystalline drug production by milling technology*. Curr. Pharm. Des. (2013).

[34] Hou, T.-H., Su, C.-H., et al.: *Parameters optimization of a nano-particle wet milling process using the Taguchi method, response surface method and genetic algorithm*. Powder Technol. (2007).

[35] Azizian-Kalandaragh, Y., Khodayari, A., et al.: *Ultrasound-assisted synthesis of ZnO semiconductor nanostructures*. Mater. Sci. Semicond. Process. (2009).

[36] Pal, U., Kim, C. W., et al.: *Ultrasound-assisted synthesis of mesoporous ZnO nanostructures of different porosities*. J. Phys. Chem. C (2009).

[37] Xu, Z. P., Zhang, J., et al.: *Catalytic applications of layered double hydroxides and derivatives*. Appl. Clay Sci. (53) (2011) 139–150.

[38] Baikousi, M., Stamatis, A., et al.: *Thiamine pyrophosphate intercalation in layered double hydroxides (LDHs): An active bio-hybrid catalyst for pyruvate decarboxylation*. Appl. Clay Sci. (75–76) (2013) 126–133.

[39] Machado, G. S., Wypych, F., et al.: *Anionic iron(III) porphyrins immobilized on zinc hydroxide chloride as catalysts for heterogeneous oxidation reactions*. Appl. Catal. A Gen. (413–414) (2012) 94–102.

[40] Kozai, N., Mitamura, H., et al.: *Synthesis and characterization of nickel-copper hydroxide acetate, NiCu(OH)3.1(OCOCH3)0.9 ??? 0.9H2O*. Microporous Mesoporous Mater. (89) (2006) 123–131.

[41] Tagaya, H., Sasaki, N., et al.: *Preparation of New Inorganic—Organic Layered Compounds, Hydroxy Double Salts, and Preferential Intercalation of Organic Carboxylic Acids into Them*. Mol. Cryst. Liq. Cryst. Sci. Technol. Sect. A. Mol. Cryst. Liq. Cryst. (341) (2000) 413–418.

[42] Tagaya, H., Sasaki, N., et al.: *Preferential intercalation of isomers of naphthalenecarboxylate ions into the interlayer of layered double hydroxides*. Chem. Mater. (1993) 1431:1433.

[43] Komarneni, S., Menon, V. C., et al.: *Microwave-Hydrothermal Processing of BiFeO3 and CsAl2PO6*. J. Am. Ceram. Soc. (79) (1996) 1409–12.

[44] Rives, V., Del Arco, M., et al.: *Layered double hydroxides as drug carriers and for controlled release of non-steroidal antiinflammatory drugs (NSAIDs): A review*. J. Control. Release (169) (2013) 28–39.

[45] Rojas, R., and Giacomelli, C. E.: *Effect of structure and bonding on the interfacial properties and the reactivity of layered double hydroxides and Zn hydroxide salts*. Colloids Surfaces A Physicochem. Eng. Asp. (419) (2013) 166–173.

[46] Rojas, R., and Giacomelli, C. E.: *Size-tunable LDH–protein hybrids toward the optimization of drug nanocarriers*. J. Mater. Chem. B (2015).

[47] Lonkar, S. P., Kutlu, B., et al.: *Nanohybrids of phenolic antioxidant intercalated into MgAl-layered double hydroxide clay*. Appl. Clay Sci. (71) (2013) 8–14.

[48] Li, D., Tuo, Z., et al.: *Preparation of 5-benzotriazolyl-4-hydroxy-3-sec-butylbenzenesulfonate anion-intercalated layered double hydroxide and its photostabilizing effect on polypropylene*. J. Solid State Chem. (179) (2006) 3114–3120.

[49] Cursino, A. C. T., Gardolinski, J. E. F. C., et al.: *Intercalation of anionic organic ultraviolet ray absorbers into layered zinc hydroxide nitrate*. J Colloid Interface Sci. (347) (2010) 49–55.

[50] Audebrand, N., Auffredic, J. ., et al.: *X-ray-diffraction study of the early stages of the growth of nanoscale zinc-oxide crystallites obtained from thermal-decomposition of 4 precursors - general concepts on precursor-dependent microstructural properties*. Chem. Mater. (1998) 2450:2461.

[51] Markov, L., Ioncheva, R., et al.: *Synthesis and thermal decomposition of Cu(II)-Zn(II) hydroxide nitrate mixed crystals*. Mater. Chem. Phys. (1990) 493:504.

[52] Wang, Z., Han, E., et al.: *Influence of nano-LDHs on char formation and fire-resistant properties of flame-retardant coating*. Prog. Org. Coatings (53) (2005) 29–37.

[53] Camino, G., Maffezzoli, A., et al.: *Effect of hydroxides and hydroxycarbonate structure on fire retardant effectiveness and mechanical properties in ethylene-vinyl acetate copolymer*. Polym. Degrad. Stab. (2001) 457:464.

[54] Allmann, R.: *The crystal structure of pyroaurite*. Acta Crystallogr. Sect. B Struct. Crystallogr. Cryst. Chem. (1968).

[55] Taylor, H. F. W.: *Segregation and cation-ordering in sjogrenite and pyroaurite*. Mineral. Mag. (1969).

[56] Arizaga, G. G. C., Satyanarayana, K. G., et al.: *Layered hydroxide salts: Synthesis, properties and potential applications*. Solid State Ionics (178) (2007) 1143–1162.

[57] Boshkov, N., Petrov, K., et al.: *Galvanic alloys Zn-Mn - Composition of the corrosion products and their protective ability in sulfate containing medium*. Surf. Coatings Technol. (194) (2005) 276–282.

[58] Hawthorne, F. C., and Sokolova, E.: *Simonkolleite, Zn5 (OH)8 Cl2 (H2O), a decorated interrupted-sheet structure of the form [MΦ2]4*. Can. Mineral. (40) (2002) 939–946.

[59] Schmetzer, K., Schnorrer-Köhler, G., et al.: *Wülfingite, ε-Zn(OH)2, and simonkolleite, Zn5(OH)8Cl2•H2O, two new minerals from Richelsdorf, Hesse, F.R.G.* Neues Jahrb. Miner. Monatsh. (1985) 145:154.

[60] Zhu, Y., Zhang, X., et al.: *Hydrogen bonding directed assembly of simonkolleite aerogel by a sol–gel approach*. Mater. Des. (93) (2016) 503–508.

[61] Khamlich, S., Bello, A., et al.: *Hydrothermal synthesis of simonkolleite microplatelets on nickel foam-graphene for electrochemical supercapacitors*. J. Solid State Electrochem. (17) (2013) 2879–2886.

[62] Khamlich, S., Mokrani, T., et al.: *Microwave-assisted synthesis of simonkolleite nanoplatelets on nickel foam–graphene with enhanced surface area for high-performance supercapacitors*. J. Colloid Interface Sci. (461) (2016) 154–161.

[63] Momodu, D. Y., Barzegar, F., et al.: *Simonkolleite-graphene foam composites and their superior electrochemical performance*. Electrochim. Acta (151) (2015) 591–598.

[64] Sithole, J., Ngom, B. D. D., et al.: *Simonkolleite nano-platelets: Synthesis and temperature effect on hydrogen gas sensing properties*. Appl. Surf. Sci. (2012).

[65] Merzlyakov, M., and Schick, C.: *Thermal conductivity from dynamic response of DSC*, in Thermochim. Acta, (2001).

[66] Singh, N., Mittal, S., et al.: *Controlling the flow of nascent oxygen using hydrogen peroxide results in controlling the synthesis of ZnO/ZnO2*. Chalcogenide Lett. (7) (2010) 275–281.

[67] Ullah, M. H., Kim, I., et al.: *One-step synthetic route for producing nanoslabs: Zn-oriented polycrystalline and single-crystalline zinc oxide*. J. Mater. Sci. (2006).

[68] Moezzi, A., Cortie, M., et al.: *Formation of Zinc Hydroxide Nitrate by H^+ -Catalyzed Dissolution-Precipitation*. Eur. J. Inorg. Chem. (2013) (2013) 1326–1335.

[69] Mohsin, S. M. N., Hussein, M. Z., et al.: *Synthesis of (cinnamate-zinc layered hydroxide) intercalation compound for sunscreen application.* Chem. Cent. J. (2013).

[70] Kozawa, T., Onda, A., et al.: *Effect of water vapor on the thermal decomposition process of zinc hydroxide chloride and crystal growth of zinc oxide*. J. Solid State Chem. (2011).

[71] Yoshimura, H.N., Molisani, A.L., et al.: *Mechanical Properties and Microstructure of Zinc Oxide Varistor Ceramics*. Materials Science Forum. (530-531) (2011) 408-413.

[72] Li, S., Zhao, J., et al.: *Maximum packing densities of basic 3D objects*. Chin. Sci. Bull.. (55) (2010) 114-119.

List of Student's Published Works

Author's publication related to the dissertation topic:

Articles in specialized journals

Gorodylova, N., **Cousy, S**., Šulcová, P., Svoboda, L. (2017).
Thermal transformation of layered zinc hydroxide chloride: A review.
Journal of Thermal Analysis and Calorimetry, 127 (2017), 675–683. https://doi.org/10.1007/s10973-016-5517-4

Cousy S., Gorodylova N., Svoboda L., Zelenka J.
Influence of synthesis conditions over simonkolleite/ZnO precipitation
Chemical Papers, (2017) 1-10

Matysová E., **Cousy S**., Zelenka J., Svoboda L.
Preparation of zinc oxide nanopaticles for polymeric systems
Scientific Papers of the University of Pardubice, Serie A 23 (2017) 157-168

Participation in international conferences

Zelenka J., Matysová E., Zelenková M., **Cousy S**., Vlček T.
Polymeric systems modified by ZnO nanoparticles
Nanocon 2014, Brno, Czech Republic, 5.-7.11.2014, poster, ISBN 978-80-87294-55-0.

Zelenka J., Matysová E., Zelenková M., **Cousy S**., Vlček T.
Polymeric systems modified by ZnO nanoparticles
6th Workshop on Green Chemistry and Nanotechnologies in Polymer Chemistry, Braganca, Portugal, 15.-17.7.2015, přednáška, str. 52, ISBN 978-972-745-188-3

Cousy S., Svoboda L., Zelenka J.

Basic precipitation of simonkolleite nanoplatelets

NANOCON 2013 - Conference Proceedings, 5th International Conference, (2013) 265-268

Gorodylova N., **Cousy S**., Svoboda L., Zelenka J.

Peculiarities of thermal decomposition of synthetic simonkolleite.

3rd Central and Eastern European Conference on Thermal Analysis and Calorimetry, At Ljubljana, Slovenia (2015)

Cousy S., Svoboda L., Zelenka J.

Influence of synthesis conditions on ZnO/Zn5(OH)8Cl2.H2O formation

NANOCON 2014 - Conference Proceedings, 6th International Conference, (2014), at Brno, Czech Republic

Cousy S., Svoboda L., Zelenka J.

Effect of layered zinc hydroxide chloride nanoparticle insertion in an epoxy matrix

TRENDY – Conference Proceedings (2014), at Prague, Czech Republic

Cousy S., Svoboda L., Zelenka J.

Synthesis and modification of zinc hydroxide choride for nano-composite preparation

EIDS – Workshop proceedings (2014), at Lázně Bohdaneč, Czech Republic

Participation in domestic conferences

Matysová E., **Cousy S**., Zelenka J., Zelenková M., Vlček T., Svoboda L.

Příprava nanočástic ZnO pro různé polymerní systémy

62. konference chemického a procesního inženýrství, Seč - Ústupky, Česká republika, 9.-12.11.2015, poster, str. 127.

Gorodylova N., **Cousy S**., Svoboda L., Zelenka J.

Correlations between eExperimental conditions and thermal behaviour of layered zinc hydroxide chloride

Conference of Special Pigments and Powder Materials, At Pardubice, Czech Republic (2015)

Other publishing activities by the author:

Articles in specialized journals

Ferjencik M., Pelikan V., **Cousy S.**

Is our apparatus foolproof?: Examination of safety-important characteristics of an electrostatic discharge tester for explosives

Process Safety Progress, 32(2013), 283–297. https://doi.org/10.1002/prs.11573